Title
Effects of Nonuniform Potential and Current Distributions in Electrochemical Systems

Author
West, A.

Publication Date
1989-12-01

Lawrence Berkeley Laboratory
UNIVERSITY OF CALIFORNIA

Materials & Chemical Sciences Division

Effects of Nonuniform Potential and Current Distributions in Electrochemical Systems

A.C. West
(Ph.D. Thesis)

December 1989

Prepared for the U.S. Department of Energy under Contract Number DE-AC03-76SF00098.

DISCLAIMER

LBL-28076

Effects of Nonuniform Potential and Current Distributions in Electrochemical Systems

A. C. West
Ph.D. Thesis

Department of Chemical Engineering
University of California
Berkeley, CA 94720

and

Materials and Chemical Sciences Division
Lawrence Berkeley Laboratory
University of California
Berkeley, CA 94720

December 1989

This work was supported by the U.S. Department of Energy under
Contract No. DE-AC03-76SF00098.

Effects of Nonuniform Potential and Current Distributions in Electrochemical Systems

Alan C. West

Abstract

We examine the effects that nonuniform current and potential distributions have on electrochemical systems. Chapter 1 provides definitions used by researchers studying these phenomena. In chapter 2, we discuss boundary integral techniques, which are powerful numerical methods used in such studies. In chapters 3 and 4, an asymptotic solution is developed that shows explicitly how the extreme characteristics of a primary current distribution are approached when the ohmic resistance of the cell becomes large compared to the resistance of the faradaic reaction. It is shown how these results can be used to complement and verify more common numerical analyses. Chapters 5 and 6 show how to determine exchange current densities and transfer coefficients when the reaction rate along the electrode is nonuniform. The results can be used to design experiments that provide for a more straightforward interpretation of data. The ohmic resistance and current distribution for a recessed disk electrode are given in chapter 7. Chapter 8 discusses briefly experimental work intended to elucidate whether the dissolution kinetics of ferrous-sulfate films must be included in mathematical descriptions of the complicated dynamic behavior of iron dissolution in sulfuric acid.

John Newman

Acknowledgements

I wish to acknowledge everyone. In particular, John Newman. He never forgets that the education of the student is one of the primary goals of graduate research. I also wish to thank Professors Tobias and Devine for serving on my thesis committee.

Deserving special mention are all of my former and current colleagues from the group. In particular, Chrys, Gregg, Jennifer, Paul, Sudoh, Tom, Tony, and Vince. I also thank Sholeh for useful suggestions about eliminating noise in my experiments. Finally, John Sukamto deserves a special acknowledgement. He performed calculations relevant to chapters 4 and 5.

This work was supported by the Assistant Secretary for Conservation and Renewable Energy, Office of Energy Storage and Distribution, Energy Storage Division, of the U. S. Department of Energy under Contract No. DE-AC03-76SF00098.

Contents

CHAPTER 1
Introduction

This chapter defines terms that are used by researchers studying how reaction rates, electrochemical potentials, and surface concentrations are distributed along an electrode.

The best known parameter used in characterizing current distributions is the Wagner number. Its importance was established by Hoar and Agar [1] and was clarified by Wagner in 1951 [2]. In general, the Wagner number does not characterize completely the current and potential distributions in the solution. In 1966, Newman [3] showed for the rotating disk electrode which parameters are important for the various limiting cases and for the general problem. With his 1966 paper, the study of the distribution of current density on planar electrodes becomes a well-defined science. The study of current distributions in porous electrodes is also understood [4].

Wagner Number

The Wagner number represents the ratio of the kinetic to ohmic resistances to the flow of current. As the Wagner number approaches zero, the current approaches a "primary current distribution." When the kinetic resistance dominates, the distribution of current density is uniform. Since the Wagner number is defined by different variables for different reaction regimes, Newman does not explicitly use it.

Mass-Transfer Controlled Current Distributions

An important limiting case is the mass-transfer controlled (limiting) current distribution. In the absence of migration, the limiting current density is determined by procedures that are common in the heat and mass-transfer literature [5,6,7]. Newman showed [8] that, for boundary-layer flows, migration at the limiting current does not affect the distribution of current but does change its magnitude.

Primary Current Distributions

In the absence of concentration variations, Laplace's equation determines the current distribution. When the kinetic resistance of the interfacial reaction is zero compared to the ohmic resistance, the current distribution is known as *primary*. This case is important because it may be desirable to compare different cell designs to minimize the ohmic resistance. The ohmic potential drop increases with the size of an electrochemical system; therefore the primary current distribution is approached as a system is scaled-up. The primary current distribution is also approximately valid, for example, for short times after a step change in the electrode potential.

Secondary Current Distributions

In practical situations, the kinetics of a reaction are important. When an interfacial resistance is included but mass-transfer effects are neglected, the current distribution is known as *secondary*. To study the effects of finite kinetics, it is instructive to

study the two limiting cases of the Butler-Volmer equation, known as linear and Tafel kinetics. The behavior of a system, for a given Wagner number, depends on which reaction regime is applicable. A dimensionless exchange current density is the important parameter for linear kinetics, and a dimensionless average current density is important in characterizing the distribution for Tafel kinetics.

For linear kinetics, analogous boundary conditions are found in heat-transfer problems, and experience obtained from these studies can provide insight into the behavior of current distributions. For Tafel kinetics, analogous boundary conditions do not exist, and it is necessary to develop intuition specifically for this important limiting case. For example, Smyrl and Newman [9] show that, under certain well-defined conditions, the current density at the edge of an electrode is proportional to the square of the average current density.

Tertiary Current Distributions

Below the limiting current, when both ohmic potential drop and convective diffusion are important, the problem is complicated. Newman discussed this class of problems [10]. Complete characterization of a tertiary current distribution can require many parameters.

Porous Electrodes

Newman and Tiedemann [4] reviewed the solution procedure for the determination of current distributions in porous electrodes. The same limiting cases discussed above are important. Intuition developed from studying planar electrodes aids in understanding the

current distribution in porous electrodes.

Summary

Significant progress in studying current distributions requires useful numerical procedures. Chapter 2 discusses a numerical method that we have used for studying primary and secondary current distributions. Chapters 3 through 7 present results that are obtained with this method. It is hoped that these results are directly useful to the reader. If not, they elucidate behavior that is helpful in understanding phenomena observed in other current distribution studies.

Chapter 8 discusses experimental observations of the Fe/H_2SO_4 system. The complicated behavior that is observed for this system is, in part, a result of nonuniform potential and current distributions. This is a passivating system, which makes it quite sensitive to the potential distribution along the electrode.

To allow for leisurely reading, the chapters have been largely written so that they can be read independently. Particularly, the details of the numerical method given in chapter 2 are unnecessary for the rest of the thesis.

References

[1] T. P. Hoar and J. N. Agar, "Factors in Throwing Power Illustrated by Potential-Current Diagrams," *Discussions of the Faraday Soc.*, 1, 162 (1947).

[2] Carl Wagner, "Theoretical Analysis of the Current Density Distribution in Electrolytic Cells," *J. Electrochem. Soc.*, **98**, 116 (1951).

[3] John Newman, "Current Distribution on a Rotating Disk below the Limiting Current," *J. Electrochem. Soc.*, **113**, 1235 (1966).

[4] John Newman and William Tiedemann, "Porous-Electrode Theory with Battery Applications," *AICHE Journal*, **21**, 25 (1975).

[5] Veniamin G. Levich, *Physicochemical Hydrodynamics*, Prentice-Hall, Englewood Cliffs, N. J. (1962).

[6] Hermann Schlichting, *Boundary Layer Theory*, McGraw-Hill, New York (1968).

[7] John Newman, *Electrochemical Systems*, chapter 17, Prentice-Hall, Englewood Cliffs, N. J. (1973).

[8] John Newman, "The Effect of Migration in Laminar Diffusion Layers," *Int. J. Heat and Mass Transfer*, **10**, 983 (1967).

[9] William H. Smyrl and John Newman, "Current Distributions at Electrode Edges at High Current Densities," *J. Electrochem. Soc.*, **136**, 132, (1989).

[10] John Newman, *Electrochemical Systems*, chapter 21, Prentice-Hall, Englewood Cliffs, N. J. (1973).

CHAPTER 2
An Iterative, Boundary Integral Technique

Laplace's equation often arises in mathematical descriptions of electrochemical systems. This chapter discusses the use of boundary integral methods for solving it. For a more general discussion of numerical methods used in current distribution problems, see references [1], [2], [3], and [4]. Greenberg [5] and Ramkrishna and Amundson [6] gave details pertaining to the application of boundary integral techniques to other linear operators.

Boundary-elements have become increasingly popular since the mid-1970's [7], [8], [9]. Also becoming popular are the finite-element methods. Comparisons of these methods are found in papers by Hume *et al.* [10] and by Dukovic and Tobias [11]. Most of the advantages and disadvantages of boundary integral techniques apply regardless of how the equations are formulated or solved.

Boundary-element methods require fewer nodes, at which the finite-difference approximations to the equations are solved, than finite-element methods. However, the resulting equations form a dense matrix (as opposed to a banded matrix). Therefore, computation time is not greatly reduced, even though the number of unknowns can be considerably less.

Contrary to many techniques [7], [8], [9], the solution procedure that we discuss does not pose the problem as one to be solved by the method of weighted residuals. The method permits any type of

basis function† and allows for the form of the basis function to vary with position. This is particularly important for primary current distributions.

Although the formalism of certain boundary-element methods is relatively new, boundary integral methods have existed for a long time [12]. Wagner [13] used integral equations for the analytic solution of current distribution problems. Newman [3] and Cahan *et al.* [14] discussed the use of boundary integral equations to calculate current distributions numerically.

The technique of Cahan *et al.* discretizes the boundary conditions and solves for the potential near, but not on, the boundary. In this manner, the method avoids evaluating the singularities that arise in equations (5), (12), and (14). We prefer handling directly these singularities because errors that arise from their procedure are avoided. This becomes particularly important in the calculation of primary current distributions.

Green's Theorem

Boundary integral methods are based on the second form of Green's theorem (see [15], for example),

$$\int_V \left(g\nabla^2\Phi - \Phi\nabla^2 g\right) dV = \int_{\partial V} \mathbf{n}\cdot\left(g\nabla\Phi - \Phi\nabla g\right) dA. \qquad (1)$$

---

† *Basis functions* is a term borrowed from traditional finite and boundary-element methods. It describes the manner in which a function is interpolated between nodes.

If Φ satisfies Laplace's equation, equation (1) becomes

$$-\int_V \Phi\nabla^2 g \, dV = \int_{\partial V} \mathbf{n}\cdot\left(g\nabla\Phi - \Phi\nabla g\right) dA. \tag{2}$$

A clever choice of g greatly facilitates the determination of the potential. Specifically, g is chosen to satisfy

$$\nabla^2 g = \delta(x-x_q, y-y_q, z-z_q), \tag{3}$$

where δ is the three-dimensional Dirac delta function, x, y, and z are the Cartesian coordinates, and x_q, y_q, z_q specifies a point. One Green's function g that satisfies equation (3) is $g = \frac{1}{\xi_3}$, where

$$\xi_3 = \left[(x-x_q)^2 + (y-y_q)^2 + (z-z_q)^2\right]^{1/2}. \tag{4}$$

Physically, g can be thought of as the potential at x_q, y_q, z_q due to a point source of current at x, y, z.

Substituting g into equation (2) gives

$$-\alpha_3\Phi(x_q, y_q, z_q) = \int_{\partial V} \mathbf{n}\cdot\left(\frac{1}{\xi_3}\nabla\Phi - \Phi\nabla\frac{1}{\xi_3}\right) dA, \tag{5}$$

where α_3 is 4π for a point, x_q, y_q, z_q, in the domain of the problem, 2π for a point on a smooth boundary, and zero for a point outside the domain. In general,

$$\alpha_3 = \lim_{R_o \to 0} \frac{A_s}{R_o^2}, \tag{6}$$

where A_s is the surface area of the portion of a sphere around x_q, y_q, z_q which falls within the domain of the problem [7]. Figure 1 shows the two-dimensional analog to α_3. Equation (5) shows that the solution for Φ is reduced to a problem on the boundary of the domain.

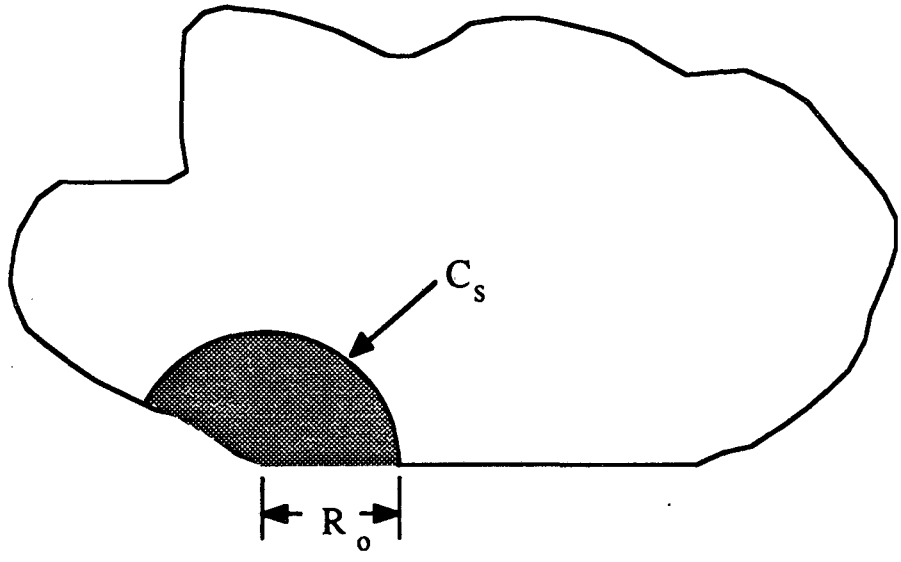

Three Dimensions

$$\alpha_3 = \lim_{R_o \to 0} \left(\frac{A_s}{R_o^2} \right)$$

Two Dimensions

$$\alpha_2 = \lim_{R_o \to 0} \left(\frac{C_s}{R_o} \right)$$

Figure 1. Schematic showing the coefficient given in equation (6) for two-dimensional geometries. A_s is the surface area of the portion of the sphere that falls within the domain of the problem, and C_s is the arc length of the portion of a circle that falls within the domain.

Once the potential and current density are known everywhere on the boundary, the potential can be found anywhere in the domain.

Since equation (3) is linear, solutions for g can be superposed. Specifically, if g_h satisfies Laplace's equation, $\frac{1}{\xi_3} + g_h$ satisfies equation (3). Choosing g_h so that $\mathbf{n}\cdot\nabla(\frac{1}{\xi_3} + g_h) = 0$ everywhere along the boundary of the domain can reduce greatly the numerical computation necessary for a solution since equation (5) becomes

$$-\alpha_3\Phi(x_q,y_q,z_q) = \int_{\partial V} \mathbf{n}\cdot\left[(\frac{1}{\xi_3} + g_h)\nabla\Phi\right]dA. \tag{7}$$

This approach is taken, for example, by Alkire and Mirarefi [16] and has been used extensively by mathematical physicists [17]. A good discussion of these methods is given by Greenberg [5].

Many electrochemical cells are approximated as two dimensional or axisymmetric. The next two sections give boundary integral equations that are more conveniently used for these cases.

Two-Dimensional Geometries

If the geometry of interest contains no z dependence, equation (2) can be written as

$$-\left[\int_A \Phi\nabla^2 g\,dx\,dy\right]\Delta z = \left[\int_{\partial A} \mathbf{n}\cdot\left[g\nabla\Phi - \Phi\nabla g\right]d\ell\right]\Delta z, \tag{8}$$

where $d\ell$ is a differential line element. If g is now chosen to satisfy

$$\frac{\partial^2 g}{\partial x^2} + \frac{\partial^2 g}{\partial y^2} = \delta(x-x_q, y-y_q), \tag{9}$$

then equation (8) reduces to

$$\alpha_2 \Phi(x_q, y_q) = \int_{\partial A} \left(\Phi \frac{\partial g}{\partial n} - g \frac{\partial \Phi}{\partial n} \right) d\ell, \tag{10}$$

where $\partial/\partial n$ implies the component of the gradient that is normal to the boundary. α_2 is 2π for a point inside the domain, zero for a point outside the domain, and π for a point on a smooth boundary. Figure 1 shows α_2 for a point where the slope of the line drawn tangent to the boundary is discontinuous.

The two-dimensional Green's function g is $g = \ln \xi_2$, where

$$\xi_2 = \left[(x-x_q)^2 + (y-y_q)^2 \right]^{1/2}. \tag{11}$$

g is the potential at x_q, y_q due to a line source of current that is perpendicular to the $\overline{xy}$ plane and passes through the point x, y. Substituting g into equation (10) gives

$$\alpha_2 \Phi(x_q, y_q) = \int_{\partial A} \left(\frac{\Phi}{\xi_2} \frac{\partial \xi_2}{\partial n} - \ln \xi_2 \frac{\partial \Phi}{\partial n} \right) d\ell. \tag{12}$$

Axisymmetric Geometries

For axisymmetric geometries, equation (5) can be written as

$$-\alpha_3 \Phi(r_q, z_q) = \int_{\partial V} \mathbf{n} \cdot \left(\frac{1}{\xi_3} \nabla \Phi - \Phi \nabla \frac{1}{\xi_3} \right) r d\theta d\ell, \tag{13}$$

where r, θ, z are the cylindrical coordinates, r_q, z_q specifies a location, and $r d\theta d\ell$ is the differential surface area.

Since by assumption the problem is axisymmetric, the θ dependence of equation (13) can be eliminated to give

$$-\alpha_3\Phi(r_q,z_q) = \int_{\partial A} \left(g \frac{\partial \Phi}{\partial n} - \Phi \frac{\partial g}{\partial n}\right) r d\ell, \tag{14}$$

where we now set

$$g = \frac{4K(m)}{\left[(r+r_q)^2 + (z-z_q)^2\right]^{1/2}} . \tag{15}$$

g can be thought of as the potential at r_q,z_q due to a ring of point sources of current at r,z. $K(m)$ is the complete elliptic integral of the first kind,

$$K(\bar{m}) = \int_0^{\pi/2} \frac{d\theta}{(1 - m \sin^2\theta)^{1/2}} , \tag{16}$$

and the modulus m is given by

$$m = \frac{4rr_q}{(r+r_q)^2 + (z-z_q)^2} . \tag{17}$$

Approximate forms of $K(m)$ are given in Abramowitz and Stegun [18]. After integration over θ, $d\ell$ signifies the length element for the path enclosing the region in the r,z half plane and n signifies a direction normal to this path. Where the path coincides with the z-axis, the integrand of equation (14) is zero.

Wrobel and Brebbia gave [19]

$$\frac{\partial g}{\partial n} = \frac{-2/r}{\left[(r+r_q)^2 + (z+z_q)^2\right]^{1/2}} \left[K(m) + \frac{r^2 - r_q^2 - (z-z_q)^2}{(r-r_q)^2 + (z-z_q)^2} E(m)\right] \mathbf{e}_r \tag{18}$$

$$- \frac{4E(m)(z-z_q)}{\left[(r+r_q)^2 + (z+z_q)^2\right]^{1/2}\left[(r-r_q)^2 + (z-z_q)^2\right]} e_z$$

where e_r and e_z are the unit vectors in the r and z directions,† and $E(m)$ is the complete elliptic integral of the second kind,

$$E(m) = \int_0^{\pi/2} (1 - m \sin^2\theta)^{1/2} d\theta. \tag{19}$$

Approximations of $E(m)$ are also given in Abramowitz and Stegun [18].

Interpolation Methods

The numerical solution of differential (or integral) equations requires finite-difference approximations. It, therefore, is important to interpolate accurately between nodes. In modern texts concerned with boundary-element or finite-element methods some discussion of interpolation methods is found under the discussion of basis functions [20]. Popular (local) basis functions are known as quadratic or linear. These terms indicate the order of the interpolating polynomial. For example, a linear basis function varies linearly between two successive nodes. Quadratic basis functions, then, fit a quadratic equation between three successive nodes.

---

† Useful relations for deriving these and similar equations are:

$$\frac{dK(m)}{dm} = -\frac{K(m)}{2m} + \frac{E(m)}{2m(1-m)}$$

and

$$\frac{dE(m)}{dm} = \frac{1}{2m}\left[E(m) - K(m)\right] .$$

Many textbooks give few details on interpolating functions that vary in a strongly nonlinear manner. For example, one might try to interpolate the primary current density near the edge of a disk electrode, where [21]

$$\frac{i(r)}{i_{avg}} = \frac{0.5}{(1 - r^2/r_o^2)^{1/2}} \quad (20)$$

It is proper to interpolate the primary current density on a disk by assuming that it varies linearly with respect to $(1 - r^2/r_o^2)^{-1/2}$. Of course, for problems to be solved numerically, the exact functional relation is not known *a priori*. Asymptotic solutions, though, predict the manner in which the current density varies, and can be used to avoid numerical errors (such as an artificial wiggle in the current distribution near the edge of an electrode) that commonly occur in the solution of primary current distributions. The interpolation procedures that we use assume a linear variation in the appropriately stretched coordinates between two succesive nodes.

Away from insulator/electrode interfaces, variations in current density and potential are sufficiently mild that special interpolation procedures are unnecessary, although they may still improve accuracy and computational efficiency. Near an electrode edge, variations may be large. For primary current distributions, the current density is infinite at the edge of the electrode if the interior angle of intersection between the insulator and electrode is obtuse [22].

In reality, kinetic resistances become important, and the current density at the edge remains finite. If the kinetic resistances are included, it, therefore, is less important to know *a priori* how the current density varies. Nevertheless, asymptotic equations are useful for understanding and verifying results.

Smyrl and Newman [23] described current distributions for large, finite ohmic resistances for a coplanar electrode and insulator. Previously, Nişancioğlu and Newman [24] showed the behavior for large ohmic resistances for linear kinetics on a disk electrode. Chapter 3 generalizes these results.

Integration Procedures

For two-dimensional geometries, when the potential or current density is interpolated linearly with respect to Cartesian coordinates, the integrals (between two successive nodes) resulting from equation (12) can be evaluated analytically.

The integrals appearing in the axisymmetric equations must be solved numerically. Standard integration methods are used for well-behaved functions. Functions containing singularities are handled by the subtraction and addition of a similarly behaved singularity or by changing the variable of integration. Edwards [25] discussed these procedures. For primary distributions, accurate solutions require knowledge of the asymptotic behavior of the current distribution.

In addition to the numerical difficulties that arise because of singularities in the current distribution, the axisymmetric Green's

function is singular as $r,z \longrightarrow r_q,z_q$ since [18]

$$\lim_{m\longrightarrow 1} K(m) = \frac{1}{2} \ln\left(\frac{16}{1 - m}\right) . \tag{21}$$

This logarithmic singularity is integrated numerically by the addition and subtraction of a similarly behaved singularity.

When knowledge of the correct asymptotic behavior is used, interpolation and integration methods can yield highly accurate solutions. For the calculation of the primary current distribution on a disk electrode, the integration techniques can give solutions accurate to within a relative error of 10^{-8}.

As a concrete example of these methods, it is instructive to look at the integral equations written for the disk geometry. The potential distribution on the disk electrode and insulating plane is given by [3]

$$\Phi(r_q) = \frac{2}{\pi\kappa} \int_0^{r_o} \frac{i_n(r)K(m)r}{r + r_q}\, dr , \tag{22}$$

where r_o is the radius of the disk electrode. For a primary current distribution, the potential Φ_o is specified on the electrode, and the current density, if it were unknown, can be described by

$$i_n(r_q) = -\frac{2\kappa}{\pi} \int_{r_o}^{\infty} \frac{(\Phi(r) - \Phi_o)E(m)r}{(r-r_q)^2(r+r_q)}\, dr . \tag{23}$$

For secondary current distributions, equation (23) is unnecessary since a kinetic rate equation relates $\Phi_o(r_q)$ and $i_n(r_q)$.

Equation (22) contains examples of integrable singularities. For primary distributions, equation (5) of chapter 3 suggests that

$i_n \propto (r_o - r)^{-\frac{1}{2}}$, which suggests changing the variable of integration to $x = (r_o - r)^{\frac{1}{2}}$. After substituting for the exact form of i_n, as given by equation (20), equation (22) becomes

$$\Phi(r_q) = \frac{2r_o i_{avg}}{\pi\kappa} \int_0^{\sqrt{r_o}} \frac{K(m)(r_o - x^2)dx}{(2r_o - x^2)^{\frac{1}{2}}(r_q + r_o - x^2)} , \tag{24}$$

which eliminates the singularity caused by the current density.

$K(m)$, though, still presents a problem because it contains a logarithmic singularity when $r \longrightarrow r_q$. To handle this singularity, if $r_q = r_o$, the integral could be written as

$$\Phi(r_o) = \frac{2r_o i_{avg}}{\pi\kappa} \int_0^{\sqrt{r_o}} \left[\frac{(r_o - x^2)K(m)}{(2r_o - x^2)^{3/2}} + \frac{2r_o ln(x)}{(2r_o)^{3/2}} \right] dx \tag{25}$$

$$- \frac{\sqrt{2r_o} i_{avg}}{\pi\kappa} \left(\sqrt{r_o} \ln(\sqrt{r_o}) - \sqrt{r_o} \right) .$$

Logarithmic singularities can also be handled by a special Gaussian quadrature procedure [26].

To handle some of the singularities that arise in these problems, Brebbia [27] suggests a device in which the evaluation of the integrals near some of the singular points is avoided. His trick recognizes that a system with constant potential everywhere has no current flowing. Therefore, equation (14), for example, becomes

$$\alpha_3 = \int_{\partial A} \frac{\partial g}{\partial n} \, r d\ell . \tag{26}$$

In his method, this integral is split into the regions between node

points, and the region containing the singularity is evaluated by difference so that the above equation is satisfied. This does not seem like a good idea because all of the numerical errors arising through the evaluation of the other elements of the integral are incorporated into the term that is the largest contributor. His idea, though, is useful because equation (26) provides a test on the accuracy of the integration procedures. Another approach that can test the accuracy of a solution is to evaluate equation (5), (12), or (14) at points outside the domain, where $\alpha_3 = 0$.

Solution Method

As was stated earlier, equation (12) or equation (14), when written for each node on the boundary, results in a "dense" matrix. This matrix equation is often solved by Gaussian elimination, but can also be solved by the method of successive substitutions. Edwards [25] discussed these two approaches. She concluded that the method of successive substitutions works well if a good initial guess is provided and a reasonable damping factor is used. The savings in computation time can be substantial for a large matrix. The disadvantage is that it is often more difficult to make the method of successive substitutions converge.

Despite her reported problems, we used this method. We also found that convergence depends on the value of the damping factor. With a proper choice and a good initial guess, the method of successive substitutions requires fewer calculations than a Gaussian-elimination procedure. For example, substantial savings can be

obtained if the results from a run with fewer node points is used as the initial guess.

To make the method of successive substitutions an attractive alternative to a Gaussian-elimination/Newton-Raphson procedure, an efficient algorithm to determine the optimum damping factor must be developed. This was not pursued since computer costs continue to decrease, and thus, for many applications, speed can be sacrificed for robustness.

Summary

A rigid method is not presented in this chapter. In fact, we purposely avoid the formalism of other methods in favor of tailoring the procedure to the particular problem. By using asymptotic solutions to guide the development of a method, greater accuracy, lower computation costs, and greater physical insight are possible. Using asymptotic results with more formal methods is possible, although this may require sacrificing generality, which is a major advantage to such procedures.

List of Symbols

A	indicates integration over the boundary, cm^2
A_s	surface area shown in figure 1, cm^2
C_s	arc shown in figure 1, cm
$E(m)$	complete elliptic integral of the second kind

$\mathbf{e}_r, \mathbf{e}_z$	unit normal vectors
g	Green's function, cm^{-1}
i_n	normal component of the current density, A/cm^2
ℓ	variable of integration in two dimensions, cm
$K(m)$	complete elliptic integral of the first kind
r	radial position coordinate, cm
r_o	radius of the disk, cm
R_o	radius shown in figure 1, cm
V	indicates integration over the entire domain, cm^3
x, y, z	Cartesian coordinates, cm
α_2, α_3	coefficients shown in figure 1
β	interior angle of intersection between electrode and insulator, radians
δ	Dirac delta function
ζ	variable of integration in cylindrical coordinates, cm
θ	cylindrical coordinate, radians
κ	solution conductivity, S/cm
ξ_2	distance for two-dimensional geometries, cm
ξ_3	distance for three-dimensional geometries, cm
π	3.141592654
Φ	potential of the solution, V

Subscripts

avg	average
edge	electrode/insulator interface
q	coordinate at which the potential is being solved

References

[1] Geoffrey A. Prentice and Charles W. Tobias, "A Survey of Numerical Methods and Solutions for Current Distribution Problems," *J. Electrochem. Soc.*, **129**, 72 (1982).

[2] N. Ibl, "Current Distribution," *Comprehensive Treatise of Electrochemistry*, **6**, Ernest Yeager, J. O'M. Bockris, Brian E. Conway, S. Sarangapani, Editors, p. 239, Plenum Press, New York (1983).

[3] John Newman, "The Fundamental Principles of Current Distribution and Mass Transport in Electrochemical Systems," in *Electroanalytical Chemistry*, A. J. Bard, Editor, pp. 187-351, Marcel Dekker, Inc., New York (1973).

[4] Alan C. West and John Newman, "Current Distributions Determined by Laplace's Equation," to be published.

[5] Michael D. Greenberg, *Applications of Green's Functions in Science and Engineering*, Prentice-Hall, Englewood Cliffs, N. J. (1971).

[6] Doraiswami Ramkrishna and Neal R. Amundson, *Linear Operator Methods in Chemical Engineering with Applications to Transport and Chemical Reaction Systems*, Prentice-Hall, Englewood Cliffs, N. J. (1985).

[7] C. A. Brebbia, *The Boundary Element Method for Engineers*, John Wiley and Sons, New York (1978).

[8] P. K. Banerjee and R. Butterfield, *Boundary Element Methods for Engineering Science*, McGraw-Hill, Inc., New York (1981).

[9] J. A. Liggett and P. L-F. Liu, *The Boundary Integral Equation Method for Porous Media Flow*, Allen and Unwin, Boston (1983).

[10] E. C. Hume III, R. A. Brown, and W. M. Deen, "Comparison of Boundary and Finite Element Methods for Moving-Boundary Problems Governed by a Potential," *Int. J. Num. Meth. Eng.*, 21, 1295 (1985).

[11] J. O. Dukovic and C. W. Tobias, *Studies on Current Distribution in Electrochemical Cells*, Ph. D. Thesis, University of California, Berkeley, (August, 1986).

[12] James Clerk Maxwell, *A Treatise on Electricity and Magnetism*, vol. 1, 3rd edition, Clarendon Press, Oxford (1906).

[13] Carl Wagner, "Theoretical Analysis of the Current Density Distribution in Electrolytic Cells," *J. Electrochem. Soc.*, 98, 116 (1951).

[14] B. D. Cahan, Daniel Scherson, and Margaret A. Reid, "I-BIEM. An Iterative Boundary Integral Equation Method for Computer Solutions of Current Distribution Problems with Complex Boundaries—A New Algorithm," *J. Electrochem. Soc.*, 135, 285 (1988).

[15] Francis B. Hildebrand, *Advanced Calculus for Applications*, p. 301, Prentice-Hall, Inc., Englewood Cliffs, N. J. (1976).

[16] Richard Alkire and Ali Asghar Mirarefi, "The Current Distribution Within Tubular Reactors under Laminar Flow," *J. Electrochem. Soc.*, **120**, 1507 (1973).

[17] John David Jackson, *Classical Electrodynamics*, 2nd ed., John Wiley & Sons, New York (1975).

[18] M. Abramowitz and I. Stegun, *Handbook of Mathematical Functions*, National Bureau of Standards, Washington (1964).

[19] L. C. Wrobel and C. A. Brebbia, "Axisymmetric Potential Problems," *New Developments in Boundary Element Methods, Proceedings of the Second International Seminar*, Southampton, pp. 77-89 (1980).

[20] Leon Lapidus and George F. Pinder, *Numerical Solution of Partial Differential Equations in Science and Engineering*, John Wiley and Sons, New York (1982).

[21] John Newman, "Resistance for Flow of Current to a Disk," *J. Electrochem. Soc.*, **113**, 501 (1966).

[22] John Newman, *Electrochemical Systems*, p. 343, Prentice-Hall, Englewood Cliffs, N. J. (1973).

[23] William H. Smyrl and John Newman, "Current Distributions at Electrode Edges at High Current Densities," *J. Electrochem. Soc.*, **136, 132 (1989).**

[24] Kemal Nişancioğlu and John Newman, "The Short-Time Response of a Disk Electrode," *J. Electrochem. Soc.*, 123, 523 (1974).

[25] Victoria Edwards, *Design of Thin-Gap Channel Flow Cells*, Ph. D. Thesis, University of California, Berkeley, p. 26 (July, 1986).

[26] A. H. Stroud and Don Secrest, *Gaussian Quadrature Formulas*, Prentice-Hall, Englewood Cliffs, N. J. (1966).

[27] C. A. Brebbia, *The Boundary Element Method for Engineers*, p. 58, John Wiley and Sons, New York (1978).

CHAPTER 3
Current Distribution near an Electrode Edge as a Primary Distribution is Approached

It is well known [1] that the primary current density is infinite at an edge of an electrode if the angle of intersection between the electrode and insulator is obtuse. Also, the primary current density at the edge is zero for an acute angle. In all practical cases, the kinetics of the interfacial reaction enters, and these extreme values do not occur.

This chapter demonstrates how the potential and current approach a primary distribution as the kinetic resistance becomes negligible (compared to the ohmic resistance). The analysis is valid in the edge region of an electrode and insulator, is a function of the angle, β, shown in figure 1, and is independent of the geometric details of the rest of the electrochemical cell. Results from this abstract geometry can be use to verify numerical investigations of actual geometries. Additionally, an *a priori* estimate of the behavior in an edge region can aid in the development of more efficient and more accurate numerical procedures.

Nişancioğlu and Newman [2] solved this problem for linear kinetics in the edge region of a disk electrode. Smyrl and Newman [3] extended the results for the linear kinetics case and gave results for Tafel kinetics. Their results are valid when $\beta = \pi$.

In both of these papers, it was recognized that, for high ohmic resistances, the current distribution could be described adequately

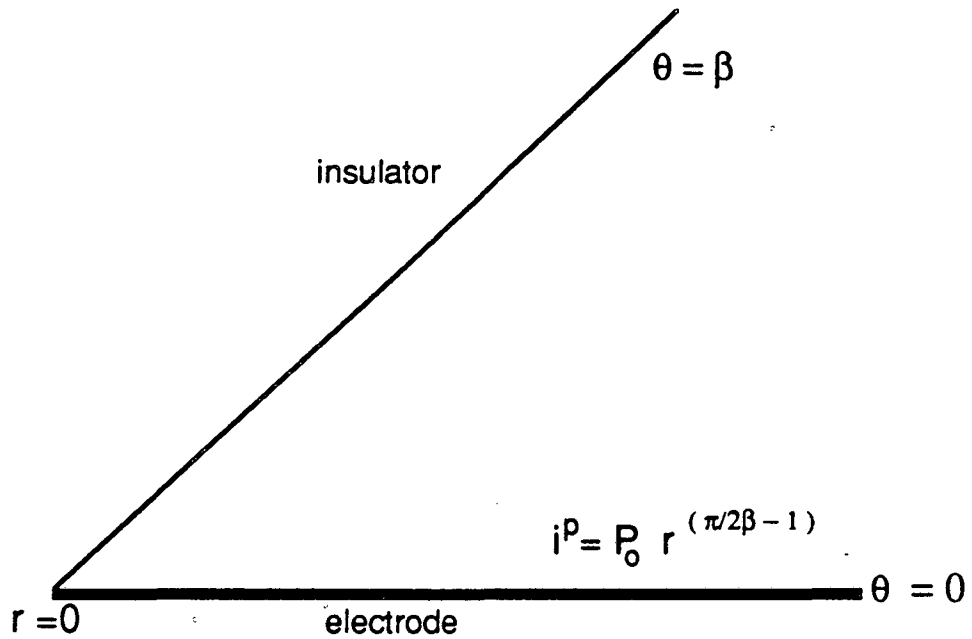

Figure 1. Primary current distribution in the *edge region* of an electrode and insulator.

by the primary distribution away from the edge region but showed large deviations from this distribution near the edge. Stated another way, the resistance of the faradaic reaction is important only in the edge region. They realized that this suggests that the problem is treated properly by a singular-perturbation analysis.

Primary Current Distribution

The primary current distribution in the edge region shown in figure 1 can be determined by Laplace's equation in cylindrical coordinates, which reduces to

$$\frac{1}{r}\frac{\partial}{\partial r}\left(r\frac{\partial \Phi}{\partial r}\right) + \frac{1}{r^2}\left(\frac{\partial^2 \Phi}{\partial \theta^2}\right) = 0. \tag{1}$$

The boundary conditions are

$$\frac{\partial \Phi}{\partial \theta} = 0 \quad \text{at} \quad \theta = \beta. \tag{2}$$

and

$$\Phi = 0 \quad \text{at} \quad \theta = 0. \tag{3}$$

The solution (for small r) to equations (1) through (3) is

$$\Phi^P = -\frac{2\beta}{\pi\kappa} P_o r^{\pi/2\beta} \sin\left(\frac{\pi\theta}{2\beta}\right), \tag{4}$$

where P_o relates to the magnitude of the primary current distribution:

$$i^P(r) = -\frac{\kappa}{r}\frac{\partial \Phi^P}{\partial \theta} = P_o r^{(\pi/2\beta - 1)}. \tag{5}$$

It is necessary to introduce P_o because equations (1) through (3) do not completely specify the solution, and the magnitude of the

current can be changed by changing the cell potential. The placement of the counterelectrode and the geometric details of the working electrode in the region *away* from the corner region are not given. To do so would eliminate the possibility of a general analysis. In a region sufficiently close to the corner, the distribution of current density behaves in a manner independent of these details. In general, the details of the geometry away from the edge region are incorporated into P_o, which is determined through comparisons of equation (4) with the primary current distribution valid for the entire geometry. Smyrl and Newman [3] showed that $P_o = i_{avg}\sqrt{r_o/8}$ for the rotating disk electrode. They also gave P_o for the flow-channel geometry.

Linear Kinetics

For linear kinetics, the boundary condition along the working electrode becomes

$$-\frac{\kappa}{r}\frac{\partial\Phi}{\partial\theta} = \frac{(\alpha_a+\alpha_c)Fi_o}{RT}(V - \Phi_o) , \qquad (6)$$

where V is the potential of the electrode and Φ_o is the potential of the solution adjacent to the electrode. For large values of the exchange current density, the current is given adequately by equation (5) for large (but not too large) values of r. Near the corner, though, kinetics is important, and the current deviates from the primary distribution. To emphasize this corner region, a stretched radial distance should be defined by

$$\bar{r} = rS_L = r \frac{(\alpha_a+\alpha_c)Fi_o}{RT\kappa} , \tag{7}$$

and a stretched potential by

$$\bar{\phi} = (\Phi - V) \frac{\kappa S_L^{\pi/2\beta}}{P_o} . \tag{8}$$

The problem, in terms of these variables, is given by

$$\frac{1}{\bar{r}} \frac{\partial}{\partial \bar{r}}\left[\bar{r} \frac{\partial \bar{\phi}}{\partial \bar{r}}\right] + \frac{1}{\bar{r}^2} \left[\frac{\partial^2 \bar{\phi}}{\partial \theta^2}\right] = 0 , \tag{9}$$

with the boundary conditions,

$$\frac{\partial \bar{\phi}}{\partial \theta} = 0 \quad \text{at} \quad \theta = \beta \tag{10}$$

and

$$\frac{1}{\bar{r}} \frac{\partial \bar{\phi}}{\partial \theta} = \bar{\phi}_o \quad \text{at} \quad \theta = 0. \tag{11}$$

Finally, for large $\bar{r}$ (but small r) $\bar{\phi}$ must satisfy the condition that

$$\bar{\phi} \longrightarrow - \frac{2\beta}{\pi} \bar{r}^{\pi/2\beta} \sin\left(\frac{\pi\theta}{2\beta}\right) \quad \text{as} \quad \bar{r} \longrightarrow \infty . \tag{12}$$

($\bar{r} \longrightarrow \infty$ because S_L becomes large.)

It should be noted that V has effectively been set equal to zero in the matching condition given by equation (12). This is justified for obtuse angles because the primary current density (see equation (5)) decreases for large $\bar{r}$. Acute angles require the treatment outlined in the appendix.

Details of the numerical solution for $\bar{\phi}$ are given below. It should be recognized that the equations are free of parameters and that $\bar{\phi}$ is therefore independent of the stretching parameter S_L.

An important result of this section is that, for high exchange current densities, the current density in the corner region is given by

$$\frac{i(r)}{P_o} = -\left[\frac{(\alpha_a+\alpha_c)Fi_o}{RT\kappa}\right]^{(1-\pi/2\beta)} \bar{\phi}_o \ . \tag{13}$$

That the current density at the edge of the electrode approaches infinity as a power of a parameter involving the exchange current density should not be too surprising since previous experience [4] suggests that such a parameter dictates the distribution of current for linear kinetics.

Tafel Kinetics

For anodic Tafel kinetics, the boundary condition along the electrode is

$$-\frac{\kappa}{r}\frac{\partial\Phi}{\partial\theta} = i_o \exp\left[\frac{\alpha_a F}{RT}(V - \Phi_o)\right] \ . \tag{14}$$

The exchange current density is no longer a key variable in determining the distribution of current. Previous experience suggests that a dimensionless average current density is the important parameter. Since a characteristic length is missing from this problem, no such parameter can be defined. P_o, though, is analogous in that it specifies the magnitude of the current, and it may be expected to be important for Tafel kinetics.

If P_o is large—so that the ohmic resistance is large and the analysis is valid—the current distribution far from the edge is

given adequately by the primary distribution. To investigate the region where the primary distribution does not apply, the potential should be stretched as

$$\bar{\phi} = \frac{\alpha_a F}{RT} (\Phi - V) - \ln(S_T) + \ln\left[\frac{\alpha_a F i_o}{RT\kappa}\right], \tag{15}$$

and the radial distance by

$$\bar{r} = rS_T = r \left[\frac{\alpha_a F P_o}{RT\kappa}\right]^{2\beta/\pi} . \tag{16}$$

In terms of these variables, equations (9) and (10) apply, and the boundary condition along the electrode becomes

$$\frac{1}{\bar{r}} \frac{\partial \bar{\phi}}{\partial \theta} = - \exp(-\bar{\phi}_o) \quad \text{at} \quad \theta = 0. \tag{17}$$

For large $\bar{r}$, $\bar{\phi}$ must approach the asymptotic solution suggested by Smyrl and Newman [3]:†

$$\bar{\phi} \longrightarrow - \frac{2\beta}{\pi} \bar{r}^{\pi/2\beta} \sin\left[\frac{\pi\theta}{2\beta}\right] + \left[\frac{\pi}{2\beta} - 1\right] \ln(\bar{r}) \quad \text{as} \quad \bar{r} \longrightarrow \infty. \tag{18}$$

The numerical procedure used to solve for $\bar{\phi}$ is discussed in the next section. For large values of P_o, the current in the edge region is given by

$$\frac{i(r)}{P_o} = \left[\frac{\alpha_a F P_o}{RT\kappa}\right]^{(2\beta/\pi - 1)} \exp(-\bar{\phi}_o) . \tag{19}$$

Again, the parameter that is important for specifying the current

---

† A complication which could arise in the analysis is that Tafel kinetics may no longer apply at distances at which the primary distribution is approached. The possibility of entering a linear kinetics regime before the primary distribution is approached was not investigated.

density in the edge region is consistent with previous experience.

Numerical Analysis

Since, in two dimensions, currents can not flow to infinity without an infinite potential drop, it is necessary to calculate deviations from the primary potential distribution. A new potential, ψ, is defined as

$$\psi = \bar{\phi} - \bar{\phi}^{P} \quad , \tag{20}$$

where $\bar{\phi}^{P}$ is given by equation (12). To facilitate the solution for ψ, the geometry of figure 1 can be mapped conformally so that the insulator and electrode are coplanar. The coordinates of this new geometry are related to the original coordinates through

$$x = \bar{r}^{\pi/\beta} \quad \text{and} \quad \theta = \frac{\theta\pi}{\beta} \quad . \tag{21}$$

In terms of these new variables, the problem can be stated as

$$\frac{1}{x}\frac{\partial}{\partial x}\left(x\,\frac{\partial\psi}{\partial x}\right) + \frac{1}{x^2}\left(\frac{\partial^2\psi}{\partial\theta^2}\right) = 0 \quad , \tag{22}$$

with the boundary conditions:

$$\frac{\partial\psi}{\partial\theta} = 0 \quad \text{at} \quad \theta = \pi \tag{23}$$

and

$$\frac{1}{x}\frac{\partial\psi}{\partial\theta} = \frac{\beta}{\pi}\left(f(\psi_o)\,x^{(\beta/\pi-1)} + x^{-1/2}\right) \quad \text{at} \quad \theta = 0 \quad . \tag{24}$$

For linear kinetics, $f(\psi_o) = \psi_o$, and for Tafel kinetics, $f(\psi_o) = -\exp(-\psi_o)$.

The boundary integral equation describing the potential of the solution adjacent to the electrode is

$$\psi_o(x_q) = \frac{\beta}{2\pi^2} \int_0^\infty \ln(x-x_q)^2 \left[f(\psi_o)\, x^{(\beta/\pi-1)} + x^{-1/2} \right] dx. \qquad (25)$$

For linear kinetics and $\beta \leq \pi/2$, the integrand does not approach zero quickly enough for the integral to converge. The appendix demonstrates the modification to the solution procedure necessary to obtain convergence.

A finite-difference approximation to equation (25) was solved with an iterative procedure. An upper limit of integration, x_{max}, was chosen to set a finite domain of integration. The contribution of the integral for $x > x_{max}$ was assumed to be negligible, which is consistent with requiring that the primary current distribution be approached at x_{max}.

The accuracy of this procedure was verified by increasing x_{max} until the value of the current at the corner changed by some small amount. A procedure of node-point doubling was also used. The results for the case of $\beta = \pi$ were compared with the results from references (2) and (3). Finally, an integral constraint can be used to check the accuracy of the answer. This arises from the asymptotic behavior expressed in equations (12) and (18) and takes the form, for linear kinetics (obtuse angles),

$$0 = \int_0^\infty \left[\psi_o x^{(\beta/\pi-1)} + x^{-1/2} \right] dx \ , \qquad (26)$$

and, for Tafel kinetics,

$$\pi \left(1 - \frac{\pi}{2\beta}\right) = \int_0^\infty \left[x^{-1/2} - \exp(-\psi_o)x^{(\beta/\pi-1)}\right]dx. \qquad (27)$$

The reported values are estimated to be accurate within 0.5 percent.

Results and Discussion

Results for linear kinetics are shown in figures 2 and 3. These figures, along with equation (13), give a good estimate of the current density in the corner region only for large values of $(\alpha_a+\alpha_c)Fi_o/RT\kappa$. Figure 4 shows results for Tafel kinetics. It can be used with equation (19) to predict current distributions near corner regions for high values of $\alpha_a FP_o/RT\kappa$.

Our experience has shown (and this analysis suggests) that numerical difficulties can arise when ohmic resistances begin to dominate. In other words, the results of this chapter become applicable when other numerical analyses begin to become suspect. A practical use, then, of these results could be as a tool for the verification of other results. One test which could be made for linear kinetics is to determine whether

$$\frac{i_{edge}}{P_o} = A_L(\beta)\left[\frac{(\alpha_a+\alpha_c)Fi_o}{RT\kappa}\right]^{(1-\pi/2\beta)} \qquad (28)$$

as the right side of the equation goes to infinity. The test for Tafel kinetics is whether

$$\frac{i_{edge}}{P_o} = A_T(\beta)\left[\frac{\alpha_a FP_o}{RT\kappa}\right]^{(2\beta/\pi-1)} \qquad (29)$$

as the right side of the equation goes to infinity. Smyrl and Newman [3] have demonstrated such tests for the case of $\beta = \pi$. The

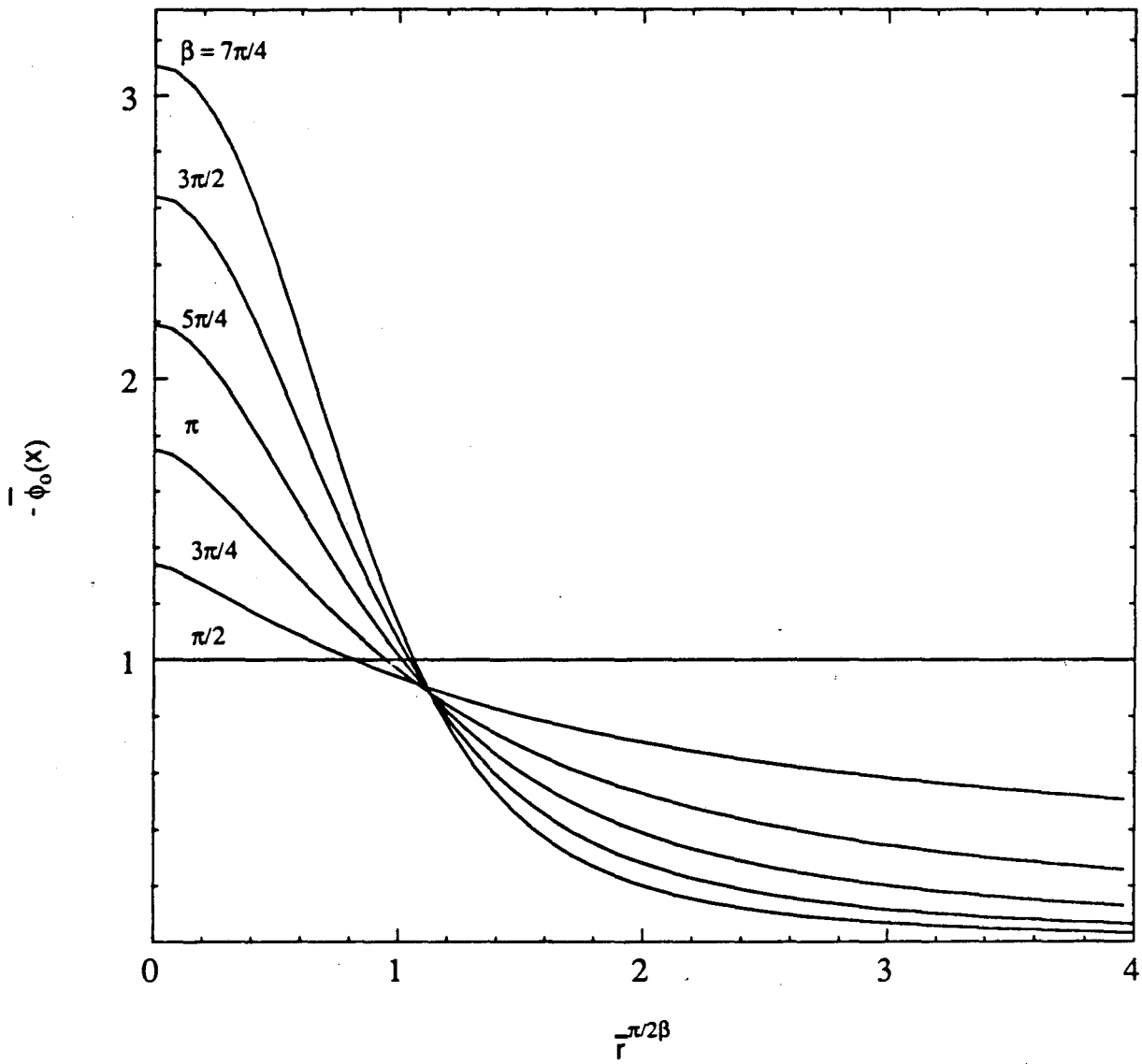

Figure 2. Current distribution for linear kinetics (obtuse angles).

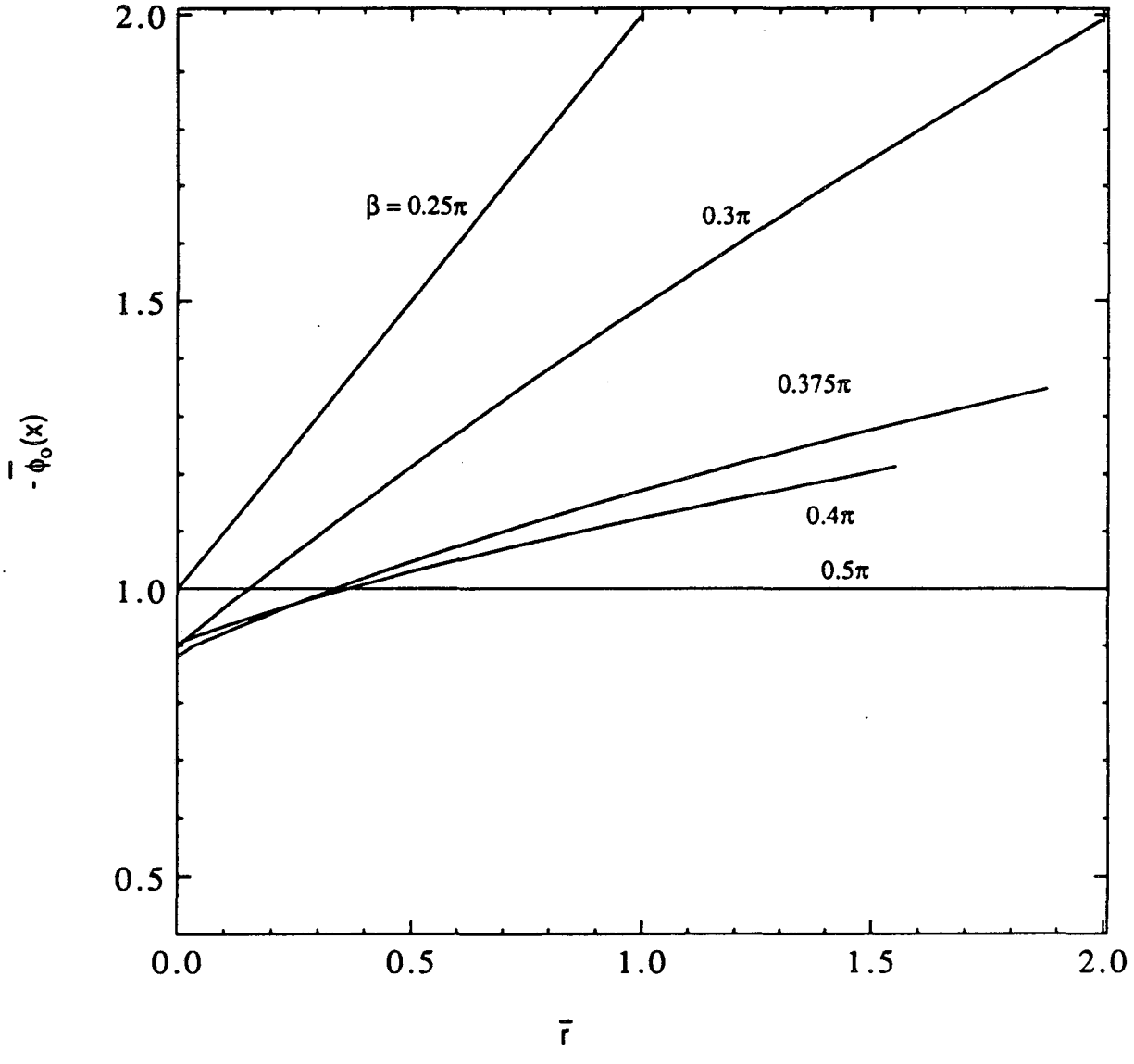

Figure 3. Current distribution for linear kinetics (acute angles).

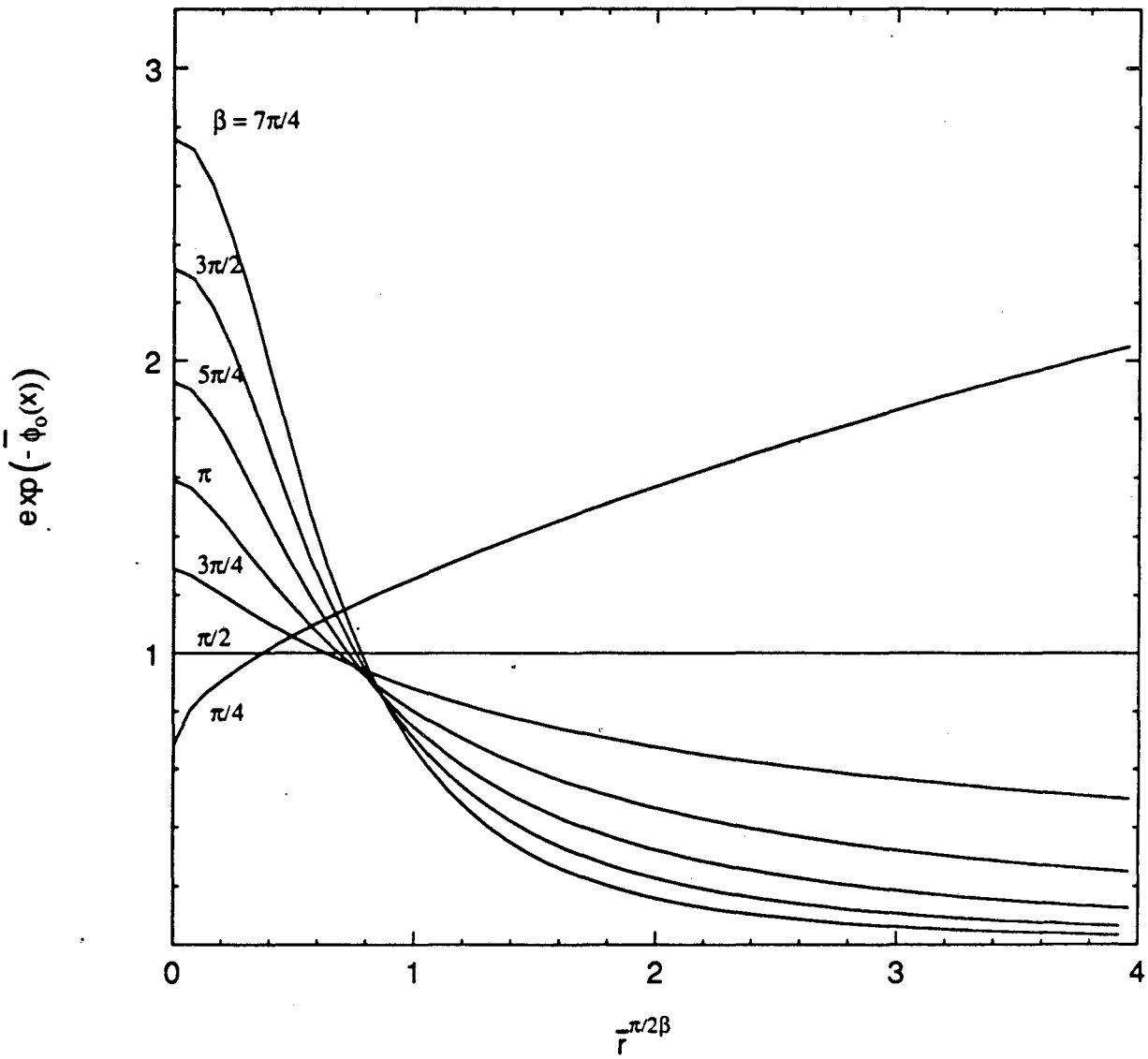

Figure 4. Current distribution for Tafel kinetics.

coefficients, $A_L(\beta)$ and $A_T(\beta)$, are shown in figure 5. The appendix shows that the value of A_L is 6.0 for an angle of $\beta = \pi/8$.

By solving the *primary* current distribution for an actual cell, it is possible to relate P_o to measureable electrochemical and geometric variables. It might, though, not be desired to take the time to determine the exact relation between P_o and these other variables. As a quick check, one might recall that P_o is proportional to i_{avg} and determine whether the proper relationship, suggested by equation (28) or (29), is followed.

The analysis can also be used to establish the proper mesh-spacing for an accurate and efficient finite-difference procedure. For linear kinetics, the region where the primary distribution does *not* apply is of the order $\left[\frac{(\alpha_a+\alpha_c)Fi_o}{RT\kappa}\right]^{-1}$. For Tafel kinetics, the region where the kinetic resistance is important is of the order $\left[\frac{\alpha_a FP_o}{RT\kappa}\right]^{-2\beta/\pi}$.

Conclusions

A singular-perturbation analysis has shown explicitly the manner in which the current density near an electrode edge approaches extreme values as the primary current distribution is approached. The results are consistent with previous analyses of a coplanar electrode and insulator and also with the special case of $\beta = \pi/2$.

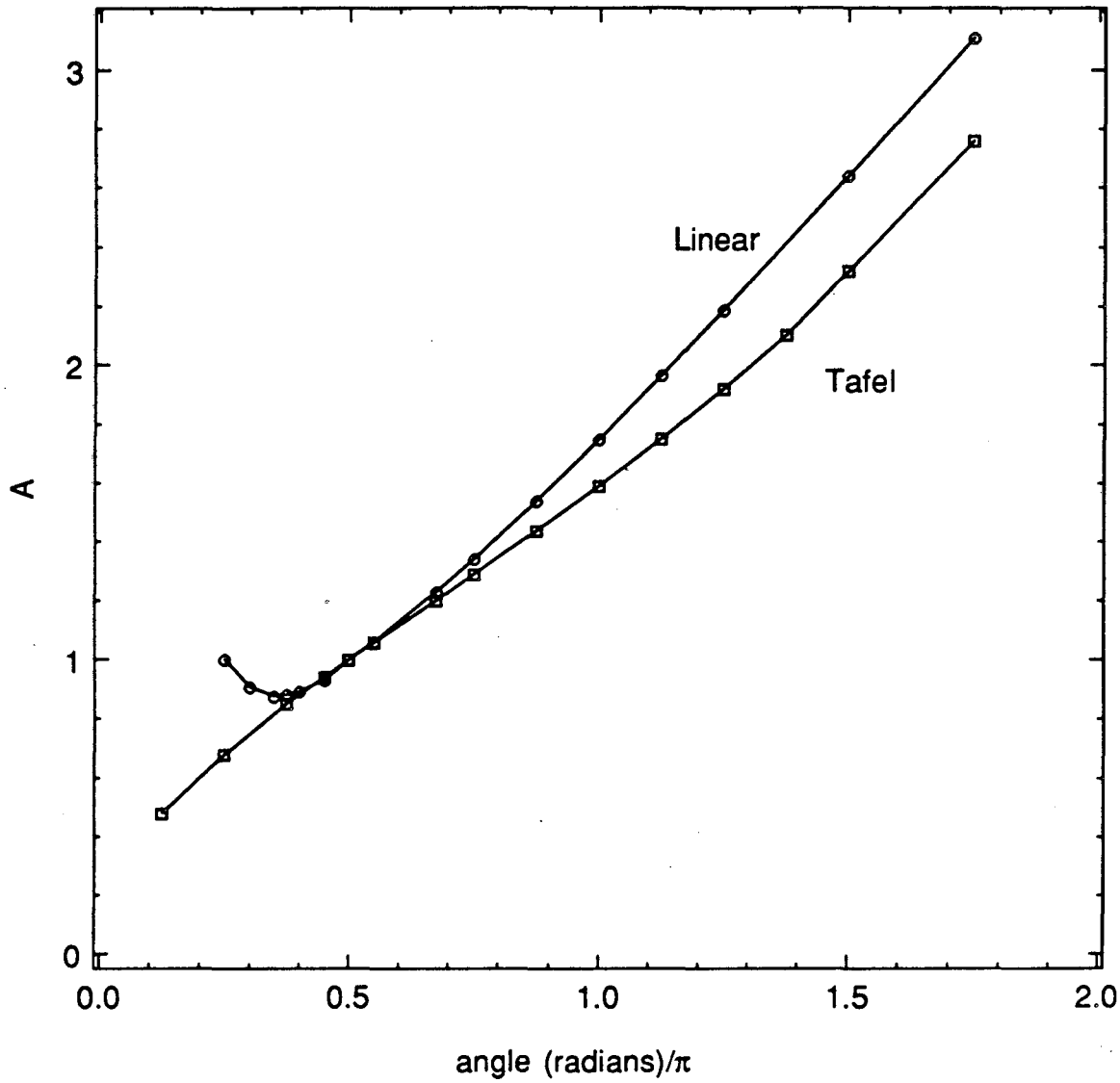

Figure 5. Dimensionless coefficient which specifies the value of the stretched current density at the edge. See equations (28) and (29).

Appendix

For linear kinetics, the solution to equations (9) through (12) might be approximated by

$$\bar{\phi} = \sum_{i=0} A_i \bar{r}^{n_i} \cos\left[n_i(\beta - \theta)\right], \tag{A.1}$$

where n_i and A_i are determined through the boundary conditions and the matching condition. This series diverges except for certain angles, β, where it terminates. Three angles which terminate are $\beta = \pi/2$, $\beta = \pi/4$, and $\beta = \pi/8$. For these angles, the potential of the solution adjacent to the electrode edge is given by

$$\bar{\phi}_o = -1 \quad (\beta = \pi/2), \tag{A.2}$$

$$\bar{\phi}_o = -1 - \bar{r} \quad (\beta = \pi/4), \tag{A.3}$$

and

$$\bar{\phi}_o = -6 - 14.4852\bar{r} - 7.2464\bar{r}^{\,2} - \bar{r}^{\,3} \quad (\beta = \pi/8). \tag{A.4}$$

As $\bar{r} \longrightarrow \infty$, the difference between the actual stretched current and the stretched primary current (in terms of x) is of the order given by

$$\psi_o x^{(\beta/\pi - 1)} + x^{-1/2} \propto x^{-(1/2+\beta/\pi)}. \tag{A.5}$$

For angles β less than $\pi/2$, the integral equation (25) is unbounded since the first neglected term is of order greater than x^{-1}.

Stated another way, for linear kinetics and acute angles, the first neglected term in the matching condition is sufficiently large

along the electrode surface that the integral does not converge. For $\pi/4 < \beta \leq \pi/2$, equations (30) and (34) suggest that an equation which calculates the deviations of the current density from the first *two* terms of the series will converge. A potential defined in this manner is

$$\psi' = \bar{\phi} + \frac{2\beta}{\pi}\bar{r}^{\pi/2\beta}\cos\left[\frac{\pi}{2\beta}(\beta - \theta)\right] \qquad (A.6)$$

$$- A_1\bar{r}^{(\pi/2\beta-1)}\cos\left[(\frac{\pi}{2\beta} - 1)(\beta - \theta)\right].$$

A_1 is determined by applying the matching and boundary conditions:

$$A_1 = \frac{-1}{\sin(\beta)}. \qquad (A.7)$$

The integral equation which gives ψ' is

$$\psi_o' = \frac{\beta}{2\pi^2}\int_0^\infty \ln(x-x_q)^2\left[\psi_o' x^{(\beta/\pi-1)} - A' x^{(-1/2-\beta/\pi)}\right]dx, \qquad (A.8)$$

where

$$A' = \left[\frac{\pi}{2\beta} - 1\right]\frac{-1}{\tan(\beta)}. \qquad (A.9)$$

The matching condition used numerically for ψ_o' is given by the next term of the series:

$$\psi_o' \longrightarrow A_2\bar{r}^{(\pi/2\beta-2)}\cos\left[\frac{\pi}{2} - 2\beta\right] \text{ as } \bar{r} \longrightarrow \infty. \qquad (A.10)$$

For example, for $\beta = 3\pi/8$, the potential at the electrode surface is

$$\bar{\phi}_o = -\bar{r}^{1/3} - 0.13807\bar{r}^{-2/3} + \ldots . \qquad (A.11)$$

For $\beta \leq \pi/4$, additional terms need to be subtracted from ψ'. The

number of additional terms is given by equation (30), the solution for $\bar{\phi}$ as $\bar{r} \longrightarrow \infty$.

To obtain results for $\beta \leq \pi/2$, this appendix is necessary. It can also be used with obtuse angles because it shows how asymptotic corrections can be used to relax the assumption that the integrand in equation (25) is zero for $x > x_{max}$. This reduces the value of x_{max} needed to obtain accurate results.

Appendix B of Smyrl and Newman [3] can be used to show that, for Tafel kinetics, the difference between the current density and the primary current density is sufficiently small that the integral equation (25) converges for acute, as well as obtuse, angles.

List of Symbols

A_L, A_T	dimensionless coefficients given in figure 5
F	Faraday's constant, 96487 C/equiv
i	current density, A/cm^2
i_{avg}	average current density, A/cm^2
i_{edge}	current density at the electrode/insulator edge, A/cm^2
i_o	exchange current density, A/cm^2
P_o	parameter defined in equation (5), A/cm$^{(1+\pi/2\beta)}$
R	universal gas constant, 8.3143 J/mol-K
r	radial distance variable, cm
$\bar{r}$	stretched, dimensionless radial distance variable, defined by equation (7) or (16)

S_L	stretching variable for linear kinetics, cm^{-1}
S_T	stretching variable for Tafel kinetics, cm^{-1}
T	absolute temperature, K
x, x_q	dimensionless position in transformed coordinate system
V	electrode potential, V
α_a, α_c	transfer coefficients
β	angle defined in figure 1, radians
θ	angular coordinate in cylindrical coordinates
Θ	angular coordinate of transformed geometry
π	3.141592654
κ	specific conductivity, $ohm^{-1}cm^{-1}$
Φ	potential, V
Φ^p	primary potential, V
$\bar{\phi}$	stretched, dimensionless potential
ψ	dimensionless potential defined by equation (20)
ψ'	dimensionless potential defined by equation (35)

References

[1] John S. Newman, *Electrochemical Systems*, p. 343, Prentice-Hall, Englewood Cliffs, N. J. (1973).

[2] Kemal Nişancioğlu and John Newman, "The Short-Time Response of a Disk Electrode," *J. Electrochem. Soc.*, **121**, 523 (1974).

[3] William H. Smyrl and John Newman, "Current Distribution at Electrode Edges at High Current Densities," *J. Electrochem. Soc.*,

136, 132 (1989).

[4] John S. Newman, *Electrochemical Systems*, p. 346, Prentice-Hall, Englewood Cliffs, N. J. (1973).

CHAPTER 4
A Criterion to Verify Current Distribution Calculations

This chapter provides a practical demonstration and partial verification of the abstract results of chapter 3. Specifically, it shows how the results provide a criterion by which the validity of current distribution calculations can be tested. The geometry used to demonstrate the procedure is a slotted-electrode cell for which the primary current distribution was given by Orazem and Newman [1]. Previously, Smyrl and Newman [2] applied similar results to the rotating disk and flow channel cells.

A summary of the results of chapter 3 is given below. To generalize the treatment, a parameter P_o is used. It sets the magnitude of the current density for small distances from the edge:

$$i^P = P_o \, r^{(\pi/2\beta - 1)} \quad . \tag{1}$$

The angle β and the radial coordinate r are shown in figure 1 of chapter 3. P_o is determined by the cell potential and the details of the entire geometry. It is obtained by comparing the primary current distribution of the cell with equation (1), the asymptotic form valid near the edge.

For large polarization parameters, chapter 3 shows:

1. that the current density deviates appreciably from the primary current density where

$$r \approx \left[\frac{(\alpha_a+\alpha_c)Fi_o}{RT\kappa}\right]^{-1} \tag{2}$$

for linear kinetics, and

$$r \approx \left[\frac{\alpha_a FP_o}{RT\kappa}\right]^{-2\beta/\pi} \tag{3}$$

for Tafel kinetics.

2. that the current density near an electrode edge behaves as

$$\frac{i_{edge}}{i_{avg}} \propto \left[\frac{(\alpha_a+\alpha_c)Fi_o}{RT\kappa}\right]^{(1 - \pi/2\beta)} \tag{4}$$

for linear kinetics, and

$$\frac{i_{edge}}{i_{avg}} \propto \left[\frac{\alpha_a FP_o}{RT\kappa}\right]^{(2\beta/\pi - 1)} \tag{5}$$

for Tafel kinetics.

3. detailed distributions in the edge region for various angles, β.

Numerical Analysis

The primary current distribution of the slotted-electrode cell shown in figure 1 was determined by a technique that utilizes two numerical, Schwarz-Christoffel transformations. Conformal mapping techniques such as this one are often used for the determination of primary current distributions. When coupled with other numerical procedures, problems with more complicated boundary conditions can be analyzed.

Orazem and Newman [2] gave the transformation relating the coordinates of figure 1a and figure 1c. Since this is a conformal

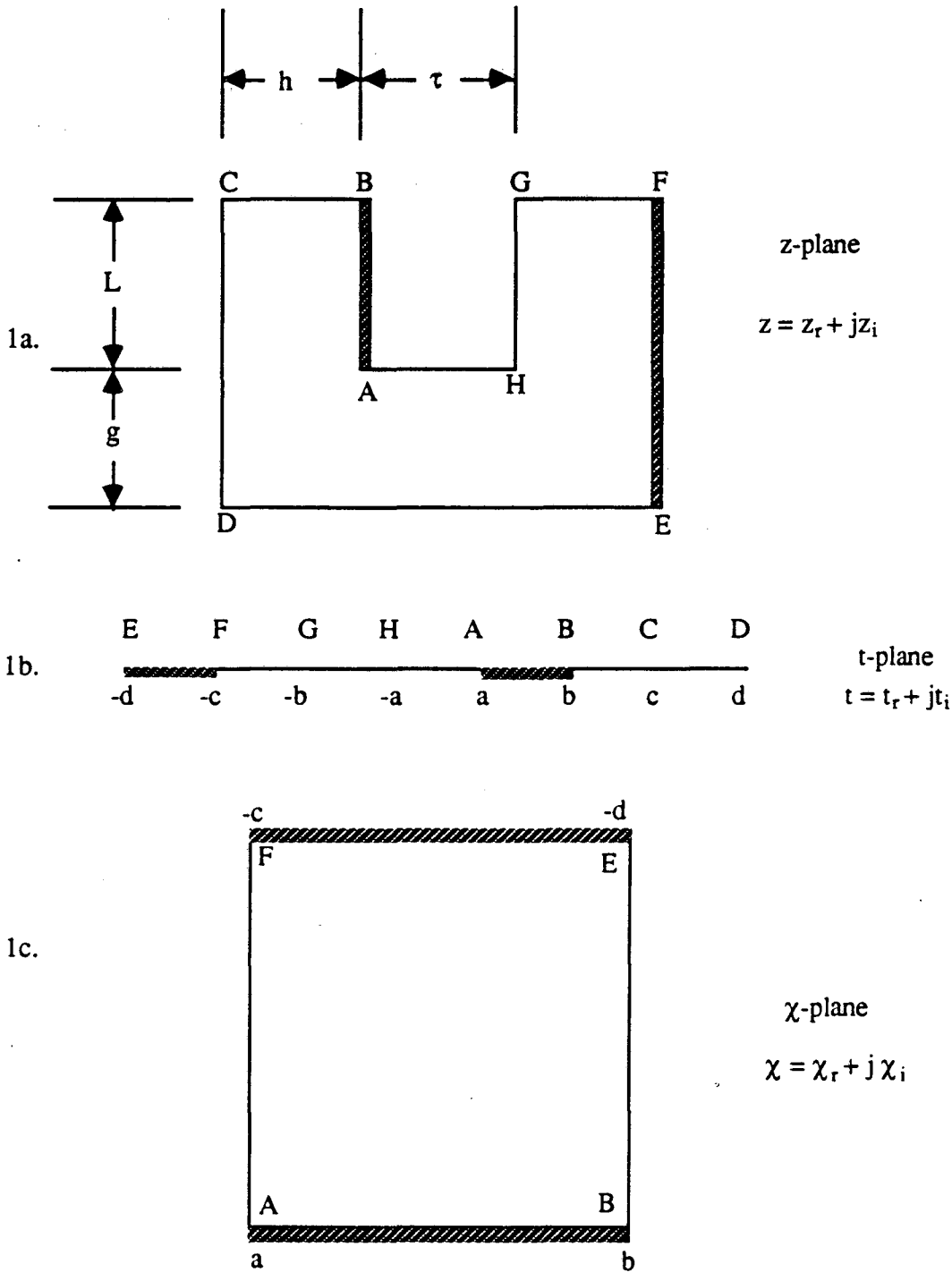

Figure 1. Schematic diagram of the slotted-electrode cell. Figure 1a shows the cell in the original coordinate system. To facilitate solution of Laplace's equation it is mapped conformally to the coordinate system of figure 1c, with the coordinate system shown in figure 1b as an intermediate coordinate system. See reference [1] for details.

mapping, Laplace's equation maintains the same form. Insulator boundary conditions also remain the same. Along the counterelectrode, the kinetics are assumed to be infinitely fast, and the constant potential boundary condition is unchanged. At the working electrode, the boundary condition becomes

$$\frac{\partial \Phi}{\partial \chi_i} = f(\Phi_o)\gamma(\chi), \tag{6}$$

where

$$f(\Phi_o) = -\frac{(\alpha_a+\alpha_c)Fi_o}{RT\kappa}(V - \Phi_o) \tag{7}$$

for linear kinetics, and

$$f(\Phi_o) = -\frac{i_o}{\kappa}\exp\left[\frac{\alpha_a F}{RT}(V - \Phi_o)\right] \tag{8}$$

for anodic, Tafel kinetics.

$\gamma(\chi)$ relates the normal derivatives along the working electrode in the two coordinate systems and is given by

$$\gamma(\chi_r) = \frac{\sqrt{t-a}\,\sqrt{t-a}\,\sqrt{t+a}}{\sqrt{t+b}\,\sqrt{c-t}\,\sqrt{d-t}} \tag{9}$$

where t is related to χ through

$$\chi = \int_a^t \frac{j\,dt}{\sqrt{t-a}\,\sqrt{t-b}\,\sqrt{t+d}\,\sqrt{t+c}}, \tag{10}$$

and the original coordinate z is related to t through

$$z = \int_0^t \frac{\sqrt{t-a}\,\sqrt{t+a}\,dt}{\sqrt{t-b}\,\sqrt{t+b}\,\sqrt{t-c}\,\sqrt{t+c}\,\sqrt{t-d}\,\sqrt{t+d}}. \tag{11}$$

This problem was solved with a boundary-integral technique.

In this chapter, the geometric ratios used are $L/h = 0.5$, $r/g = 0.1$, and $h/G = 6.0$, where L, h, r, and g are shown in figure 1. The polarization parameter for linear kinetics is

$$J = \frac{(\alpha_a+\alpha_c)FLi_o}{RT\kappa} \tag{12}$$

and for Tafel kinetics is

$$\delta = \frac{\alpha_a FL|i_{avg}|}{RT\kappa}. \tag{13}$$

The length L used in defining J and δ is chosen arbitrarily.

Applicability of the Perturbation Analysis

Singular perturbation analyses can be quite involved. Nevertheless, their results can be simple to use. In this chapter, a tool that checks the validity of numerical calculations is established. To use it effectively, one must be aware of the limited range of applicability of the perturbation analysis. Also, a physically significant length should be used in the definitions of the polarization parameters. Otherwise, the coefficients in the series may be very different from unity.

The first neglected term in a perturbation series determines the range of applicability. Because the term arises from the details of the entire cell (and not one specific detail like β), a general conclusion is difficult to make. To estimate its magnitude, it is useful to study in detail one particular geometry: the disk electrode. For this cell, the characteristic length L in equations (12) and (13) should be replaced with r_o, the disk radius.

Linear Kinetics—For large J, the current density at the electrode edge is given by [3]

$$\frac{i_{edge}}{i_{avg}} = 0.62\ \sqrt{J} + \epsilon^{(2)}\ \frac{\ln J}{\sqrt{J}}, \tag{14}$$

where $\epsilon^{(2)}$ is determined by solving for the second order correction to the primary potential distribution.

The condition for when the first term adequately predicts the current density is

$$\sqrt{J} \gg \frac{\epsilon^{(2)}}{0.62}\ \frac{\ln J}{\sqrt{J}}. \tag{15}$$

Although a determination of $\epsilon^{(2)}$ may not be worth the effort, its value should be near unity, and one can make a reasonable estimate of the range of applicability.

Figure 2 compares calculated values of the current density at the edge of the electrode with the first term of the asymptotic prediction. The predicted behavior is approached by values of J consistent with the above inequality. Equation (14) also suggests an alternate, more sensitive way of plotting results. For example, a plot of $\frac{i_{edge}}{\sqrt{J} i_{avg}}$ *vs.* $\frac{\ln J}{J}$ could be used. For such plots, the ordinate intercept is predicted.

To comment generally about the magnitude of the next term, the relation of Nişancioğlu and Newman [4] is useful:

$$\int_0^1 (1 - \Phi_o/V) r dr = O(\tfrac{\ln J}{J}) \text{ (for high } J). \tag{16}$$

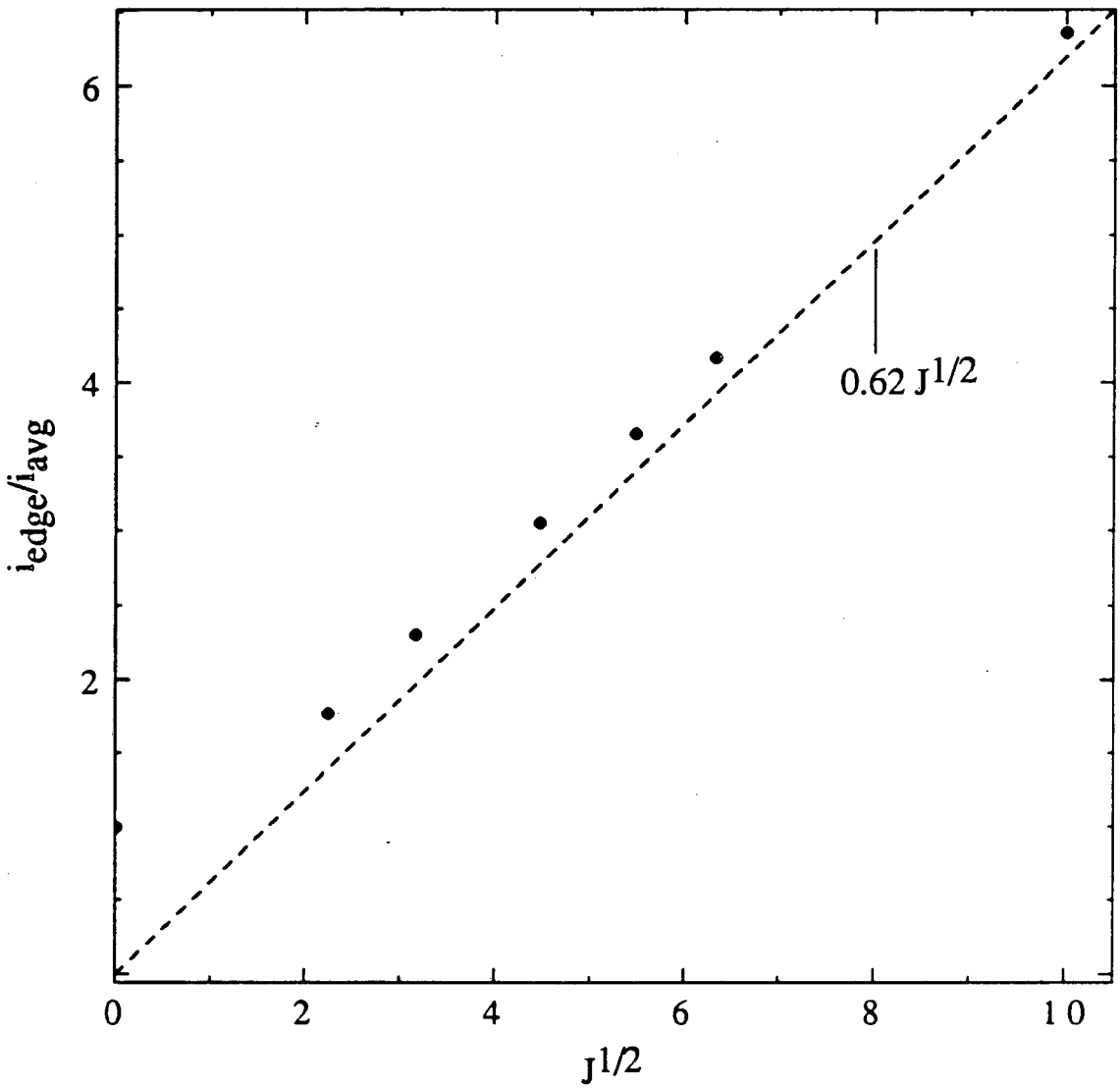

Figure 2. The current density at the edge of a disk electrode for linear kinetics. The points are calculated values, and the dashed line is the asymptotic prediction.

An analogous term should give the order of the next term for other geometries, and it is expected to be of the same magnitude. If so, for large J and $\beta > \pi/2$,

$$\frac{i_{edge}}{i_{avg}} = \epsilon^{(1)} J^{(1-\pi/2\beta)} + \epsilon^{(2)} \frac{\ln J}{J^{\pi/2\beta}} . \tag{17}$$

This implies that the analysis of chapter 3 applies when

$$J \gg \frac{\epsilon^{(2)}}{\epsilon^{(1)}} \ln J. \tag{18}$$

Tafel Kinetics—For Tafel kinetics on a disk electrode, Appendix A shows that the order of the next term in the perturbation expansion is unity with respect to δ, thus implying that

$$\frac{i_{edge}}{i_{avg}} = 0.196\ \delta + \epsilon^{(2)}. \tag{19}$$

Figure 3 compares the first term with calculated results. In harmony with equation (19), the calculated values lie on a line parallel to the asymptotic prediction. The figure shows that the last data point (near $\delta = 90$) is inaccurate. For larger δ (not shown), errors are more noticeable. A more sensitive test of numerical calculations would be to plot $\frac{i_{edge}}{\delta i_{avg}}$ *vs.* $1/\delta$, with a predicted ordinate intercept of 0.196.

Appendix A suggests that the next term of a perturbation series will be of order unity for other cell geometries. Previous calculations [4] verify this for the channel geometry (again, $\beta = \pi$). In general, for $\beta > \pi/2$, the expected relationship is

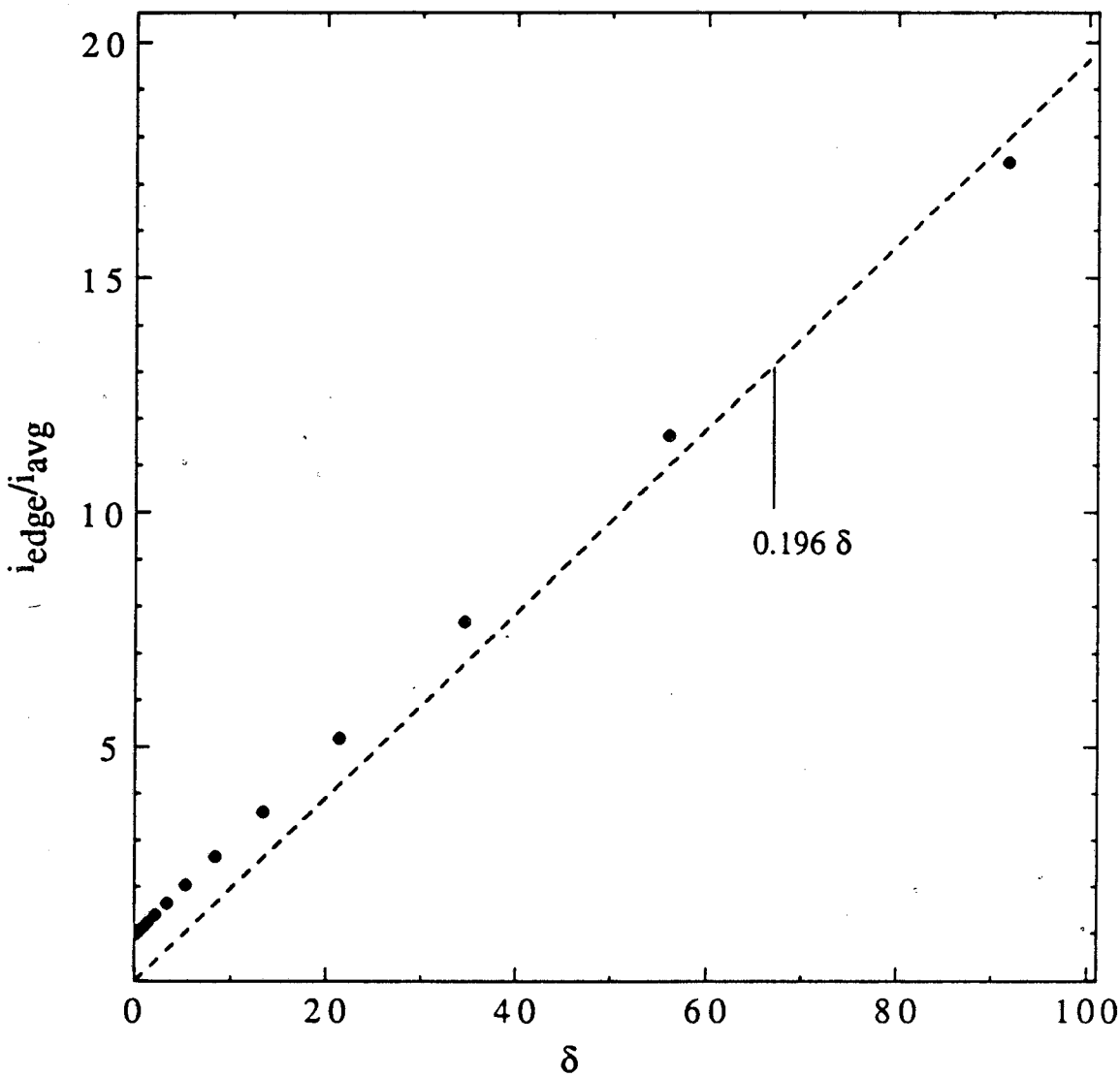

Figure 3. The current density at the edge of a disk electrode for Tafel kinetics. The points are calculated values, and the dashed line is the asymptotic prediction.

$$\frac{i_{edge}}{i_{avg}} = \epsilon^{(1)}\ \delta^{(2\beta/\pi-1)} + \epsilon^{(2)} \quad . \tag{20}$$

The third term in this series will be of order less than unity. For $\delta^{(2\beta/\pi-1)} > 10$ we can expect the numerical calculations to attain the correct slope but to be offset from a line through the origin by an amount $\epsilon^{(2)}$.

Results and Discussion

For the slotted-electrode cell, the primary current distribution near the electrode edge is

$$i_{as} = P_o r^{-2/3}, \tag{21}$$

where r is the distance along the electrode measured from point A. P_o is determined by comparing this asymptotic form with the current distribution as calculated by the method of Orazem and Newman (see figure 4):

$$P_o = 0.569\ L^{2/3} i_{avg} \quad . \tag{22}$$

For linear kinetics in the slotted-electrode cell, equation (28) of chapter 3 gives

$$\frac{i_{edge}}{i_{avg}} = 1.5\ J^{2/3} \quad . \tag{23}$$

as $J \longrightarrow \infty$. In figure 5 this relationship is compared to calculated values of i_{edge}/i_{avg}. Good agreement exists for $J^{2/3} \geq 4$.

For Tafel kinetics, equation (29) of chapter 3 gives

$$\frac{i_{edge}}{i_{avg}} = 0.426\ \delta^2 \tag{24}$$

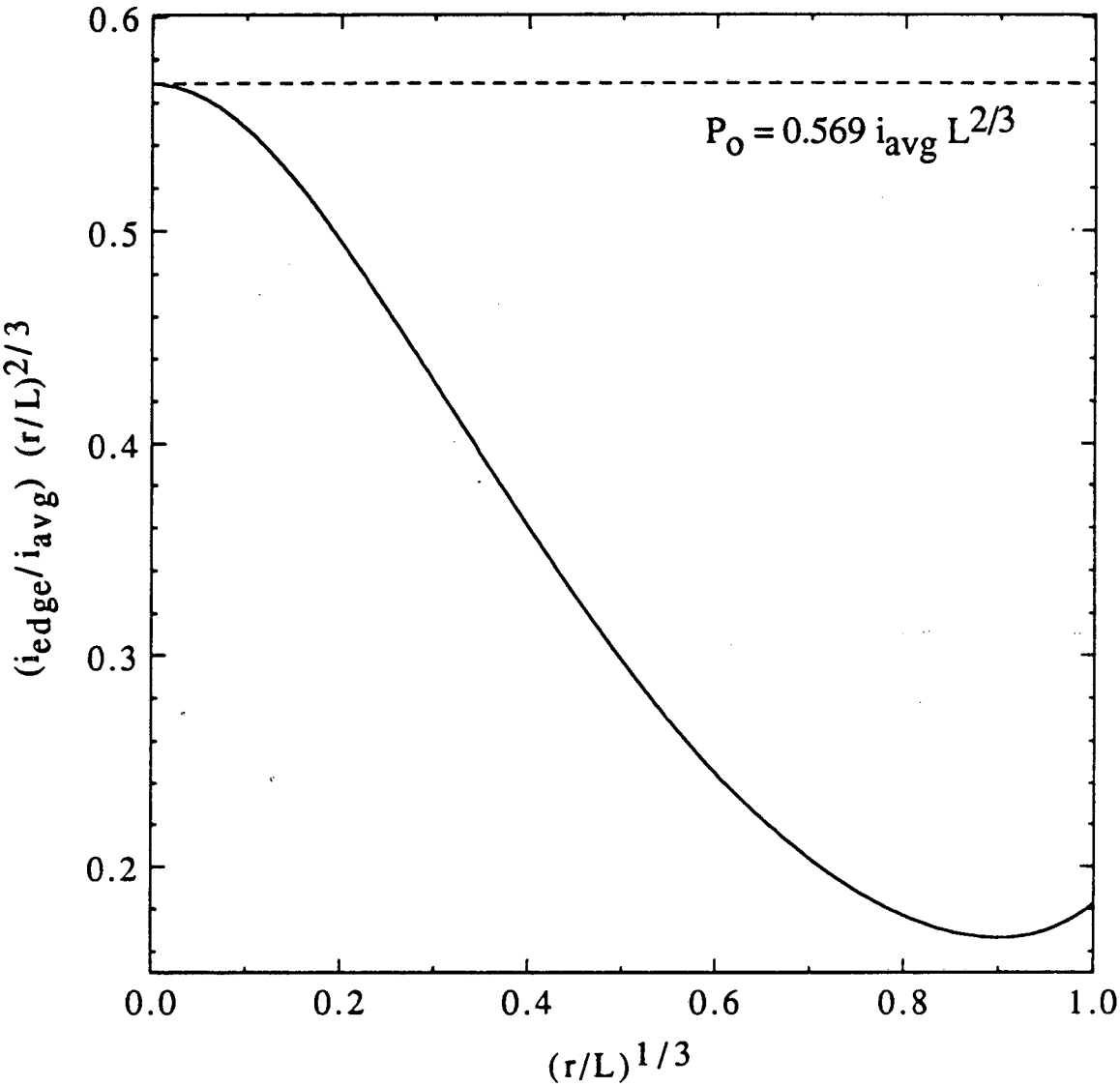

Figure 4. The primary current distribution of a slotted-electrode cell. The dashed line is the asymptotic approximation of the current distribution, given by equations (21) and (22).

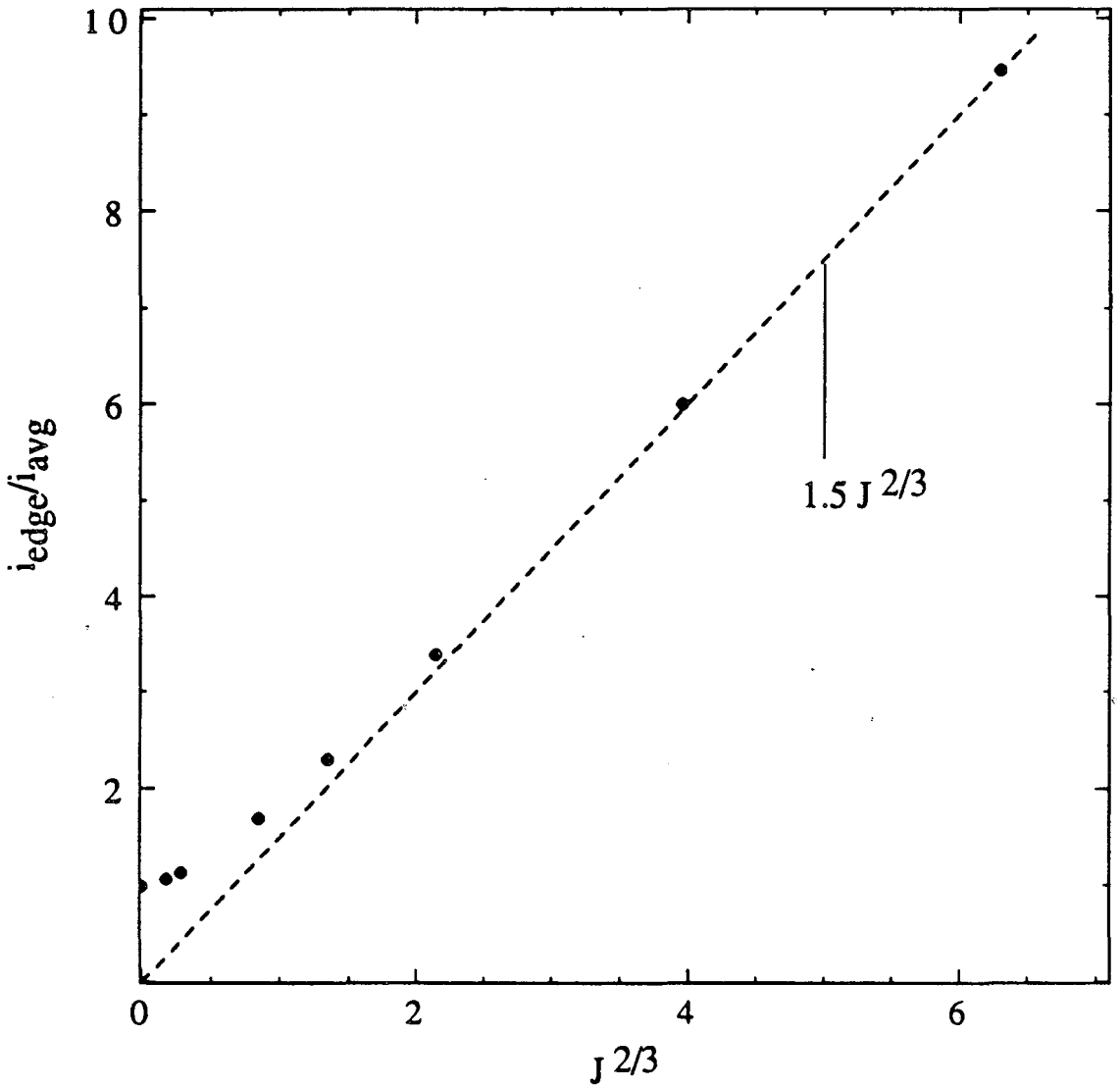

Figure 5. The current density at point *A* of the slotted-electrode cell (figure 1) as it varies with the polarization parameter for linear kinetics. The points are calculated values, and the dashed line is the asymptotic behavior predicted by equation (23).

as $\delta \rightarrow \infty$. Figure 6 compares this relationship with calculated results. An empirical curve, with the predicted slope of 0.426, is fit through the calculated results. Its intercept is determined from the slope of the curve shown in figure 7.

Figure 7 provides a sensitive test of numerical calculations. If the next term in the series is of order unity with respect to δ, the curve should be linear at high δ and have the ordinate intercept predicted by equation (24). This figure shows that the numerical calculations begin to fail near $\delta^2 = 30$. For larger δ (not shown), the numerical calculations are clearly in error. The deviation from the semi-empirical curve of figure 6 also suggests that the calculations begin to fail near $\delta^2 = 30$. Our experience suggests that it becomes difficult to obtain highly accurate solutions with traditional numerical procedures when i_{edge}/i_{avg} is much greater than 10.

Figures such as 5, 6, and 7 are recommended as checks on numerical results, where, for large polarization parameters, numerical difficulties arise. To check data quickly, the proportionalities given by equations (3) and (5) can be tested. Deviations from a linear relationship indicate that results are inaccurate.

Few numerical difficulties are expected for small polarization parameters; therefore, a perturbation analysis describing the deviations from a uniform current distribution might not be as interesting. Nevertheless, Appendix B demonstrates by example how the deviations could be predicted. For other geometries, the same functional dependence on the polarization parameter is expected, but general

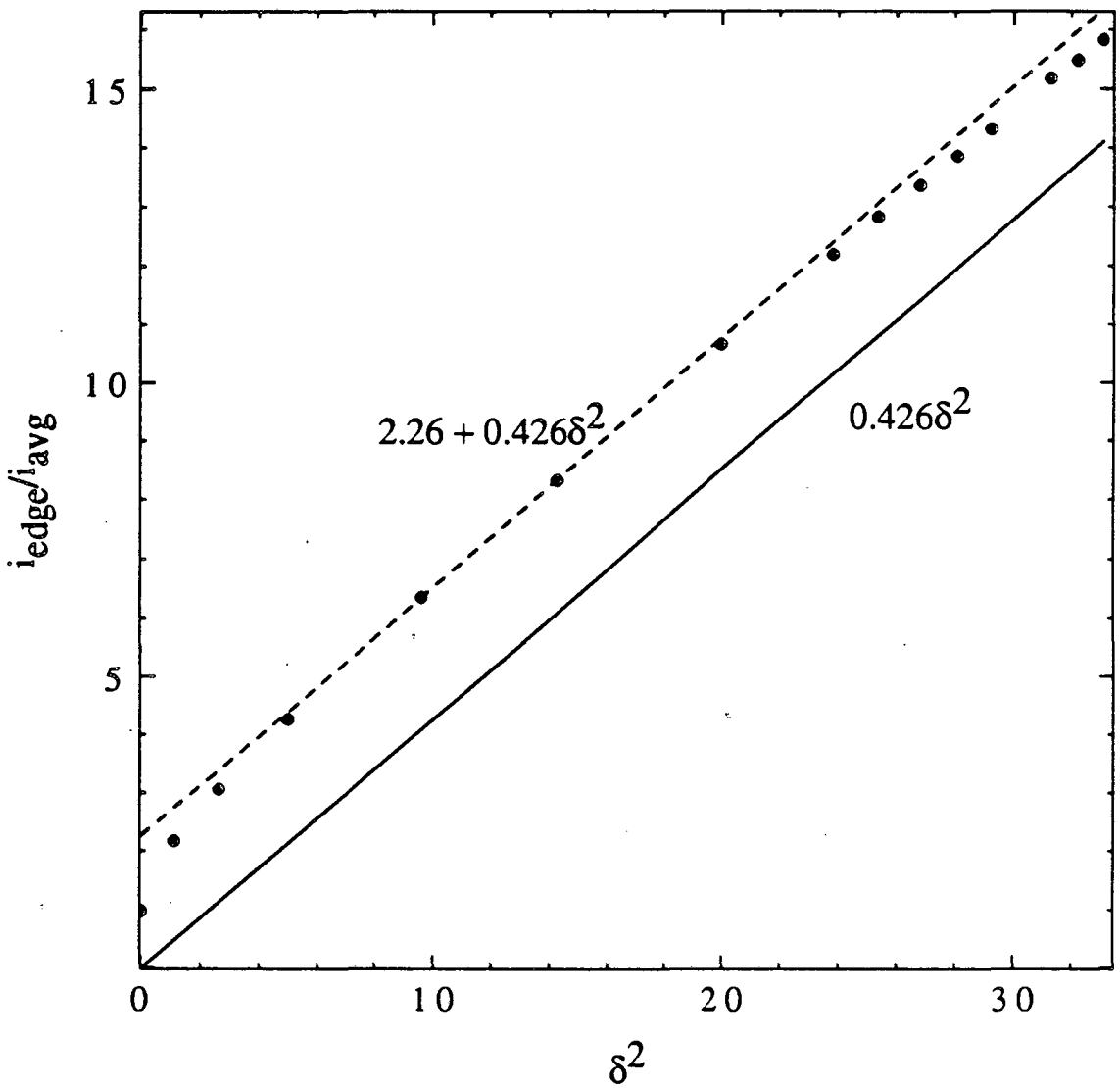

Figure 6. The current density at point *A* of the slotted-electrode cell (see figure1) as it varies with the polarization parameter for Tafel kinetics. The points are calculated values, the solid line is the asymptotic behavior predicted by equation (24), and the dashed line has the predicted slope but an empirical ordinate intercept.

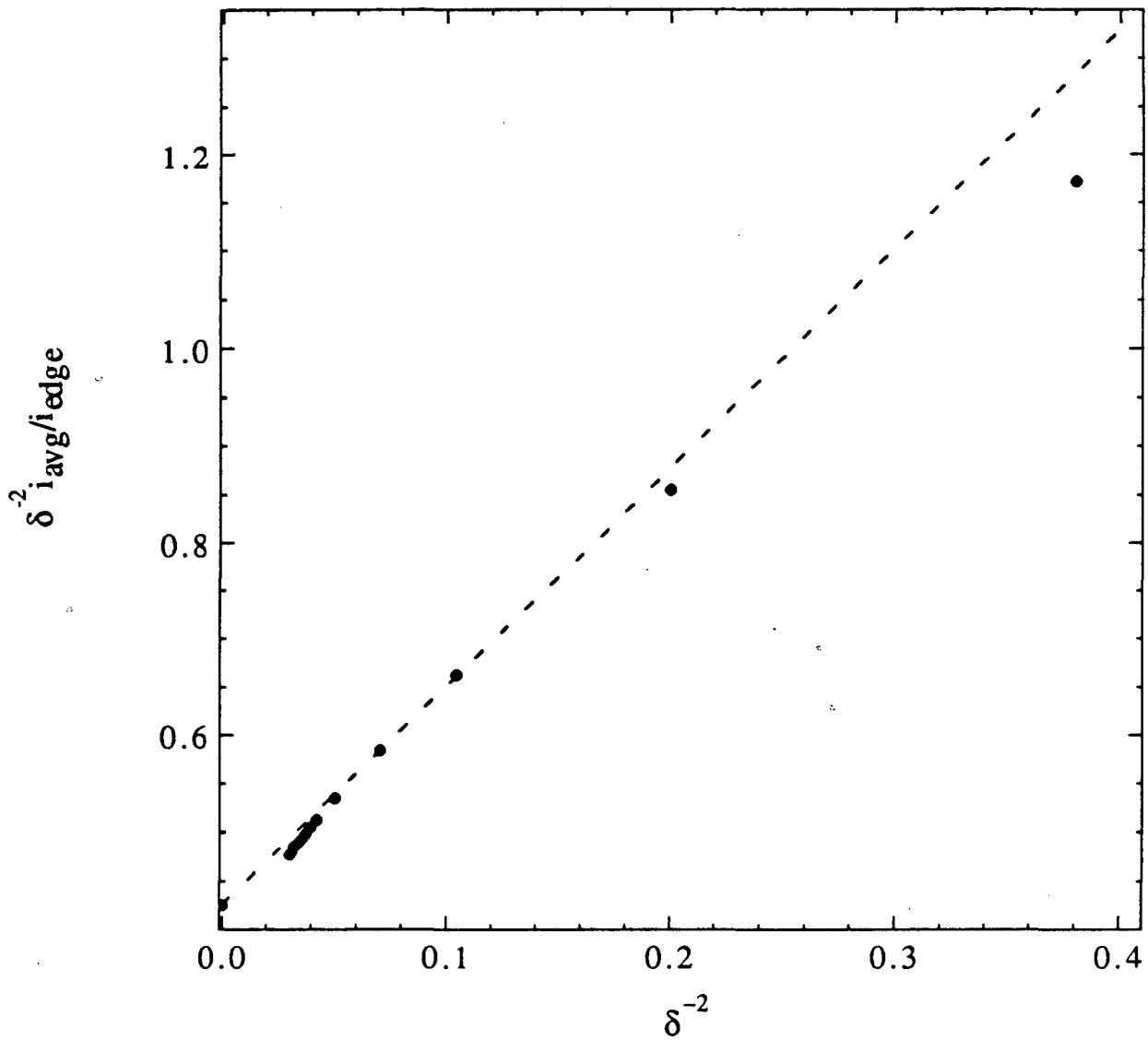

Figure 7. An alternate, more sensitive way of plotting calculated results for Tafel kinetics in the slotted-electrode cell. The ordinate intercept is predicted by the perturbation analysis, and the slope of the line gives an estimate of the next term in the series.

predictions of the coefficients in the series is not possible.

Conclusions

Applications of the results of chapter 3 are demonstrated. The results, valid for asymptotically large polarization parameters, provide a test of numerical results. The predictions do not hold for small polarization parameters, partly because $i_{edge}/i_{avg} = 1$ for a zero polarization parameter. For Tafel kinetics and obtuse angles of intersection between the electrode and insulator, the next term in a perturbation series is expected to be of order unity. Calculated values of i_{edge}/i_{avg} are expected, therefore, to fall on a line that is parallel to the predictions of chapter 3.

The importance of asymptotic analyses should not be underestimated. In addition to giving insight, they can provide checks on calculations. With the emergence of high-speed computers and sophisticated, packaged software, complicated numerical calculations are more prevalent, and simple tests of these results are necessary.

Appendix A
Tafel Kinetics on a Disk Electrode

The order of the next term in a perturbation series describing i_{edge}/i_{avg} for Tafel kinetics on a rotating disk electrode is shown to be unity. It is also suggested that a term of order unity can be expected for other geometries. $O(\epsilon)$ means of order ϵ, and $o(\epsilon)$ means of order lower than ϵ.

Following Smyrl and Newman [2], a potential ϕ is defined as

$$\phi = \frac{\pi}{4}\left[1 - \Phi/\Phi_o^p\right] , \tag{A.1}$$

where Φ_o^p is the primary potential difference, for the same total current, between the disk electrode and a reference electrode placed at infinity. The stretched variables for the outer region (away from the edge of the electrode) are $\bar{\phi} = \phi$, $\bar{\eta} = \eta$, and $\bar{\xi} = \xi$, where ξ and η are the rotational elliptic coordinates. In the inner region, the appropriately stretched variables are

$$\bar{\phi} = \delta\phi - \ln\delta , \tag{A.2}$$

$$\bar{\xi} = \delta\xi , \tag{A.3}$$

and

$$\bar{\eta} = \delta\eta . \tag{A.4}$$

The stretched potentials, $\bar{\phi}$ and $\bar{\phi}$, can be expanded in terms of δ:

$$\bar{\phi} = \bar{\phi}^{(0)} + \bar{f}_1(\delta)\bar{\phi}^{(1)} + \ldots , \tag{A.5}$$

$$\bar{\phi} = \bar{\phi}^{(1)} + \bar{f}_2(\delta)\bar{\phi}^{(2)} + \ldots . \tag{A.6}$$

Smyrl and Newman showed that $\bar{\phi}^{(0)} = \frac{1}{2}\tan^{-1}\xi$, and they determined numerically $\bar{\phi}^{(1)}$.

In the inner region, terms of order δ^{-2} are neglected in Laplace's equation. Terms can also arise from the matching and boundary conditions. The insulator boundary condition does not introduce additional terms. Along the disk electrode, the boundary condition is

$$\frac{E}{2}\, e^{\bar{\phi}_o} = \frac{1}{\bar{\eta}}\left(\frac{\partial\bar{\phi}}{\partial\bar{\xi}}\right)_{\bar{\xi}=0}, \tag{A.7}$$

where

$$E = \frac{2i_o}{i_{avg}} \exp\left[\frac{\alpha_a F}{RT}(V - \Phi_o^p)\right]. \tag{A.8}$$

It is shown [2] that

$$\ln E = 1 + \frac{1}{\delta}\ln E^{(1)} + \ldots, \tag{A.9}$$

where $\ln E^{(1)}$ is the second term in a perturbation expansion of $\ln E$.

The boundary condition, therefore, can be rewritten as

$$\frac{e}{2}\left[1 + \frac{1}{\delta}\ln E^{(1)} + o(1/\delta)\right]\exp\left[\bar{\phi}_o^{(1)} + \bar{f}_2(\delta)\bar{\phi}_o^{(2)} + o(\bar{f}_2(\delta))\right] \tag{A.10}$$

$$= \frac{1}{\bar{\eta}}\left\{\left.\frac{\partial\bar{\phi}^{(1)}}{\partial\bar{\xi}}\right|_{\bar{\xi}=0} + \bar{f}_2(\delta)\left.\frac{\partial\bar{\phi}^{(2)}}{\partial\bar{\xi}}\right|_{\bar{\xi}=0} + o(\bar{f}_2(\delta))\right\},$$

which is expanded further to yield

$$\frac{e}{2}\left[1 + \frac{1}{\delta}\ln E^{(1)} + o(1/\delta)\right]\left[1 + \bar{f}_2(\delta)\bar{\phi}_o^{(2)} + \ldots\right]e^{\bar{\phi}_o^{(1)}} \tag{A.11}$$

$$= \frac{1}{\bar{\eta}}\left\{\left.\frac{\partial\bar{\phi}^{(1)}}{\partial\bar{\xi}}\right|_{\bar{\xi}=0} + \bar{f}_2(\delta)\left.\frac{\partial\bar{\phi}^{(2)}}{\partial\bar{\xi}}\right|_{\bar{\xi}=0} + o(\bar{f}_2(\delta))\right\}.$$

Equating terms of the same order in δ suggests that $\bar{f}_2 = \frac{1}{\delta}$. To decide conclusively necessitates inspecting the matching conditions, where higher order terms due to the outer solution can arise.

In the outer region, the exact form of Laplace's equation (in rotational elliptic coordinates) was solved, and thus no terms arise from the governing equation. Also, no terms arise from the boundary condition at infinity, on the insulator, or on the axis. The boundary condition along the electrode in the outer region can be expressed by

$$\frac{1}{2} Ee^{\delta\bar{\phi}_o} = \frac{1}{\eta} \frac{\partial\bar{\phi}}{\partial\xi}\bigg|_{\xi=0} . \tag{A.12}$$

Since $\bar{\phi}_o^{(0)} = 0$, this boundary condition is rewritten as

$$\frac{e}{2} \left[1 + \frac{1}{\delta} \ln E^{(1)} + o(1/\delta)\right]\left[1 + \delta\bar{F}_2(\delta)\bar{\phi}_o^{(2)} + \ldots\right] e^{\delta\bar{F}_1(\delta)\bar{\phi}_o^{(1)}} \tag{A.13}$$

$$= \frac{1}{\eta}\left\{ \frac{\partial\bar{\phi}^{(0)}}{\partial\xi}\bigg|_{\xi=0} + \bar{F}_1(\delta) \frac{\partial\bar{\phi}^{(1)}}{\partial\xi}\bigg|_{\xi=0} + \ldots \right\} .$$

This suggests that $\bar{F}_1 = \frac{1}{\delta}$ and that

$$\bar{\phi}_o^{(1)} = -1 - \ln(\eta), \tag{A.14}$$

which is expected from a straightforward attempt to correct the potential (from the primary potential) for finite electrode kinetics. Smyrl and Newman [2], with a different approach, implied the same results.

$\bar{\phi}^{(1)}$ is described by Laplace's equation in rotational elliptic coordinates:

$$(1 - \eta^2) \frac{\partial^2\bar{\phi}^{(1)}}{\partial\eta^2} + (1 + \xi^2) \frac{\partial^2\bar{\phi}^{(1)}}{\partial\xi^2} + 2\xi \frac{\partial\bar{\phi}^{(1)}}{\partial\xi} - 2\eta \frac{\partial\bar{\phi}^{(1)}}{\partial\eta} = 0. \tag{A.15}$$

The insulator boundary condition at $\eta = 0$ is unchanged, the boundary condition at the disk electrode is given by equation (A.14) and

$\bar{\phi}^{(1)} \longrightarrow 0$ as $\xi^2+\eta^2 \longrightarrow \infty$. Furthermore, no current should flow to infinity since δ specifies the total current, and this is supplied by the primary current term, $\bar{\phi}^{(0)}$.

From separation of variables, the solution is

$$\bar{\phi}^{(1)}(\eta,\xi) = \sum_{n=1}^{\infty} B_n P_{2n}(\eta) M_{2n}(\xi), \tag{A.16}$$

where P_{2n} are the even Legendre polynomials, and M_{2n} are Legendre functions of imaginary argument [5]. The B_n are determined through the orthogonality condition (see, for example, reference [6]):

$$B_n = -(4n + 1) \int_0^1 P_{2n}(\eta) \ln(\eta) d\eta \ . \tag{A.17}$$

The asymptotic behavior (for small ξ,η) of $\bar{\phi}^{(1)}$ must be developed to provide the matching condition for the inner solution. If $r = (\xi^2+\eta^2)^{\frac{1}{2}}$ and $\theta = \tan^{-1}(\eta/\xi)$, Laplace's equation becomes

$$0 = \left[\frac{\partial^2\bar{\phi}^{(1)}}{\partial r^2} + \frac{1}{r}\frac{\partial\bar{\phi}^{(1)}}{\partial r} + \frac{1}{r^2}\frac{\partial^2\bar{\phi}^{(1)}}{\partial\theta^2}\right]\left[1 + \frac{r^2}{2}(1 - 2\sin^2\theta)\right] \tag{A.18}$$

$$+ \frac{r}{2\sin\theta\cos\theta}\left[\frac{1}{r}\frac{\partial\bar{\phi}^{(1)}}{\partial\theta} - \frac{\partial^2\bar{\phi}^{(1)}}{\partial r\partial\theta}\right]$$

$$+ 2r(1 - 2\sin^2\theta)\frac{\partial\bar{\phi}^{(1)}}{\partial r} - 4\sin\theta\cos\theta\frac{\partial\bar{\phi}^{(1)}}{\partial\theta} \ .$$

Using a coordinate expansion technique and separation of variables, and applying the appropriate boundary conditions,

$$\bar{\phi}^{(1)} = -1 - \ln r + \bar{A}_1^{(1)} r\cos\theta - r^2\cos^2\theta - \tag{A.19}$$

$$\frac{2}{7}\bar{A}_1^{(1)} r^3\cos\theta + \bar{A}_2^{(1)} r^3\cos(3\theta) + O(r^4),$$

which can be written in terms of ξ and η as

$$\tilde{\phi}^{(1)}(\eta\to 0,\xi\to 0) = -1 - \ln(\eta^2+\xi^2)^{1/2} + \tilde{A}_1^{(1)}\xi - \xi^2 - \frac{2}{7}\tilde{A}_1^{(1)}\xi(\xi^2+\eta^2) + \tilde{A}_2^{(1)}\frac{\xi(\xi^2+\eta^2)^{3/2}}{(\xi^2+9\eta^2)^{1/2}} + O((\xi^2+\eta^2)^2). \tag{A.20}$$

$\tilde{A}_1^{(1)}$ and $\tilde{A}_2^{(1)}$ would be determined by comparing this asymptotic solution with the complete solution.

Finally, the matching condition is applied. This condition is expressed formally as

$$\frac{\ln\delta}{\delta} + \frac{1}{\delta}\bar{\phi}(\bar{\eta}^2+\bar{\xi}^2\to\infty) = \tilde{\phi}(\eta\to 0,\xi\to 0) \ . \tag{A.21}$$

Agreement must be observed for all orders in δ and also all orders in $(\xi^2+\eta^2)^{1/2}$. Equation (B-8) of Smyrl and Newman can be rewritten in terms of ξ and η as

$$\bar{\phi}(\bar{\eta}^2+\bar{\xi}^2\to\infty) = \frac{\delta}{2}\xi - \ln(E\delta(\eta^2+\xi^2)^{1/2}) + \frac{1}{\delta}\frac{\bar{A}_1^{(1)}\xi}{\xi^2+\eta^2} + \frac{1}{\delta}\bar{\phi}^{(2)}(\bar{\eta}^2+\bar{\xi}^2\to\infty) + o(1/\delta), \tag{A.22}$$

where $\bar{A}_1^{(1)}$ is the same as Smyrl and Newman's A_1 and is estimated to be -3.1. Substituting for E with equation (A.9) gives

$$\frac{\ln\delta}{\delta} + \frac{\bar{\phi}(\bar{\eta}^2+\bar{\xi}^2\to\infty)}{\delta} = \frac{\xi}{2} - \frac{1}{\delta}\left[1 + \ln(\eta^2+\xi^2)^{1/2}\right] \tag{A.23}$$

$$+ \frac{1}{\delta^2}\left[\bar{\phi}^{(2)} - \ln E^{(1)} + \frac{\bar{A}_1^{(1)}\xi}{\xi^2 + \eta^2}\right] + o(1/\delta^2).$$

To specify completely the matching condition for $\bar{\phi}^{(2)}$, it is necessary to investigate the outer region expansion:

$$\tilde{\phi}(\eta\to 0, \xi\to 0) = \frac{\xi}{2} - \frac{\xi^3}{6} + O(\xi^5) + \frac{1}{\delta}\Big[-1 - \ln(\xi^2+\eta^2)^{1/2} \tag{A.24}$$

$$-\bar{A}_1^{(1)}\xi - \xi^2 + O((\xi^2+\eta^2)^{3/2})\Big] + O(1/\delta^2)$$

The leading term of $\bar{\phi}^{(2)}$ must match the highest unmatched term in $\tilde{\phi}$. Although it might not be worth the effort of solving it, for completeness, the problem statement is given.

The governing equation remains

$$\frac{\partial^2\bar{\phi}^{(2)}}{\partial\bar{\eta}^2} + \frac{\partial^2\bar{\phi}^{(2)}}{\partial\bar{\xi}^2} = 0. \tag{A.25}$$

The insulator boundary condition is

$$\frac{\partial\bar{\phi}^{(2)}}{\partial\bar{\eta}} = 0 \quad \text{at} \quad \bar{\eta} = 0. \tag{A.26}$$

Along the working electrode, the boundary condition is

$$\frac{e}{2}\, e^{\bar{\phi}_o^{(1)}}\left(\ln E^{(1)} + \bar{\phi}_o^{(2)}\right) = \frac{1}{\bar{\eta}}\left.\frac{\partial\bar{\phi}^{(2)}}{\partial\bar{\xi}}\right|_{\bar{\xi}=0}, \tag{A.27}$$

where equation (A-18) of Smyrl and Newman gives

$$\ln E^{(1)} = \int_0^\infty \left[\bar{\phi}_o^{(1)} + \ln\bar{\eta}\right] d\bar{\eta}\ . \tag{A.28}$$

Results of finite-difference calculations can be correlated by

$$\frac{E}{2} = \frac{4.3 + \delta}{4.3 + 0.7358\delta}, \tag{A.29}$$

which is expanded to suggest that $\ln E^{(1)} = -1.544$. Finally, the matching condition is

$$\bar{\phi}^{(2)}{}_{(\bar{\eta}^2+\bar{\xi}^2\to\infty)} = \bar{A}_1^{(1)}\bar{\xi}, \tag{A.30}$$

and, in principle, $\bar{\phi}^{(2)}$ can be obtained.

The next term for i_{edge}/i_{avg} would be

$$\frac{i_{edge}}{i_{avg}} = \frac{e}{2}\, e^{\bar{\phi}_o^{(1)}(\bar{\eta}=0)} \left[\delta + \ln E^{(1)} + \bar{\phi}_o^{(2)}(\bar{\eta}=0) \right]. \tag{A.31}$$

Without further numerical work, the important result is that the next term in a perturbation series is of order unity.

A thorough treatment of the rotating disk geometry is presented. The E parameter of Smyrl and Newman [3] is the key to obtaining the next term in a perturbation series. For other cell geometries, an analogous term arises, and it might be expected to behave similarly. For a coplanar electrode and insulator, a term of order unity seems likely. For other angles of intersection, the correct expansion for the primary current distribution near the edge may cause unforeseen terms to arise. This makes it difficult to draw a more general conclusion.

Appendix B
Current Distributions for Small Polarization Parameters

A perturbation analysis describing the deviations from a uniform current distribution is regular. Such an analysis is given here for linear and Tafel kinetics on a disk electrode.

Before proceeding, one should recall the integral equation relating the potential and current distributions on the disk [7]:

$$\Phi_o(r_q) = \frac{2}{\pi\kappa} \int_0^{r_o} \frac{i_n K(m) r}{r + r_q}\, dr \ . \tag{B.1}$$

$K(m)$ is the complete elliptic integral of the first kind [8], and

$$m = \frac{2\sqrt{rr_q}}{r + r_q} \ . \tag{B.2}$$

Linear Kinetics—For linear kinetics, the boundary condition along the disk electrode can be expressed as

$$i_n = \frac{(\alpha_a + \alpha_c)Fi_o}{RT}(V - \Phi_o) . \tag{B.3}$$

We solve this problem as one with a set electrode potential. It is equally valid to specify the total current, as we prefer for Tafel kinetics.

For $J = 0$, the current distribution is uniform, and $\Phi = 0$; that is, the ohmic potential drop in the solution is negligible. This fact, along with equation (B.3), suggests that the potential is appropriately expanded as

$$\frac{\Phi}{V} = J\Phi^{(1)} + J^2\Phi^{(2)} + \ . \ . \ . \ . \tag{B.4}$$

Substitution of equations (B.3) and (B.4) into equation (B.1) gives a formal solution for the potential, where terms of the same order in J are equated:

$$\Phi_o^{(1)}(r_q) = \frac{2}{\pi} \int_0^1 \frac{K(m)r}{r + r_q}\, dr \ , \tag{B.5}$$

and, for $n > 1$,

$$\Phi_o^{(n)}(r_q) = -\frac{2}{\pi} \int_0^1 \frac{\Phi_o^{(n-1)} K(m)r}{r + r_q}\, dr \ . \tag{B.6}$$

Nanis and Kesselman [9] show that

$$\Phi_o^{(1)} = \frac{2}{\pi} E(r^2/r_o^2), \tag{B.7}$$

where $E(m)$[†] is the complete elliptic integral of the second kind.

These results give

$$\frac{i_n}{i_{avg}} = 1 + J(\bar{\Phi}_o^{(1)} - \Phi_o^{(1)}) + J^2(\bar{\Phi}_o^{(2)} - \Phi_o^{(1)}\bar{\Phi}_o^{(1)} - \Phi_o^{(2)}) + O(J^3), \tag{B.8}$$

where the $\bar{\Phi}_o^{(n)}$ arise as corrections to the average current density,

$$\bar{\Phi}_o^{(n)} = 2 \int_0^1 \Phi_o^{(n)} r dr \ . \tag{B.9}$$

Nanis and Kesselman [9] showed that $\bar{\Phi}_o^{(1)} = \frac{8}{3\pi}$.

[†]Note that our argument for the elliptic integral is the square of Nanis and Kesselman's argument. We use a definition of the elliptic integral chosen to be consistent with Abramowitz and Stegun [8].

Tafel Kinetics—For Tafel kinetics,

$$i_n = i_o \exp\left[\frac{\alpha_a F}{RT}(V - \Phi_o)\right]. \tag{B.10}$$

For relatively uniform current distributions, Wagner [10] suggested that the Tafel kinetics boundary condition can be linearized:

$$i_n = \frac{\alpha_a F i_{avg}}{RT}\left[\frac{RT}{\alpha_a F} - \Phi_o\right]. \tag{B.11}$$

This suggests that the first correction to a uniform current distribution for Tafel kinetics will be identical to the first correction for linear kinetics (with a properly modified definition of J). Only for higher order corrections will differences appear.

We solve this problem by setting δ, the dimensionless average current density. As $\delta \longrightarrow 0$, the current distribution is uniform, and Φ is zero (as a zeroth approximation). This fact, along with equation (B.10), suggests that the potential of the solution can be written as

$$\frac{\alpha_a F \Phi}{RT} = \delta\phi^{(1)} + \delta^2\phi^{(2)} + \ldots . \tag{B.12}$$

The electrode potential must also be expanded:

$$\frac{\alpha_a F V}{RT} + \ln\left[\frac{\alpha_a F r_o i_o}{RT\kappa}\right] = \ln\delta + \sum_{n=1} \delta^n V^{(n)}. \tag{B.13}$$

The $\ln\delta$ term on the right side of equation (B.13) can be thought of as the zeroth order term, which is determined by requiring that the dimensionless current distribution be uniform with a magnitude specified by δ. Since this term satisfies the specified average current density, all of the higher order corrections to the potential

distribution ($\phi^{(2)}$, *etc.*) must have a zero average current density. This provides the condition to determine $V^{(n)}$.

Following the same procedure used for linear kinetics gives

$$\phi_o^{(1)} = \frac{2}{\pi} \int_0^1 \frac{K(m)r}{r + r_q}\, dr = \frac{2}{\pi} E(r^2/r_o^2), \tag{B.14}$$

$$\phi_o^{(2)} = \frac{2}{\pi} \int_0^1 \frac{K(m)(V^{(1)} - \phi_o^{(1)})r}{r + r_q}\, dr , \tag{B.15}$$

and

$$\phi_o^{(3)} = \frac{2}{\pi} \int_0^1 \frac{K(m)\left[V^{(2)} - \phi_o^{(2)} + \frac{1}{2}(V^{(1)} - \phi_o^{(1)})^2\right]r}{r + r_q}\, dr , \tag{B.16}$$

where

$$V^{(1)} = 2 \int_0^1 \phi_o^{(1)} r dr = \frac{8}{3\pi} , \tag{B.17}$$

and

$$V^{(2)} = 2 \int_0^1 \phi_o^{(2)} r dr - \int_0^1 (V^{(1)} - \phi_o^{(1)})^2 r dr . \tag{B.18}$$

These results give

$$\frac{i_n}{i_{avg}} = 1 + \delta\, (V^{(1)} - \phi_o^{(1)}) + \tag{B.19}$$

$$\delta^2 \left[V^{(2)} - \phi_o^{(2)} + \frac{1}{2}\, (V^{(1)} - \phi_o^{(1)})^2\right] + O(\delta^3).$$

Summary—These analyses demonstrate the correct procedure to calculate small deviations from a uniform current distribution. The terms in each series can be obtained by a numerical integration of

the previously determined, lower order current distribution. Since $E(1) = 1$, the current density at the edge of the the electrode for linear kinetics is

$$\frac{i_{edge}}{i_{avg}} = 1 + \frac{2}{3\pi} J \quad \text{(small } J\text{)}, \tag{B.20}$$

and for Tafel kinetics is

$$\frac{i_{edge}}{i_{avg}} = 1 + \frac{2}{3\pi} \delta \quad \text{(small } \delta\text{)}. \tag{B.21}$$

As expected [10], the first correction to a uniform distribution is the same for linear and Tafel kinetics. Figure 8 compares numerical results obtained from finite-difference calculations with these asymptotic predictions. The current density at the center of the disk is also compared with its asymptotic value. Since $E(0) = \pi/2$,

$$\frac{i_{center}}{i_{avg}} = 1 + \left(\frac{8}{3\pi} - 1 \right) J \text{ (or } \delta\text{)}. \tag{B.22}$$

These analyses show how the current densities for linear and Tafel kinetics deviate from one another for larger values of the polarization parameter. For other cell geometries, the same linear dependence on J or δ is expected.

List of Symbols

$A_n^{(i)}$	coefficients arising in matching conditions (see equations (A.19-23))
a,b,c,d	parameters used in the conformal mapping procedures, shown in figure 2, cm

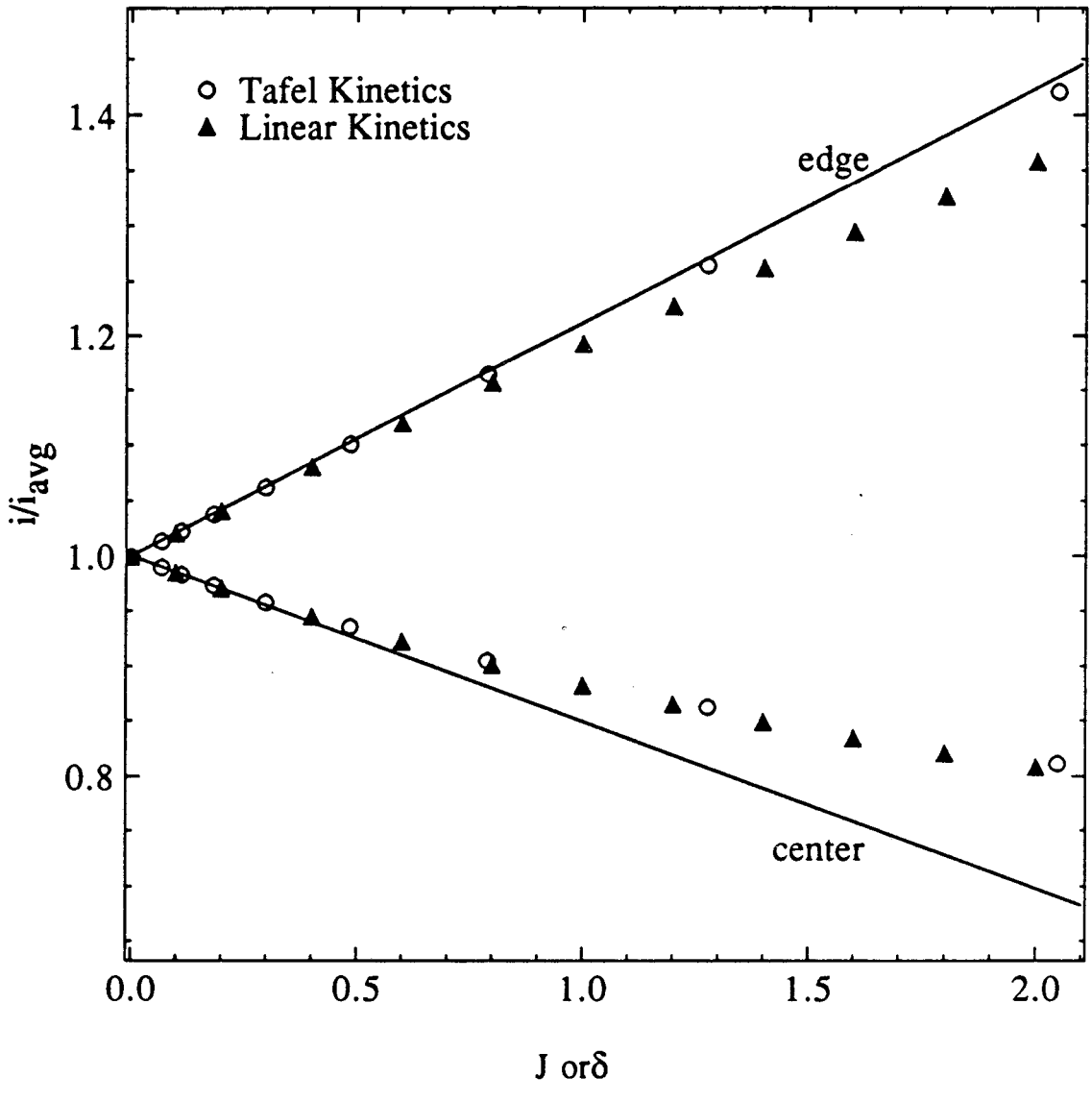

Figure 8. Calculated and predicted current densitiesfor linear and Tafel kinetics at the center and edge of a disk electrode for small polarization parameters. For linear kinetics, the current density depends on J, and, for Tafel kinetics, it depends on δ.

B_n	coefficients defined by equation (A.17)
f_n	stretching functions for the solution potential
F	Faraday's constant, 96487 C/equiv
E	parameter defined by equation (A.8)
$E(m)$	complete elliptic integral of the second kind
i	current density, A/cm^2
i_o	exchange current density, A/cm^2
j	$\sqrt{-1}$
J	dimensionless exchange current density
$K(m)$	complete elliptic integral of the first kind
L,τ,h,G	lengths characterizing the slotted electrode, cm
M_{2n}	even Legendre functions of imaginary arguments
P_o	parameter defined by equation (1), $A/cm^{(1+\pi/2\beta)}$
P_{2n}	even Legendre polynomials
r	radial distance away from the electrode/insulator edge, cm
r_o	radius of the disk electrode, cm
r_q	radial position where the potential is being determined, cm
R	universal gas constant, 8.3143 J/mol-K
S	stretching variable, cm^{-1}
T	absolute temperature, K
t,χ,z	complex coordinates
V	electrode potential, V
α_a,α_c	transfer coefficients
β	interior angle between insulator and electrode, radians

$\gamma(\chi)$	relates normal derivatives in original and transformed coordinate systems
δ	dimensionless average current density
$\epsilon^{(n)}$	n^{th} coefficient in a perturbation series
η,ξ	rotational elliptic coordinates
κ	specific conductivity, $\Omega^{-1}cm^{-1}$
π	3.141592654
ϕ	dimensionless solution potential
Φ	solution potential, V
Φ_o	solution potential adjacent to the electrode, V

Subscripts

as	asymptotic
avg	average
center	center of the disk electrode
edge	electrode/insulator interface
i,r	imaginary and real parts of a complex variable

Superscripts

p	primary
-	inner region variable
~	outer region variable

References

[1] Mark E. Orazem and John Newman, "Primary Current Distribution and Resistance of a Slotted-Electrode Cell," *J. Electrochem.*

Soc., **131**, 2857 (1984).

[2] William H. Smyrl and John Newman, "Current Distribution at Electrode Edges at High Current Densities," *J. Electrochem. Soc.*, **136**, 132 (1989).

[3] Kemal Nişancioğlu and John Newman, "The Short-Time Response of a Disk Electrode," *J. Electrochem. Soc.*, **121**, 523 (1974).

[4] William R. Parrish and John Newman, "Current Distribution on Plane, Parallel Electrodes in Channel Flow," *J. Electrochem. Soc.*, **117**, 43 (1970).

[5] John Newman, "Current Distribution on the Rotating Disk below the Limiting Current," *J. Electrochem. Soc.*, **113**, 1235 (1966).

[6] Francis B. Hildebrand, *Advanced Calculus for Applications*, 2nd edition, p. 230, Prentice-Hall, Englewood Cliffs, N. J. (1976).

[7] John Newman, "The Fundamental Principles of Current Distribution and Mass Transport in Electrochemical Systems," in *Electroanalytical Chemistry*, A. J. Bard, Editor, pp. 187-351, Marcel Dekker, Inc., New York (1973).

[8] M. Abramowitz and I. A. Stegun, eds., *Handbook of Mathematical Functions*, National Bureau of Standards, Washington (1964).

[9] Leonard Nanis and Wallace Kesselman, "Engineering Applications of Current and Potential Distributions in Disk Electrode Systems," *J. Electrochem. Soc.*, **118**, 454 (1971).

[10] Carl Wagner, "Theoretical Analysis of the Current Density Distribution in Electrolytic Cells," *J. Electrochem. Soc.*, **98**, 116 (1951).

CHAPTER 5
Corrections to Kinetic Measurements Taken on a Disk Electrode

Newman [1], [2] has suggested that a nonuniform ohmic potential drop to an electrode can lead to errors in the determination of kinetic parameters. A subsequent paper [3] showed that for linear kinetics the error in the measured exchange current density, i_o, can be as great as 300 percent, depending on the reference electrode placement and the dimensionless exchange current density, J, defined by Newman [4].

The present analysis considers the errors in kinetic parameters determined on the disk for the Tafel region in the absence of concentration variations. The apparent surface overpotential is taken to be that measured by a reference electrode of the same kind as the working electrode, with the ohmic-potential drop being determined by the interruption of the current. Since the reference electrode passes no current, it can be at equilibrium with the solution even though the working electrode is operating in the Tafel regime.

In the Tafel region, the exchange current density or J is no longer an important parameter in determining the distribution of current density and potential in the solution. Instead, the relevant parameter is a dimensionless average current density, δ, defined by

$$\delta = \frac{\alpha_a F r_o i_{avg}}{RT\kappa}. \tag{1}$$

This analysis presents the error in the measured exchange current density as a function of δ and three reference electrode placements.

Concentration variations are neglected in the analysis. Thus the ratio of the average current density to the limiting current density should be small. Since the expression for the limiting current density does not involve r_o or κ, which appear in δ, and does involve the rotation speed and the bulk concentration of the limiting reactant, which do not appear in δ, it is possible to neglect concentration variations in certain situations while still achieving moderately large values of δ. Figure 132-2 of reference 4, reproduced from reference 1, illustrates how the uniformity of current distribution is governed by the average current density, the exchange current density, and the limiting current density, as given by δ, J, and a dimensionless mass-transfer rate, N.

Analysis

The potential in solution, outside the double layer, in the absence of concentration variations, is given by Laplace's equation,

$$\nabla^2 \Phi = 0, \tag{2}$$

with boundary conditions,

$$\frac{\partial \Phi}{\partial z} = 0 \text{ for } r > r_o \text{ and } z = 0 \tag{3}$$

$$\Phi = 0 \text{ as } r^2 + z^2 \longrightarrow \infty$$

and

$$i(r) = f(\eta_s) \text{ for } r < r_o \text{ and } z = 0.$$

η_s is the local surface overpotential given by

$$\eta_s = V - \Phi(r,0), \tag{4}$$

where V is the potential of the electrode and $\Phi(r,0)$ is the potential of the solution just outside the diffuse double layer measured with a reference electrode of the same kind as the working electrode. In the Tafel region, the boundary condition describing the electrode kinetics for anodic currents is

$$i(r) = i_o \exp\left[\frac{\alpha_a F \eta_s}{RT}\right]. \tag{5}$$

Without the sectioning of an electrode, local current densities and overpotentials cannot be measured. Common practice, then, is to relate the average current density to the apparent surface overpotential, given by [5]

$$\eta_{s,app} = V - \Phi(r,z) - \bar{\Phi}(r,0) + \bar{\Phi}(r,z). \tag{6}$$

$\Phi(r,z)$ is the potential of the reference electrode, and $\bar{\Phi}(r,z) - \bar{\Phi}(r,0)$ represents the potential change observed upon interruption of the current and corresponds to the ohmic drop associated with the primary distribution of the same average current density [5].

To interpret a polarization curve obtained with a disk electrode, equation (5) may be more appropriately written as

$$i_{avg} = i_{o,app} \exp\left[\frac{\alpha_{a,app} F \eta_{s,app}}{RT}\right]. \tag{7}$$

Two defined parameters, $i_{o,app}$ and $\alpha_{a,app}$, are involved in this equation, and there are at least two possibilities for determining them from the experimental data. One is to take $\alpha_{a,app}F/RT$ to be the

slope of the line tangent to the Tafel plot of the data and $i_{o,app}$ to be an intercept obtained when this tangent line is extrapolated to $\eta_{s,app} = 0$. Then $i_{o,app}$ and $\alpha_{a,app}$ would be, in general, functions of δ, since the data will not yield exactly a straight line on a semi-logarithmic plot. Another approach is to assume that α_a is known and that its value is used for $\alpha_{a,app}$. A line of slope $\alpha_a F/RT$ is extrapolated through the data to obtain $i_{o,app}$. Again, the value obtained depends on the position along the Tafel plot through which the line is extrapolated.

Figure 1 shows a simulated Tafel plot of Ψ *vs.* $\ln(\delta)$ for three reference electrode placements. Ψ is defined in the caption of figure 1 and is used in order to make the plot valid for any (low) value of the exchange current density. Thus, in the Tafel range a decrease in the value of i_o with no change in i_{avg} would leave unchanged the current density and potential distributions. The only change would be to increase the electrode potential V, and hence η_s by an amount reflected in the definition of Ψ.

For values of $\ln(\delta) < -1$, $\alpha_a \approx \alpha_{a,app}$. Additionally, for $\ln(\delta) > 3$ and for a reference electrode placed at the center of the disk or at infinity, $\alpha_a \approx \alpha_{a,app}$. For a reference electrode placed adjacent to the edge of the disk, $\alpha_{a,app} = \alpha_a/2$ as $\delta \longrightarrow \infty$. For values of $\ln(\delta) > 4$, $\eta_{s,app}$ should be determined by the asymptotic solution shown with the dashed line. The deviation of the solid and dashed lines shows the difficulty in calculating potentials at the edge of the disk for high values of δ [6]. Only for intermediate

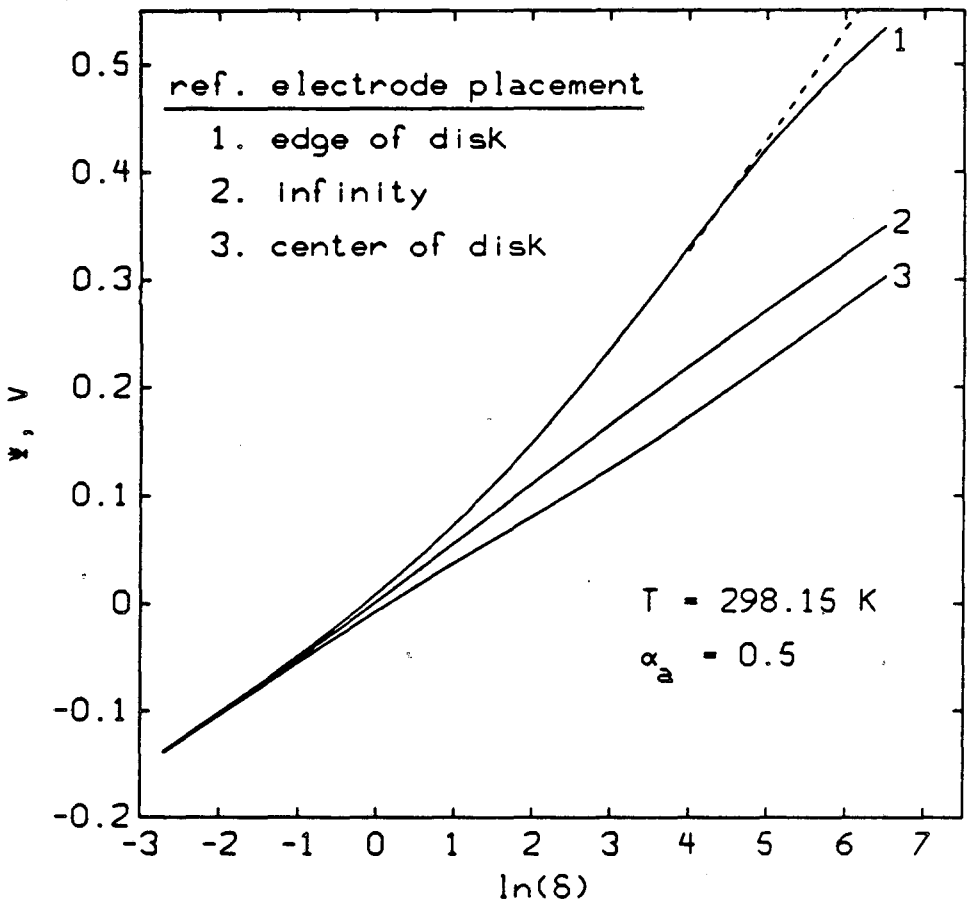

Figure 1. Average current density vs. Ψ, where

$$\Psi = \eta_{s,app} + \frac{RT}{\alpha_a F} \ln\left[\frac{i_o \alpha_a F r_o}{RT\kappa}\right]$$

values of δ will $\alpha_a \neq \alpha_{a,app}$; therefore, it is reasonable to assume that one typically has a good estimate of α_a. The following analysis will develop the equations for the more general case but will emphasize the results for the case of $\alpha_a = \alpha_{a,app}$.

To develop the relationships between the apparent parameters and the true parameters, it is convenient to introduce a new variable,

$$A = \frac{\alpha_a F r_o i_o}{RT\kappa} \exp\left[\frac{\alpha_a FV}{RT}\right]. \tag{8}$$

As is suggested in the appendix, A is a function only of δ. The relationship defined by equation (8) can be used to determine the disk potential necessary for a given average current. Originally, A was calculated by a boundary integral method. The method, as written, can not be used for high values of δ, since, as δ becomes large, the problem of the secondary current distribution becomes singular. Smyrl and Newman [6] give a parameter, E, valid for all δ, which can be related to A through

$$A = \frac{E}{2}\,\delta \exp\left[\frac{\pi\delta}{4}\right]. \tag{9}$$

E is shown in figure 2 and can be used to obtain A for any δ. It arises as a correction factor in an estimation of the potential of the disk electrode at high values of δ. The electrode potential V would be estimated by the sum of the ohmic potential drop to the center of the disk (estimated with the primary resistance) and the surface overpotential (estimated with $i/i_{avg} = 0.5$ at the center for a primary distribution):

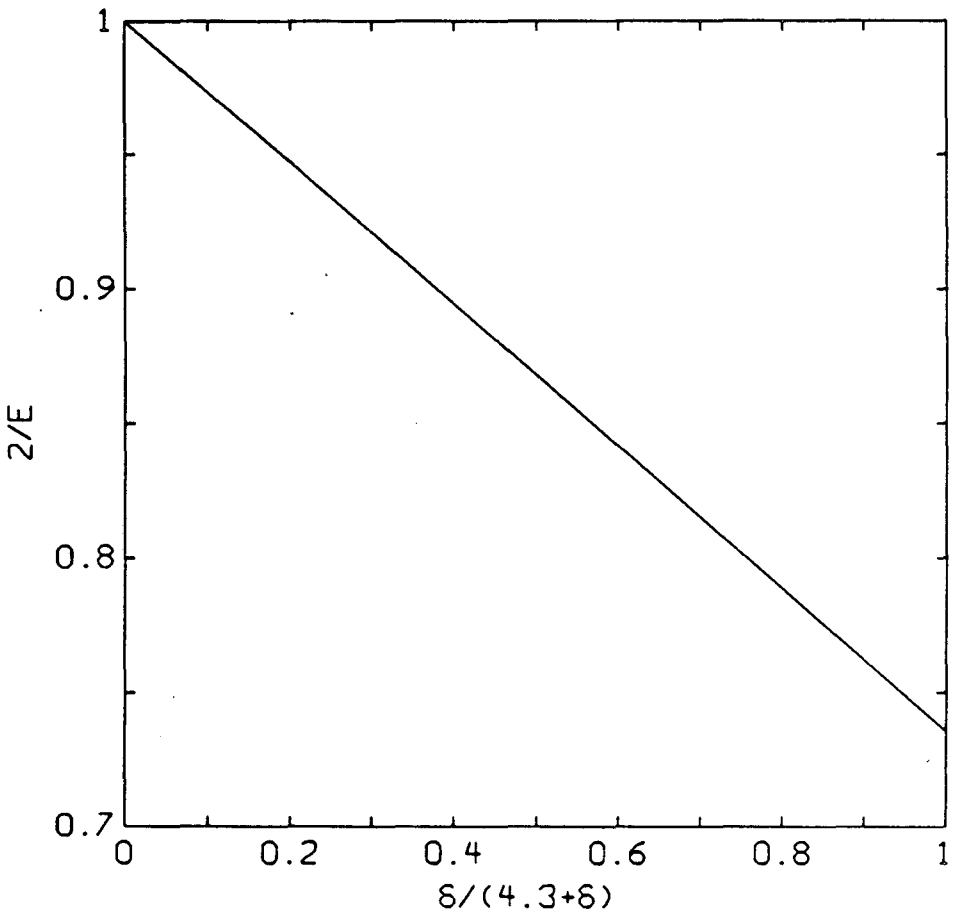

Figure 2. E vs. δ (Adopted from Smyrl and Newman [6]). As $\delta \longrightarrow \infty$, E $\longrightarrow$ e, the base of the natural logarithm.

$$\frac{\alpha_a FV}{RT} = \frac{\pi\delta}{4} + \ln\left(\frac{i_{avg}}{2i_o}\right) + \ln E \ . \qquad (10)$$

At low δ the correction factor takes on the value $E = 2$. At high δ, Smyrl and Newman [6] found by means of a singular perturbation analysis that $E \longrightarrow e$.

The ratio of the actual exchange current density to the apparent exchange current density as a function of δ can be found by combining equations (5), (7), and (8):

$$i_o/i_{o,app} = \frac{A}{\delta} \exp\left(\frac{-\alpha_a FV}{RT}\right) \exp\left(\frac{\alpha_{a,app} F\eta_{s,app}}{RT}\right). \qquad (11)$$

The ohmic drop between a disk with a primary current distribution and a reference electrode at infinity is given by

$$\bar{\Phi}(r,z) - \bar{\Phi}(r,0) = -\frac{\pi\delta RT}{4\alpha_a F} \ . \qquad (12)$$

Therefore, for a reference electrode at infinity, equation (11) becomes

$$i_o/i_{o,app} = \frac{A}{\delta} \exp\left(\frac{\alpha_a FV}{RT}\left(\frac{\alpha_{a,app}}{\alpha_a} - 1\right)\right) \exp\left(\frac{-\pi\delta\alpha_{a,app}}{4\alpha_a}\right). \qquad (13)$$

With the reference electrode placed adjacent to the surface,

$$i_o/i_{o,app} = \frac{A}{\delta} \exp\left(\frac{\alpha_a FV}{RT}\left(\frac{\alpha_{a,app}}{\alpha_a} - 1\right)\right) \exp\left(\frac{-\alpha_{a,app} F}{RT} \Phi(r,0)\right). \qquad (14)$$

The potential of the solution at the interface, $\Phi(r,0)$, is given by Smyrl and Newman [6] and is shown in figure 3 as a function of δ for $r = 0$ and $r = r_o$.

When $\alpha_a = \alpha_{a,app}$, equation (13) reduces to

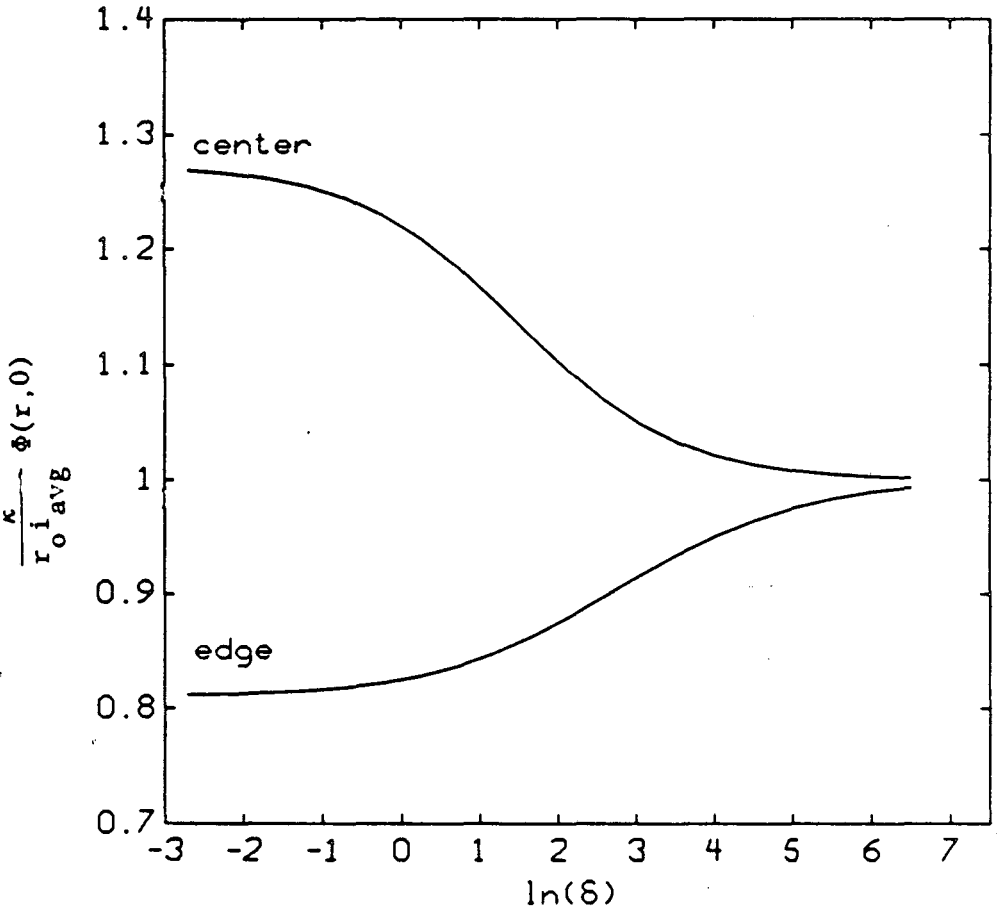

Figure 3. Dimensionless potential at the center and edge of the disk.

$$i_o/i_{o,app} = \frac{E}{2}, \tag{15}$$

and equation (14) reduces to

$$i_o/i_{o,app} = \frac{E}{2} \exp\left[\frac{\pi\delta}{4} - \frac{\alpha_a F}{RT}\,\Phi(r,0)\right]. \tag{16}$$

Equations (15) and (16), the latter for $r = 0$ and $r = r_o$, are shown in figure 4. The results of Smyrl and Newman [6] imply that, as $\delta \longrightarrow \infty$, $i_o/i_{o,app}$ goes to 0.5 for a reference electrode at the center of the disk, to infinity for a reference electrode at the edge of the disk, and to e/2 for a reference electrode at infinity, where e is the base of the natural logarithm.

Figure 1 shows that, for intermediate values of δ, α_a may not equal $\alpha_{a,app}$. In the rare case that experimental data exist only in this intermediate range, α_a, if determined by differentiation of exact data, would be given by

$$\alpha_a/\alpha_{a,app} = 1 + \frac{d\ln E}{d\ln\delta} + \frac{d\ln g(\delta)}{d\ln\delta}, \tag{17}$$

where $g(\delta)$ is one for a reference electrode at infinity and $\exp(\pi\delta/4 - \alpha_a F\Phi(r,0)/RT)$ for a reference electrode adjacent to the surface. The second term on the right side of equation (17) is shown in figure 5. The last term is shown in figure 6 for a reference electrode at the center of a disk and at the edge of a disk. The true value of α_a can be determined from figure 7, where

$$\delta_{app} = \frac{\alpha_{a,app} F r_o i_{avg}}{RT\kappa}. \tag{18}$$

For a reference electrode placed at infinity, the apparent transfer coefficient differs from the true value of the transfer coefficient

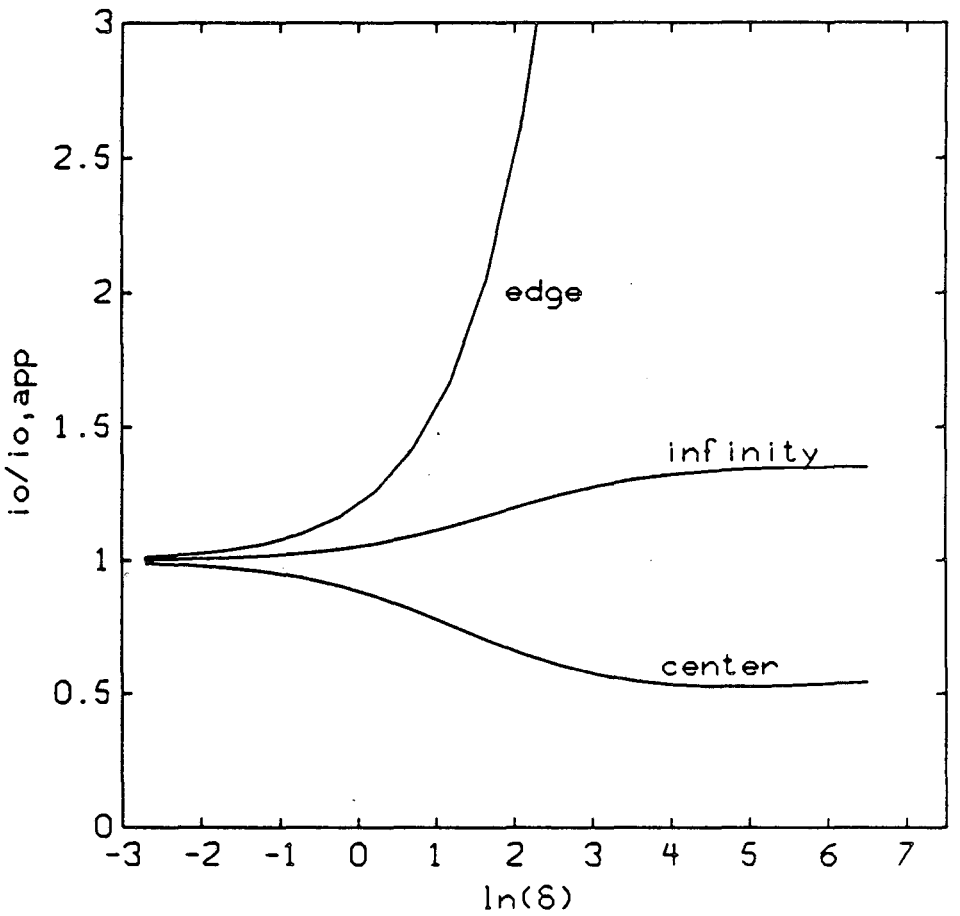

Figure 4. Correction to the exchange current density for three reference electrode placements, assuming $\alpha_a = \alpha_{a,app}$.

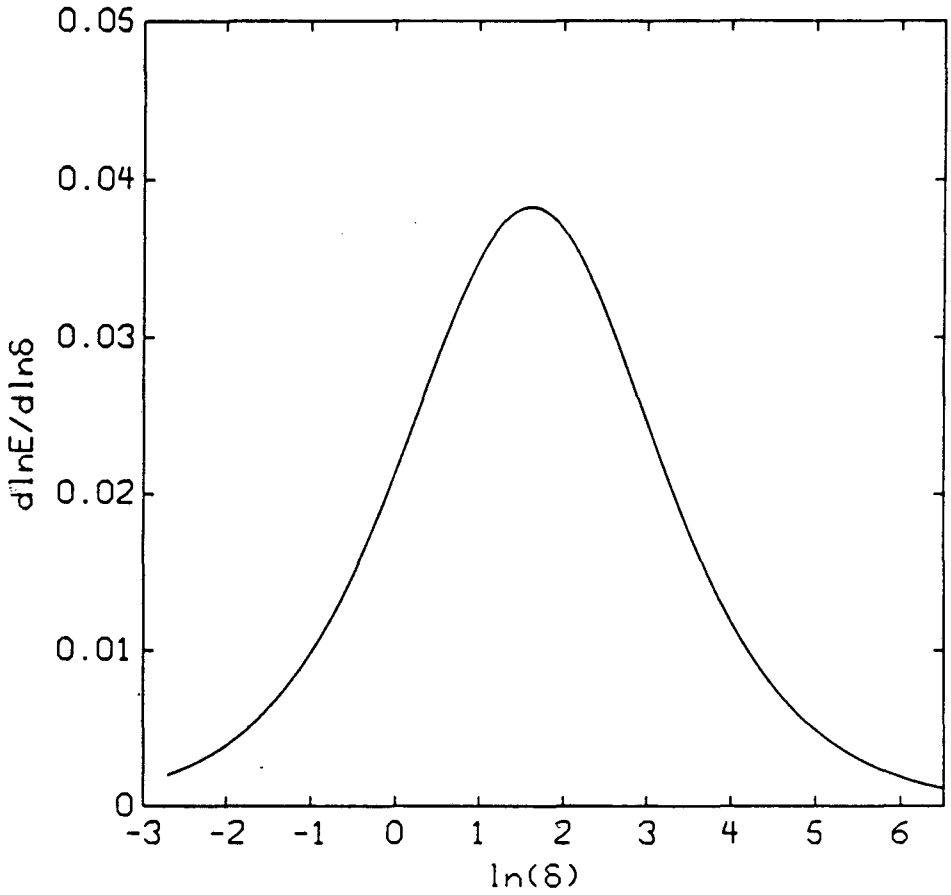

Figure 5. Correction term for the transfer coefficient, used in equation (17).

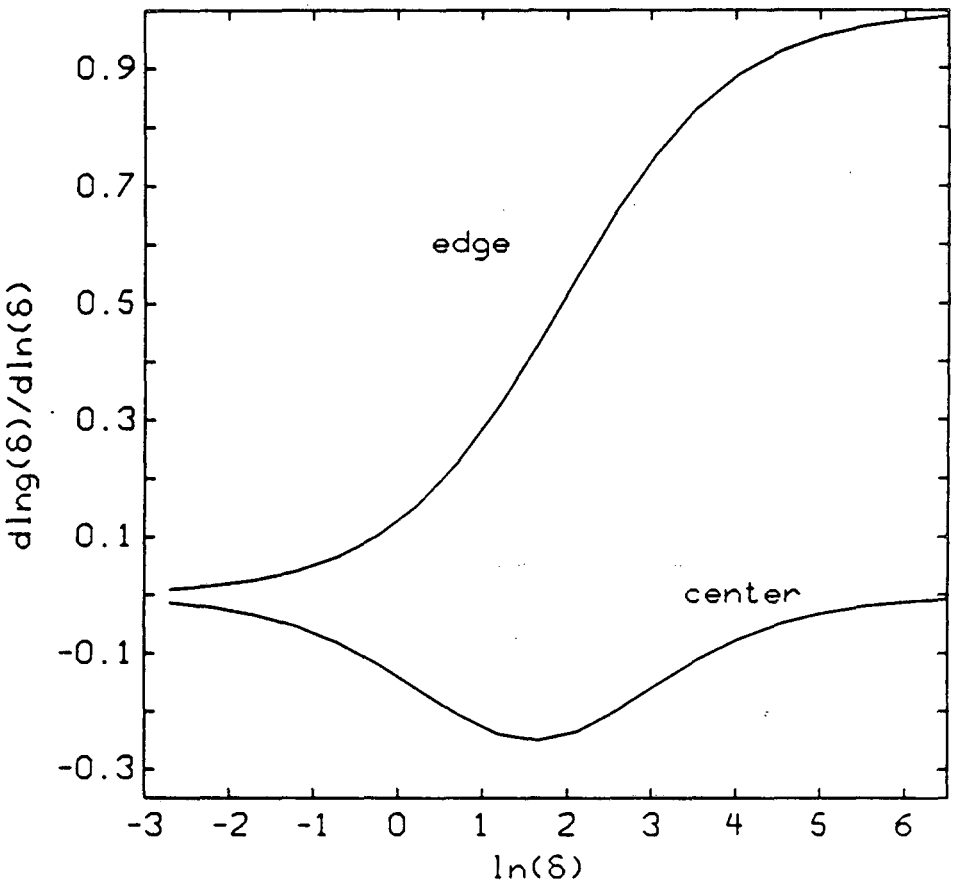

Figure 6. Correction term in equation (17) for a reference electrode at the edge and center of the disk.

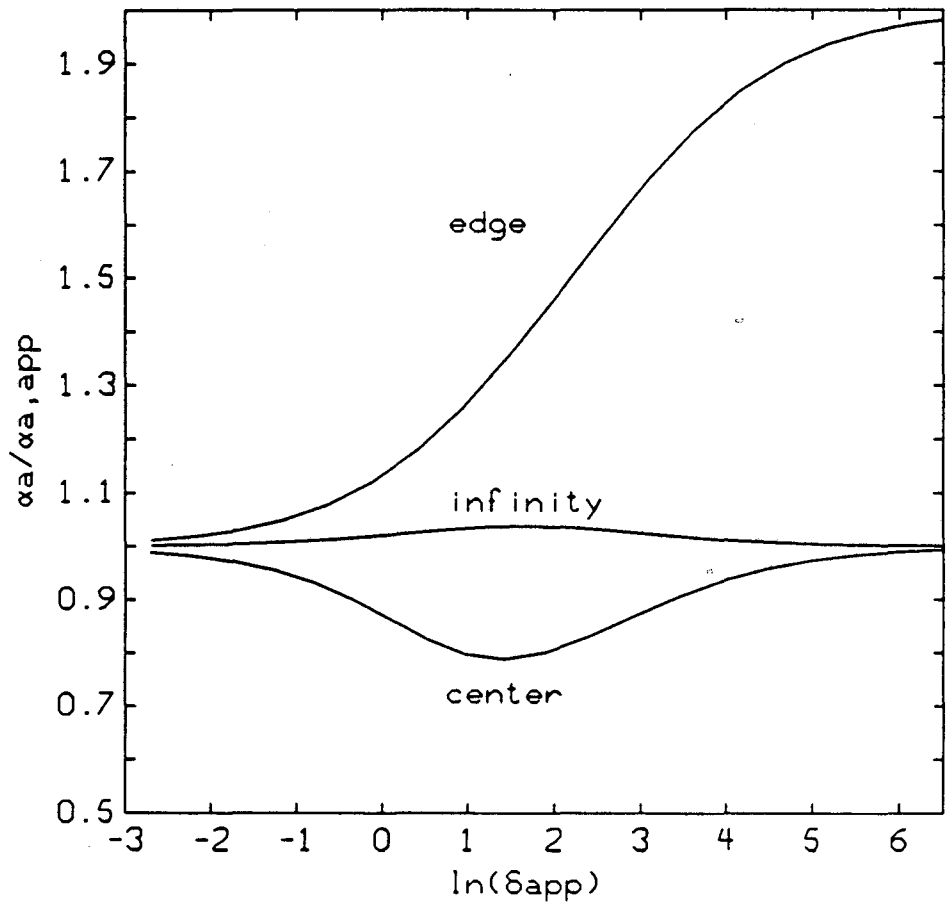

Figure 7. Correction to the transfer coefficent for three reference electrode placements as a function of δ_{app}.

by less than four percent for any value of δ. For a reference electrode placed adjacent to the disk electrode, the maximum errors can be rather large. For any reference electrode placement other than at the edge of the disk, the errors become negligible for both low and high values of δ.

Once α_a is known, two approaches are possible to determine the true value of the exchange current density. In the first approach, equation (13) or (14) could be used to obtain i_o. These equations can be rewritten as

$$\frac{i_o}{i_{o,app}} = \frac{E}{2}\, g(\delta)\, \chi^{(\alpha_{a,app}/\alpha_a - 1)} . \tag{19}$$

The last term in equation (19) can be thought of as a correction to figure 4, where

$$\chi = \exp\left(\frac{\alpha_a FV}{RT} - \frac{\pi\delta}{4}\right) g(\delta) = \frac{E}{2}\,\frac{i_{avg}}{i_o}\, g(\delta). \tag{20}$$

Unfortunately, as is suggested by the last expression of equation (20), χ can vary over many orders of magnitude.

Since χ can be very different from one, the value of i_o obtained from equation (19) is very sensitive to the value of $\alpha_{a,app}$ determined from experimental data. Any uncertainty in this value can cause even greater uncertainties in i_o. The more accurate approach would be to extrapolate a line of slope $\alpha_a F/RT$ that best fits the data to obtain a new $i_{o,app}$, where α_a was determined through figure 7. Then, equation (15) or (16) would be valid and figure 4 could be used to obtain i_o.

The above analysis can also be applied to cathodic Tafel kinetics. The appropriate kinetic boundary condition becomes

$$i(r) = - i_o \exp\left[\frac{-\alpha_c F \eta_s}{RT}\right]. \tag{21}$$

If one now takes

$$A = \frac{\alpha_c F r_o i_o}{RT\kappa} \exp\left[\frac{-\alpha_c FV}{RT}\right], \tag{22}$$

the results, equations (11), (13), and (14), will be identical if absolute values of δ and $\Phi(r,0)$ are used in the analysis. One would want to substitute cathodic transfer coefficients and apparent cathodic transfer coefficients everywhere.

Discussion

This analysis shows that $i_o/i_{o,app}$ and $\alpha_a/\alpha_{a,app}$ vary with the average current density. Therefore, a traditional plot of $\eta_{s,app}$ *vs.* $\ln(i_{avg})$ should not be expected to fall on a straight line. Figure 1 shows the range of δ over which significant variations in the slope can occur. When possible, experiments should be designed to operate mainly outside these regions of δ, since data are easier to analyze once α_a is known.

In practice, a Tafel plot of experimental data will not extend as a straight line through the abscissa since, as $\delta \longrightarrow 0$, the cathodic term of the Butler-Volmer equation becomes important. As is shown in figure 8, the common practice is to extend the straight part of the curve through $\eta_{s,app} = 0$, which gives $i_{o,app}$. By determining the value of δ at some point near which the slope of the curve

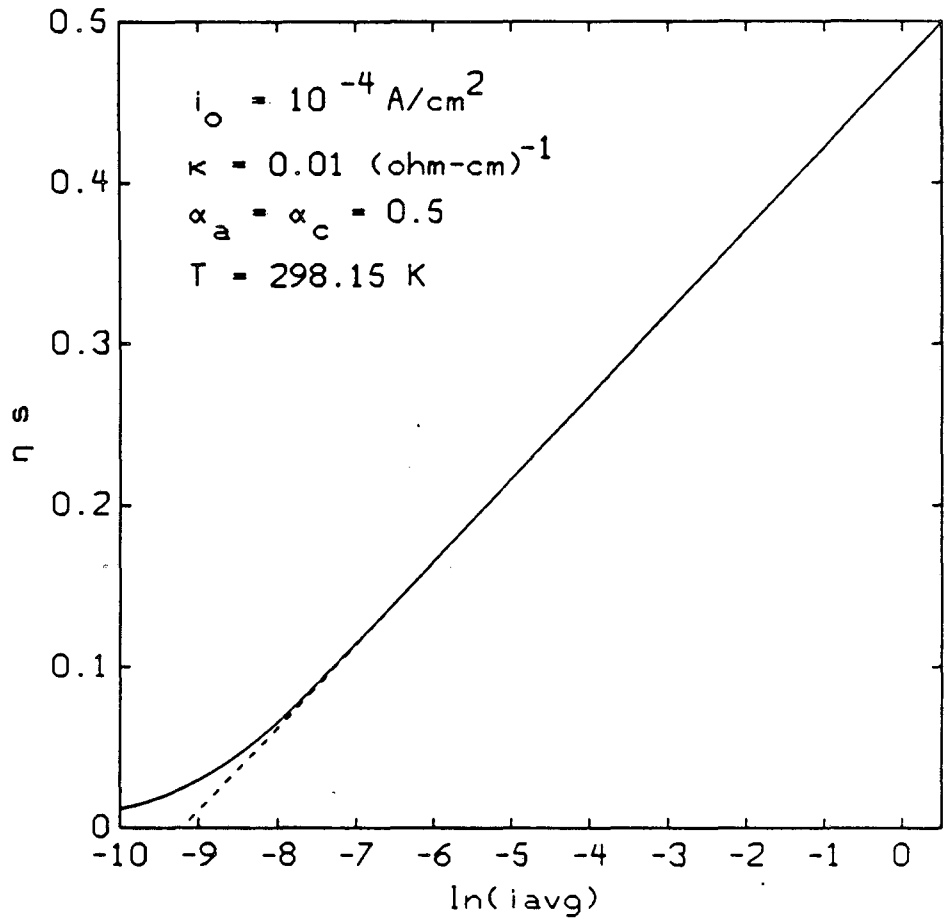

Figure 8. Simulated Butler-Volmer data, showing how experimental data may be expected to deviate from its Tafel slope.

deviates from the Tafel slope, one can use figure 4 to calculate the true exchange current density. It is important to realize that, for a given average current density, the error becomes larger for low solution conductivities and large disk radii.

Whenever possible, exchange current densities should be determined from data taken in the linear kinetics region. Errors could then be determined from reference [3]. For high exchange current densities, sufficient data should be available in this linear region. For more practical reasons, it is also desirable to use linear data, since, in the Tafel region, ohmic potential drops may dominate the measurements.

Conclusions

This analysis again confirms suggestions that the reference electrode should be placed far from the disk when possible. In addition to the reduction in measurement errors, errors caused by the distortion of current lines near the working electrode can be avoided. Contamination of the working electrode due to the reference electrode can also be minimized.

In the literature, reported exchange current densities for a given system can vary by well over one hundred percent. Therefore, depending on the application, the magnitude of the errors shown in the analysis may be considered minor. For more complicated kinetics, though, the errors may become much more significant. For example, in a study of passivation phenomena, the use of a disk electrode could

easily lead to much larger errors than those calculated unless the nonuniform current distribution is explicitly taken into account [7].

In the study of such complex kinetics or when high precision is desired, a geometry with a uniform current distribution should be chosen. Better geometries include rotating cylinder and rotating hemisphere electrodes. The disk electrode, though, is easier to manufacture and polish. Therefore, for many applications, the disk will very likely remain a popular choice.

The rotating disk electrode can be a valuable tool when mass-transfer and concentration effects can not be eliminated completely. Newman [1] outlined a method of studying electrode kinetics under such conditions. His analysis is valid for Butler-Volmer kinetics with a concentration dependent exchange current density. In the most general case, both δ and J are important parameters. Additionally, a dimensionless mass-transfer rate, the order of the reaction, α_a/α_c, and the transference number of the reactant are important. Newman's approach involves determining the current density at the center of the disk for the appropriate set of parameters. Additionally, the potential at the center of the disk can be determined through knowledge of $i(r = 0)/i_{avg}$, the disk radius, and the conductivity of the bulk electrolyte. True kinetic constants can then be determined. This approach may involve an iterative procedure.

The qualitative conclusions of this analysis are valid for any geometry with a nonuniform current distribution. In designing kinetic experiments, one should try to use a cell geometry that will

avoid these nonuniformities. Additionally, mass-transfer effects should be minimized by having uniformly accessible surfaces and operating under the proper hydrodynamic conditions.

Appendix

Axisymmetric boundary integral equations were used to calculate the current distribution (see chapter 2, equation (23)). For anodic currents, the Tafel relationship, in dimensionless form, can be written as

$$\frac{\partial \Phi^*}{\partial z^*} = -A \exp\left[- \Phi^* \right] \tag{A2}$$

where $z^* = z/r_o$,

$$\Phi^* = \frac{\alpha_a F \Phi}{RT},$$

and A is given by equation (8).

List of Symbols

A	dimensionless parameter, defined by equation (9)
E	dimensionless parameter, shown in figure 2
$g(\delta)$	function defined below equation (17)
i	current density, A/cm^2
i_o	exchange current density, A/cm^2
J	dimensionless exchange current density
$K(m)$	complete elliptic integral of the first kind
r	radial position coördinate, cm

r_o	radius of the disk, cm
r_q	radial position at which the potential is being solved, cm
R	universal gas constant, 8.3143 J/mol-K
T	absolute temperature, K
V	electrode potential, V
z	distance from electrode surface, cm
α_a, α_c	transfer coefficients
δ	dimensionless average current
η_s	surface overpotential, defined by equation (3), V
κ	solution conductivity, mho/cm
π	3.141592654
Φ	potential of the solution, V
χ	dimensionless parameter defined in equation (20)
Ψ	potential defined in figure 1, V

Subscripts

a	anodic
app	apparent
avg	average
c	cathodic

References

[1] John Newman, "Current Distribution on a Rotating Disk below the Limiting Current," *J. Electrochem. Soc.*, 113, 1235 (1966).

[2] John Newman, "Engineering Design of Electrochemical Systems," *Ind. Eng. Chem.*, **60**, no. 4, 12 (1968).

[3] W. H. Tiedemann, J. Newman, and D. N. Bennion, "The Error in Measurements of Electrode Kinetics Caused by Nonuniform Ohmic-Potential Drop to a Disk Electrode," *J. Electrochem. Soc.*, **120**, 256 (1973).

[4] John S. Newman, *Electrochemical Systems*, p. 346, Prentice-Hall, Englewood Cliffs, N. J. (1973).

[5] John Newman, "Ohmic Potential Measured by Interrupter Techniques," *J. Electrochem. Soc.*, **117**, 507 (1970).

[6] William H. Smyrl and John Newman, "Current Distributions at Electrode Edges at High Current Densities," *J. Electrochem. Soc.*, **136**, 132 (1989).

[7] Phillip Paul Russell, *Corrosion of Iron: The Active-Passive Transition and Sustained Electrochemical Oscillations*, Ph. D. Thesis, University of California, Berkeley (February, 1984).

CHAPTER 6
Interpretation of Kinetic Data Taken in a Channel Flow Cell

It has long been recognized that a nonuniform reaction distribution on an electrode can lead to difficulties in the interpretation of current-overpotential data [1]. Tiedemann *et al.* quantified this observation for linear kinetic measurements on a disk electrode [2]. Chapter 5 gives results for the more complicated case of Tafel kinetics on a disk electrode.

Measurements are sometimes taken in the channel geometry. This geometry is useful because it has well-characterized (but nonuniform) mass-transfer rates and can be useful because of ease of construction. It also approximates popular cell configurations used to study solid electrolytes. This analysis would be particularly applicable to these systems since, if the electrolyte contains only one charge carrier, concentration variations do not exist. It will also become evident that this analysis is especially relevant to solid electrolytes since their conductivities are often low (compared to aqueous solutions).

The channel geometry has already been studied extensively; see especially, papers by Wagner [3] and by Parrish and Newman [4]. The key assumption of the analysis in this paper is that concentration variations can be neglected, which implies that $\bar{i}_{avg} \ll \bar{i}_{lim}$, where $\bar{i}_{lim}$ is the average limiting current density. The validity of this assumption can be tested easily by calculating $\bar{i}_{lim}$ through knowledge of the transport properties and the flow conditions.

The channel geometry is characterized by the two lengths shown in figure 1. The ratios h/L of 1.0, 0.5, and 0.0 are investigated. Small ratios are chosen because they tend to make current distributions more uniform and tend to reduce the ohmic drop of the cell. The ratio $h/L = 0$ corresponds to a thin-gap cell, which is studied by Edwards and Newman [5], and physically means that $L \gg h$.

The average surface overpotential is assumed to be determined by the interruption of current. Additionally, the working electrode is taken to be an anode, although the results can be applied to the investigation of cathodic reactions. The counterelectrode is assumed to have the same kinetics as the working electrode, and the restrictiveness of this assumption is shown.

The emphasis of the results is on the placement of the reference electrode adjacent to the edge of the working electrode or *very far* from the electrode. To determine what can be considered *very far* from the working electrode the primary potential distribution along the insulator is shown in figure 2. At a distance h from the edge of the working electrode the potential has fallen by roughly 95% of the total potential drop to infinity. Within the resolution of the graph, the distribution for all three ratios of h/L is identical.

Analysis

In the absence of concentration variations, the distribution of current density is governed by Laplace's equation. The working and counter electrodes are assumed to operate in the same reaction regime

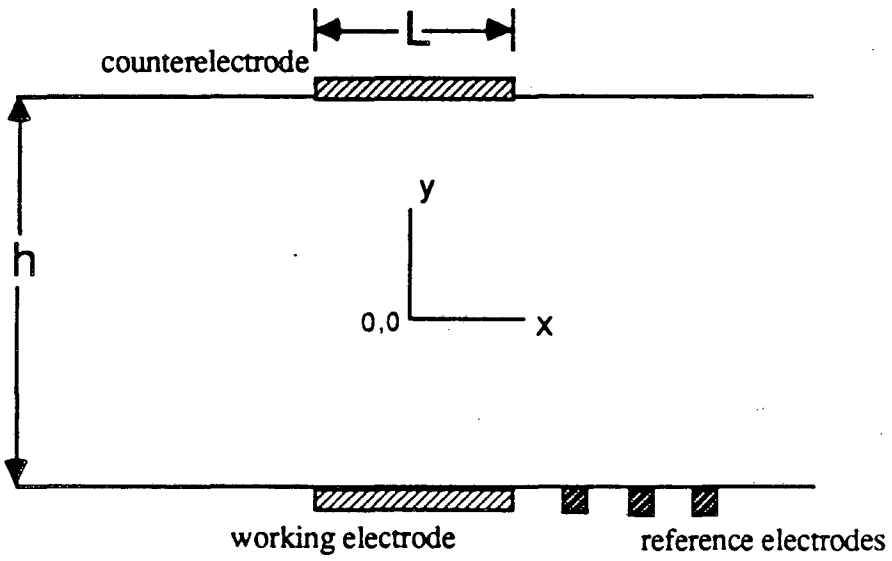

Figure 1. Cell geometry, showing the two characteristic lengths, the coordinate system, and possible reference electrode placements.

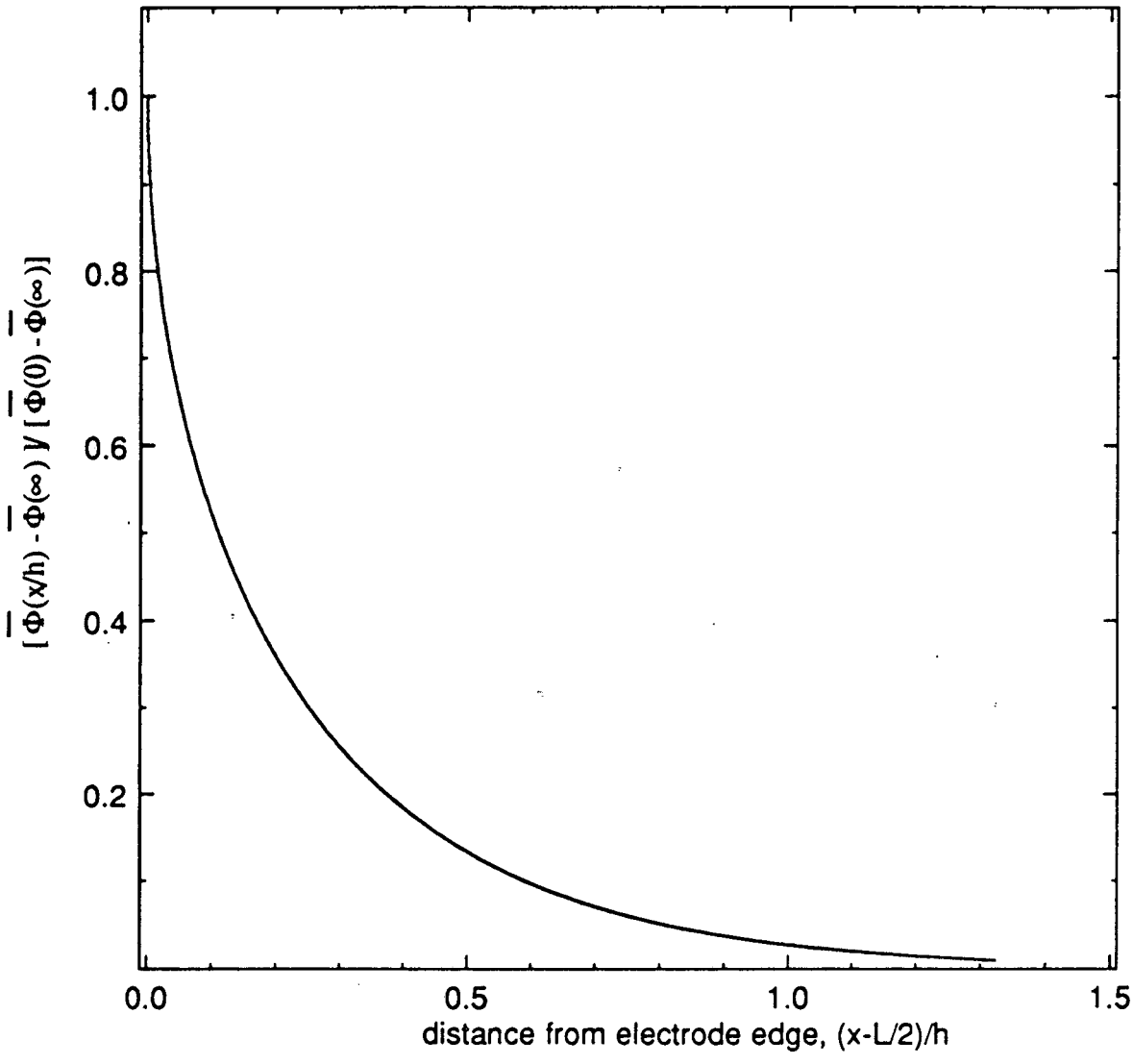

Figure 2. Primary potential distribution along the insulator, measured from the edge of the electrode, for h/L = 0, h/L = 0.5, and h/L = 1.0.

and to have identical exchange current densities and transfer coefficients. The appendix gives details of the solution procedure.

In addition to h/L, it is necessary to know the ratio of the ohmic to kinetic resistances to characterize how the data should be interpreted. Following Newman [6], the additional parameter for linear kinetics is

$$J = \frac{(\alpha_a+\alpha_c)Fhi_o}{RT\kappa} , \tag{1}$$

and for Tafel kinetics,

$$\delta = \frac{\alpha_a Fhi_{avg}}{RT\kappa} . \tag{2}$$

The characteristic length used in these definitions is chosen because it is the important length as $h/L \longrightarrow 0$.

A nonuniform potential distribution on the electrode complicates the interpretation of data taken with the aid of current interruption. The apparent surface overpotential determined by this method is [7]

$$\eta_{s,app} = V - \Phi(x,y) - \bar{\Phi}(0,h/2) + \bar{\Phi}(x,y), \tag{3}$$

where $\Phi(x,y)$ is the potential of the reference electrode,† and $\bar{\Phi}(0,h/2) - \bar{\Phi}(x,y)$ is the change in potential after the interruption of current and corresponds to the potential drop for a primary distribution with the same average current density.

---

†The reference electrode is assumed to be the same kind as the working electrode, but passes no current, and is in equilibrium with the solution.

Results for Linear Kinetics

For linear kinetics, the current density is described by

$$i = \frac{i_o(\alpha_a+\alpha_c)F\eta_s}{RT} , \tag{4}$$

where $\eta_s = V - \Phi(x,h/2)$. Assuming that $\alpha_a+\alpha_c$ is known, an apparent exchange current density can be defined by

$$i_{avg} = \frac{i_{o,app}(\alpha_a+\alpha_c)F\eta_{s,app}}{RT} . \tag{5}$$

Combining equations (4) and (5) gives

$$\frac{i_o}{i_{o,app}} = \frac{(\alpha_a+\alpha_c)Fi_o}{RT} \frac{\eta_{s,app}}{i_{avg}} . \tag{6}$$

For a reference electrode adjacent to the edge of the electrode, equation (6) reduces to

$$\frac{i_o}{i_{o,app}} = \frac{i_{edge}}{i_{avg}} . \tag{7}$$

Results obtained from equation (6) and the numerical procedure described in the appendix are shown in figures 3 and 4 for various reference electrode placements. J_{app} is introduced to facilitate the use of these figures and is defined by

$$J_{app} = \frac{(\alpha_a+\alpha_c)Fhi_{o,app}}{RT\kappa} . \tag{8}$$

Results for Tafel Kinetics

The important parameter for the characterization of Tafel kinetics is a dimensionless average current density. Since the proper interpretation of the data changes with the polarization parameter, a

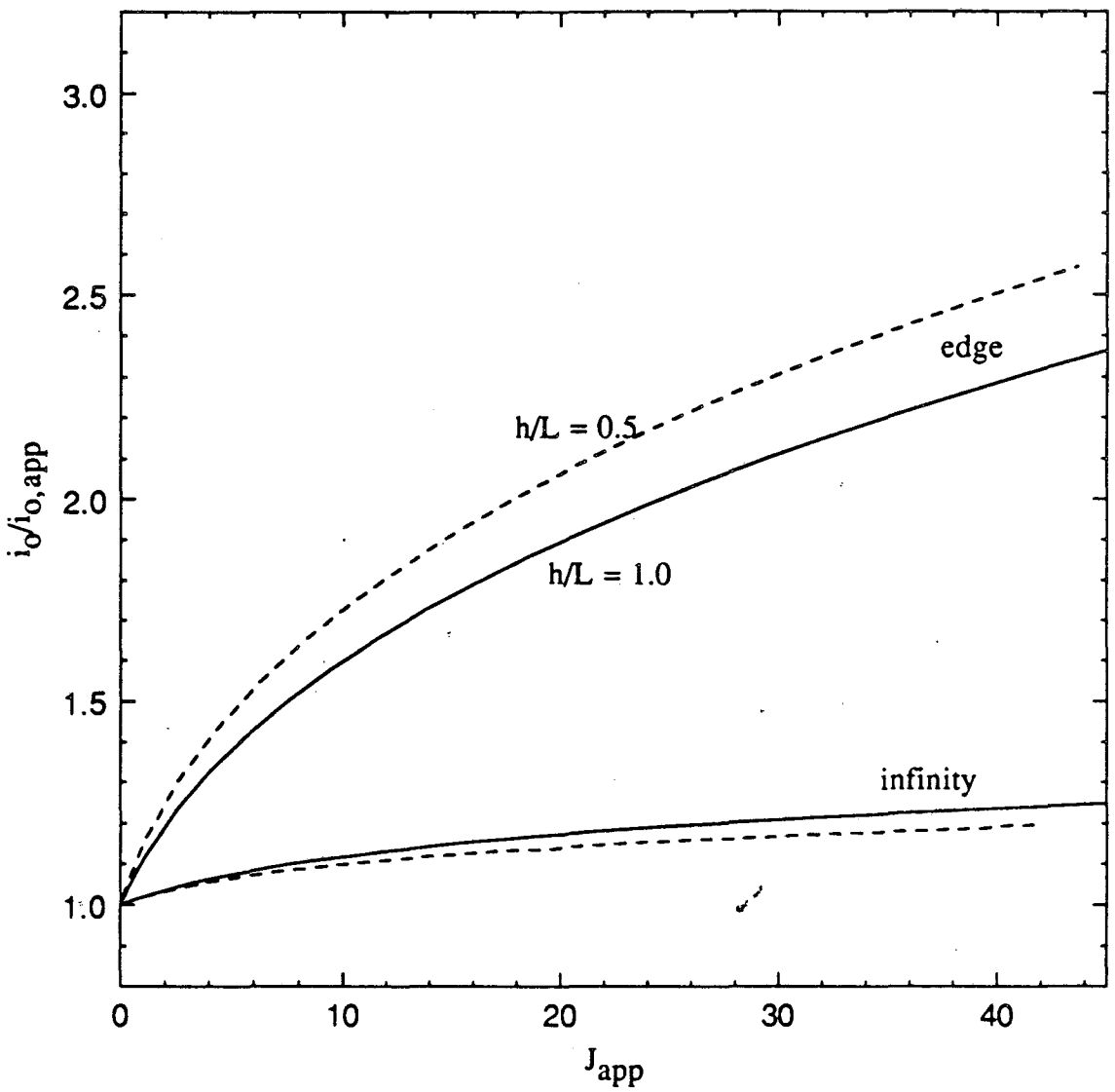

Figure 3. Correction factor for the exchange current density for linear kinetics for a reference electrode placed adjacent to the working electrode and for one placed very far from the working electrode.

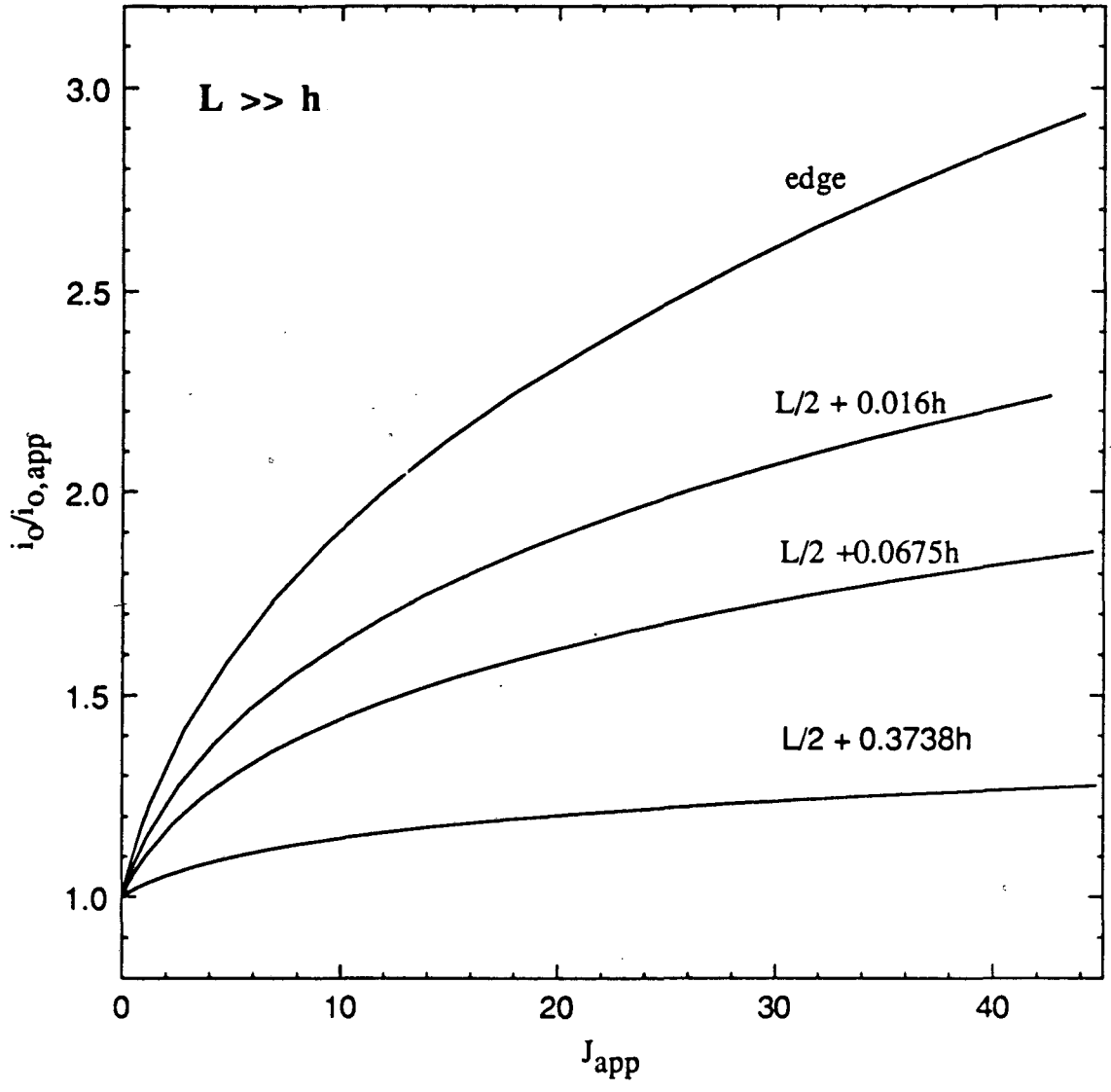

Figure 4. Correction factor for the exchange current density for linear kinetics, L >> h, and four reference electrode placements.

Tafel plot of data is not expected to fall on a straight line, even if the Tafel equation exactly describes the kinetics of the reaction. This complicates the analysis for Tafel kinetics.

Reaction rates described by Tafel kinetics are given by

$$i = i_o \exp\left[\frac{\alpha_a F \eta_s}{RT}\right] . \tag{9}$$

Since local current densities and local surface overpotentials are not measurable, apparent kinetic parameters must be defined and should be related to measured quantities:

$$i_{avg} = i_{o,app} \exp\left[\frac{\alpha_{a,app} F \eta_{s,app}}{RT}\right] . \tag{10}$$

As chapter 5 discusses, a desired procedure for analyzing data is to define more precisely $i_{o,app}$ as the apparent exchange current density obtained when a line of slope $RT/\alpha_a F$ is fitted through the experimental data. It is, therefore, most interesting to report values of $i_o/i_{o,app}$ for the case of $\alpha_a = \alpha_{a,app}$. With this assumption, equations (9) and (10) give

$$\frac{i_o}{i_{o,app}} = \frac{i_o}{i_{avg}} \exp\left[\frac{\alpha_a F \eta_{s,app}}{RT}\right] . \tag{11}$$

For a reference electrode placed adjacent to the edge of the working electrode, equation (11) reduces to equation (7). Results for various reference electrode placements are shown in figures 5 and 6.

Before i_o can be obtained from $i_{o,app}$, it is necessary to know α_a, which can be determined from $\alpha_{a,app}$:

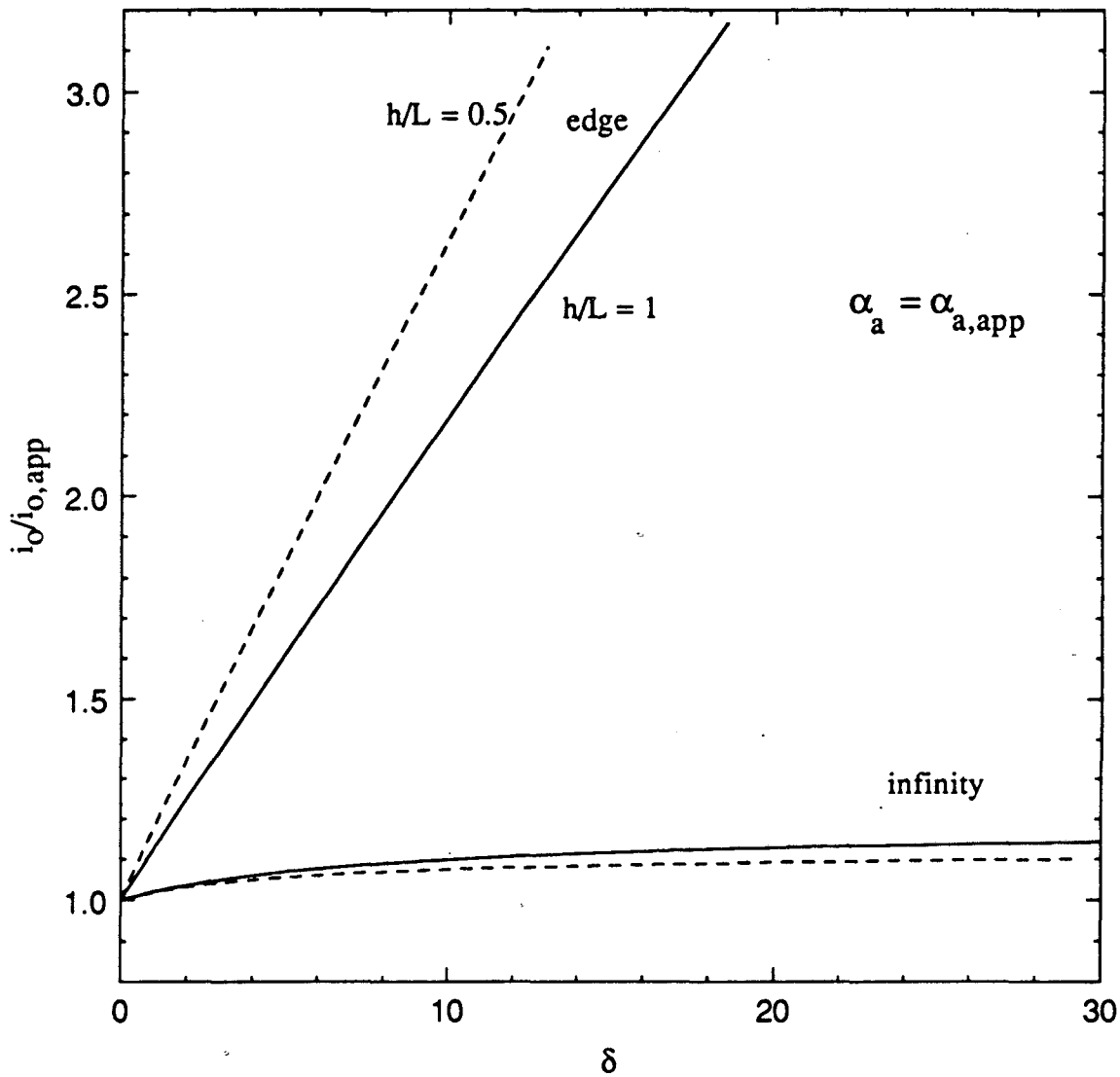

Figure 5. Correction factor for the exchange current density for Tafel kinetics, two reference electrode placements, and two ratios of h/L.

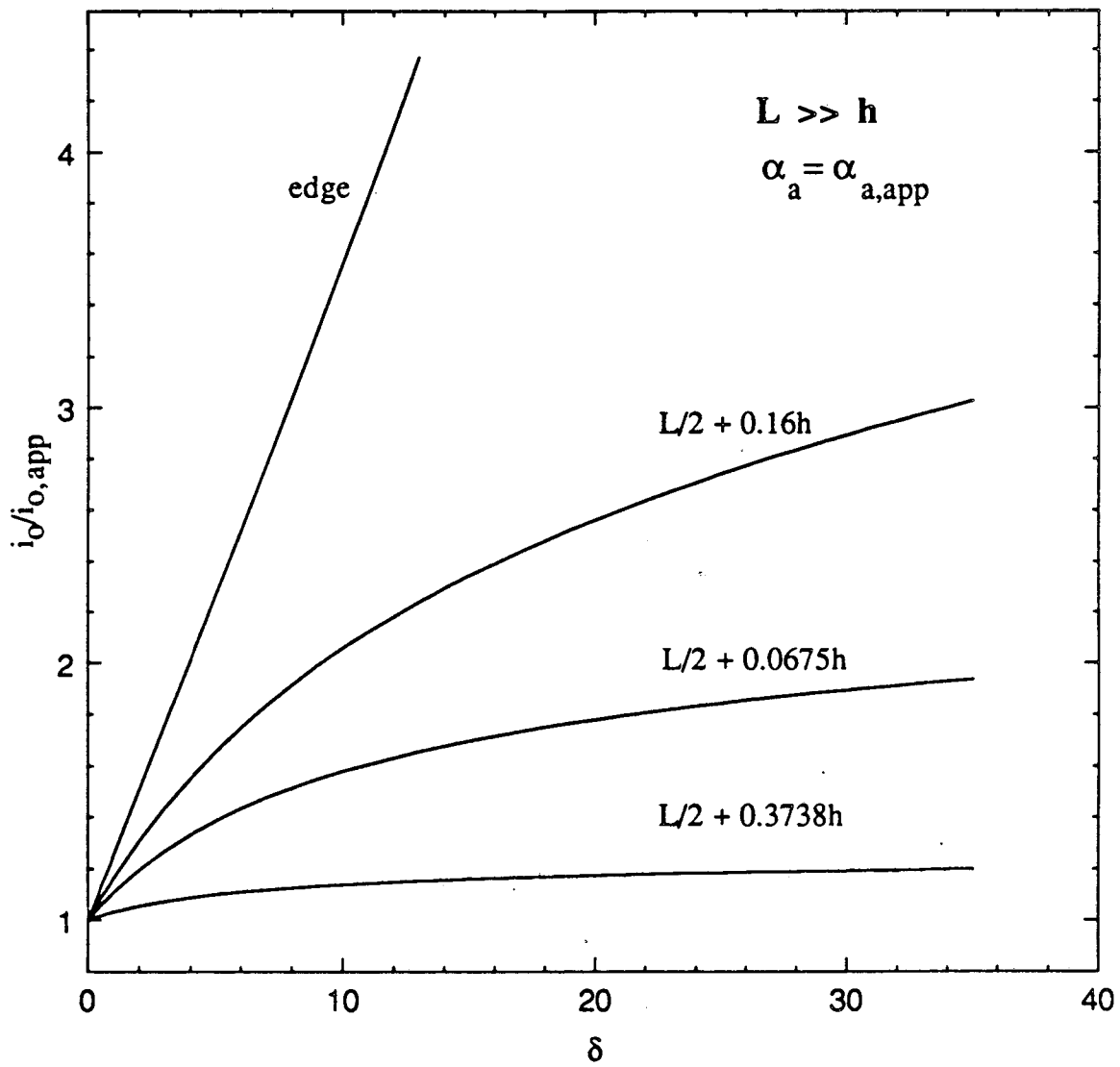

Figure 6. Correction factor for the exchange current density for Tafel kinetics, L >> h, and four reference electrode placements.

$$\alpha_{a,app} = \frac{RT}{F} \frac{d\ln i_{avg}}{d\eta_{s,app}} \quad . \tag{12}$$

Combining equations (11) and (12) gives

$$\frac{\alpha_a}{\alpha_{a,app}} = 1 + \left[\frac{d\ln(i_o/i_{o,app})}{d\ln\delta}\right]_{\alpha_a=\alpha_{a,app}} , \tag{13}$$

where the right side of equation (13) is evaluated assuming that $\alpha_a = \alpha_{a,app}$. Equation (13) is shown in figures 7 and 8, where

$$\delta_{app} = \frac{\alpha_{a,app} F h i_{avg}}{RT\kappa} , \tag{14}$$

and is introduced to determine more easily α_a. These results were obtained by differentiating fourth-degree polynomials that were fitted to logarithmic plots of the results displayed in figures 5 and 6.

Precisely obtaining i_o and α_a from Tafel data can be difficult. The procedure that one might take is outlined as follows:

1. Determine $\alpha_{a,app}$ from the slope of the data ($\ln i_{avg}$ *vs.* $\eta_{s,app}$).
2. Calculate δ_{app} from the value of i_{avg} at which the "apparent" Tafel slope was determined.
3. Obtain α_a from figure 7 or 8.
4. Determine $i_{o,app}$ from a line with the correct Tafel slope drawn through the value of i_{avg} used to calculate δ_{app}.
5. Use figure 5 or 6 to calculate i_o.

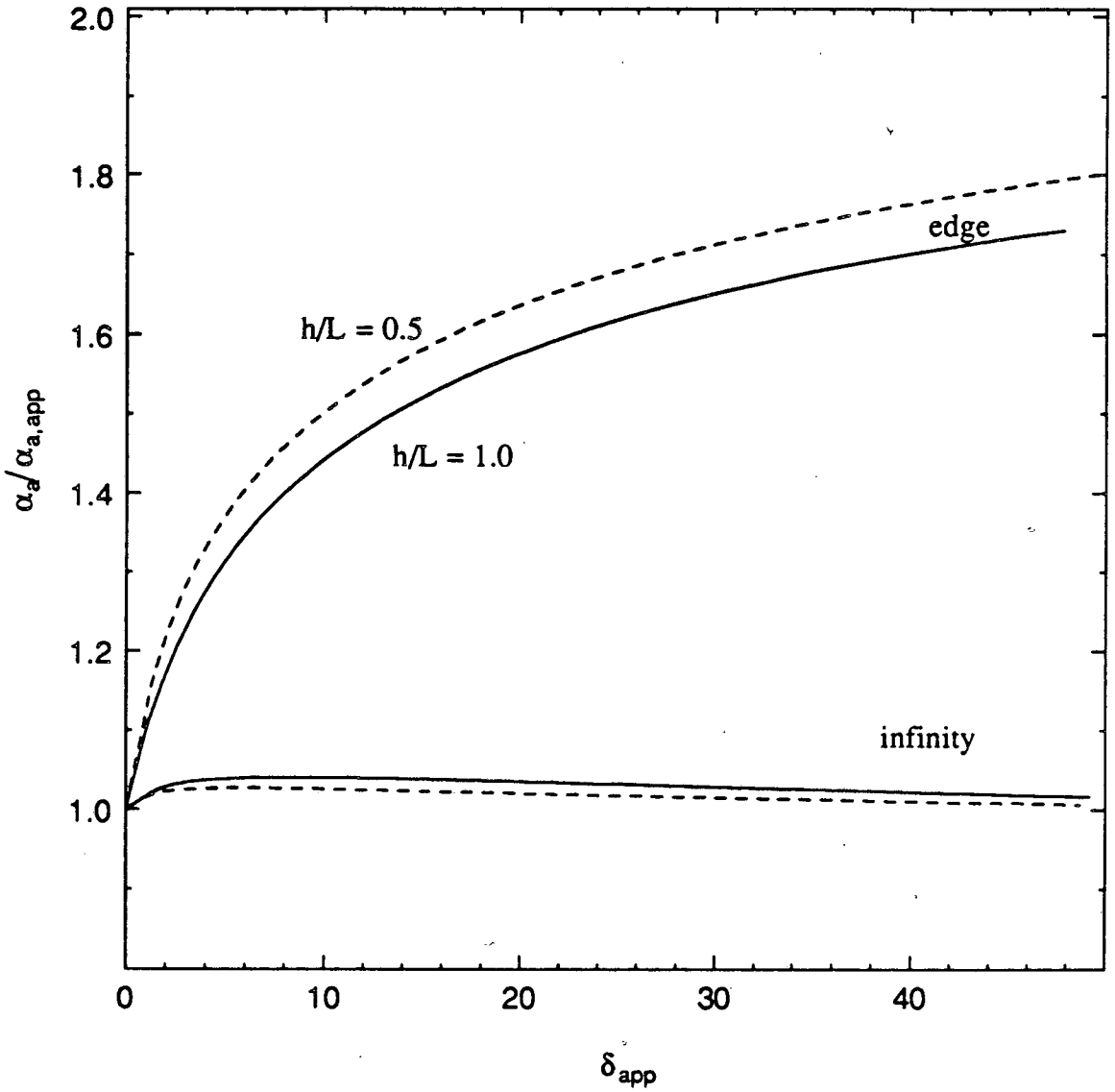

Figure 7. Correction factor for the transfer coefficient as a function of the apparent dimensionless average current density for two reference electrode placements and two ratios of h/L.

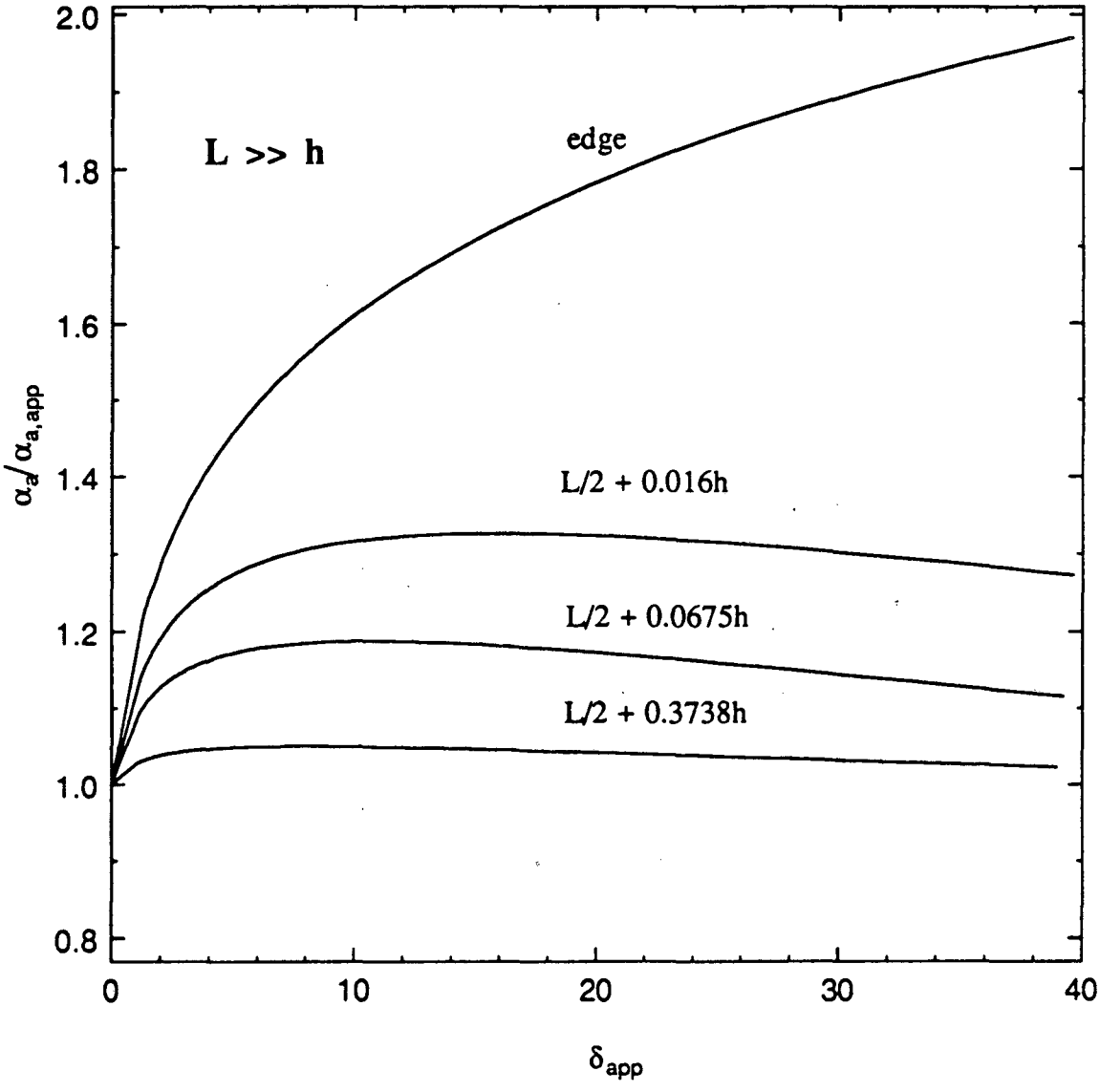

Figure 8. Correction factor for the transfer coefficient as a function of the apparent dimensionless average current density for L >> h and for various positions of the reference electrode.

Discussion

Figure 3 shows $i_o/i_{o,app}$ for linear kinetics. As might be expected [2], the correction to $i_{o,app}$ can be much lower for a reference electrode placed at infinity. Unfortunately, it is not always possible to place the reference electrode far from the working electrode because the ohmic potential may dominate the measurements.

For a reference electrode placed adjacent to the working electrode, the errors are the greater (for a given J) the smaller the ratio, h/L. This result is surprising because a smaller ratio should decrease the necessary correction. This apparent inconsistency is explained by realizing that the choice of h in the definition of J is arbitrary, and perhaps L would be a more physically significant length in describing the ratio of the ohmic to kinetic resistances. This is indeed true as $h/L \longrightarrow \infty$.

Figure 4 shows $i_o/i_{o,app}$ for linear kinetics and $L \gg h$. For this ratio, errors are always zero for a reference electrode placed at infinity. Three intermediate reference electrode placements are also given. These positions correspond to positions along the insulator where the primary potential difference, $\bar{\Phi}(0,h/2) - \bar{\Phi}(x,h/2)$, is twenty, forty, and eighty percent of $\bar{\Phi}(0,h/2) - \bar{\Phi}(\infty,h/2)$.

Figures 5 and 6 show $i_o/i_{o,app}$ for Tafel kinetics. As chapter 5 discusses, a Tafel plot of data can not be extended through $\delta = 0$ because the cathodic term of the Butler-Volmer equation becomes important. $i_{o,app}$, then, is determined by extrapolating a line of slope $RT/\alpha_a F$ through the Tafel portion of the data. A point near

which the data deviate from this Tafel slope determines the value of δ that gives the correction factor to $i_{o,app}$.

Figures 7 and 8 show $\alpha_a/\alpha_{a,app}$. As $\delta \longrightarrow 0$, $\alpha_a = \alpha_{a,app}$ for any reference electrode placement. For a reference electrode placed adjacent to the edge of the working electrode, $\alpha_a = 2\alpha_{a,app}$ as $\delta \longrightarrow \infty$. This is the same result obtained for the rotating disk electrode. Smyrl and Newman [8] show that this result holds for any reference electrode placed at the edge of a *coplanar* electrode and insulator. For any other reference electrode placement, $\alpha_a = \alpha_{a,app}$ as $\delta \longrightarrow \infty$.

For a reference electrode placed next to an electrode edge, results from chapter 3 can show that, $\alpha_a/\alpha_{a,app} = 2\beta/\pi$ as $\delta \longrightarrow \infty$, where β is the interior angle between the electrode and insulator. The results also show that, for linear kinetics, $i_o \propto i_{o,app}^{2\beta/\pi}$ as $J \longrightarrow \infty$, for a reference electrode placed adjacent to the edge. For Tafel kinetics, $i_o \propto i_{o,app} \cdot i_{avg}^{2\beta/\pi-1}$ as $\delta \longrightarrow \infty$.

The counter and working electrodes have been assumed to be in the same reaction regime and to have identical kinetic parameters. Figure 9 indicates how restrictive this assumption is. It shows $i_o/i_{o,app}$ for a reference electrode placed adjacent to the working electrode for Tafel kinetics and for a counterelectrode with very fast kinetics, very slow kinetics, and with identical kinetics to the working electrode. To simulate slow kinetics, a constant current density is used as the counterelectrode boundary condition. Fast kinetics is simulated by prescribing a current distribution on the

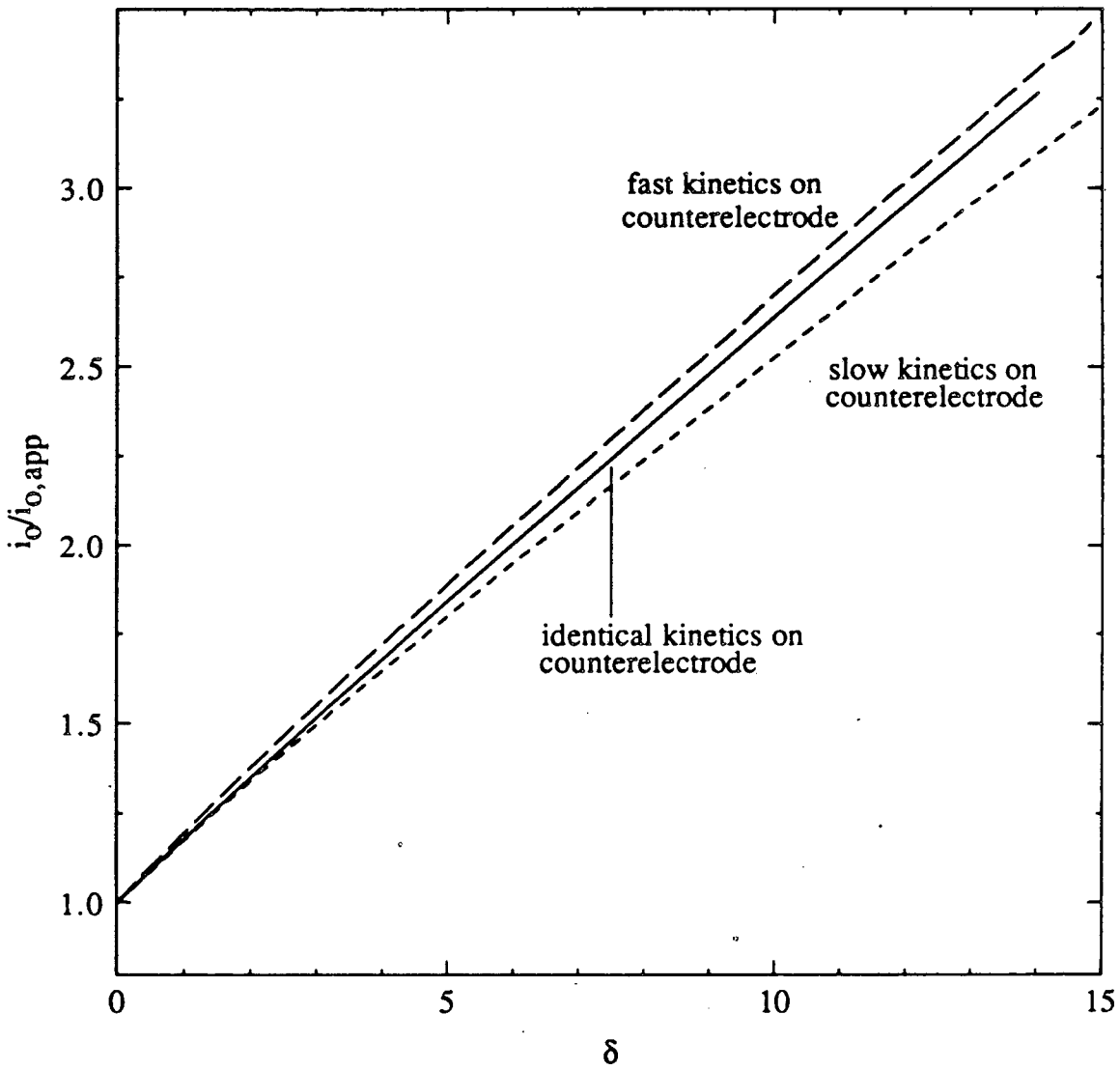

Figure 9. Correction factor to the exchange current densityfor a reference electrode placed adjacent to the working electrode for h/L = 0.5 and slow kinetics, identical kinetics, and fast kinetics on the counterelectrode.

counterelectrode identical to that obtained when the overpotential is zero on both electrodes (what might be called the primary current distribution for this two-electrode system). For other reference electrode placements, the differences are smaller.

Conclusions

Results are given for the interpretation of current-overpotential measurements taken in the linear and Tafel kinetics regimes. They show that a reference electrode should be placed far from the working electrode, and it is shown what can be considered *very far*. We also show the effect that the current distribution on the counterelectrode has on the current distribution on the working electrode. To avoid large ohmic potential drops, it may be necessary to place the reference electrode close to the working electrode. If this procedure is necessary, the apparent kinetic parameters can be corrected.

It is worth noting that uncertainty in the placement of the reference electrode causes greater uncertainties in the interpretation of data for a reference electrode placed closer to the working electrode. This is explained completely by figure 2, which shows that the potential changes most rapidly near the working electrode.

Appendix

We used boundary integral methods, discussed in chapter 2. To facilitate the use of the numerical procedure, the channel geometry was mapped conformally into the geometries shown in figure 10.

Newman [9], [10] followed a similar procedure, except that he mapped the two electrodes so that they are coplanar (which is an intermediate Schwarz-Christoffel transformation used in the conformal mapping given here).

To solve for the current and potential distributions in the transformed geometry, the boundary conditions along the electrodes are (for non-zero h/L)

$$\frac{d\Phi}{dv_r} = f(\Phi_o)\ g_v(v_i), \tag{15}$$

where $f(\Phi_o)$ is given by the right side of equation (4) or (9), and

$$g_v(v_i) = -\frac{h}{\pi}\left[\cosh^2\epsilon - w^2\right]^{\frac{1}{2}}, \tag{16}$$

where

$$w = -j\ \sinh\left[\frac{\pi z}{h}\right] \tag{17}$$

and

$$\epsilon = \frac{\pi L}{2h}. \tag{18}$$

v is related to w through

$$v = -\int_0^w \frac{dw}{(w^2-1)^{\frac{1}{2}}\ (w^2-\cosh^2\epsilon)^{\frac{1}{2}}}. \tag{19}$$

For $h/L = 0$, the boundary condition along the electrode is given by

$$\frac{d\Phi}{dt_i} = f(\Phi_o)\ g_t(t_r), \tag{20}$$

and $g_t(t_r)$ is given by

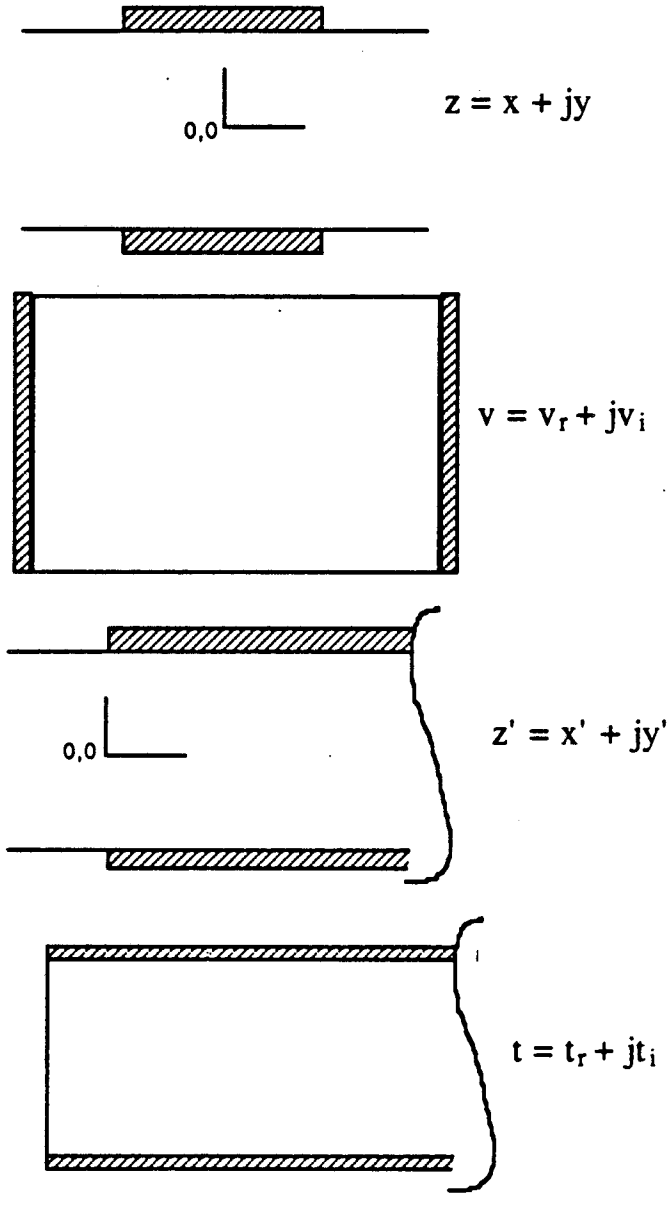

Figure 10. Original and transformed geometries, showing the working and counter-electrodes.

$$g_t(t_r) = -\frac{h}{\pi}\left(1 - e^{-2\pi x'/h}\right)^{1/2} \quad . \tag{21}$$

t is related to z' through

$$t = \sin^{-1}\exp\left(\frac{\pi z'}{h}\right) \quad . \tag{22}$$

z' is related to the original coordinate system by a shift in the origin.

The advantage of using conformal mapping prior to the boundary integral technique is that the mapping tends to provide automatically a mesh spacing appropriate for a given geometry. It can also reduce the time necessary for programming a new problem because many geometries can be mapped into one.

List of Symbols

F	Faraday's constant, 96487 C/equiv
g_t, g_v	functions relating derivatives in the transformed and original coordinate systems
h	interelectrode distance, cm
i	current density, A/cm^2
i_o	exchange current density, A/cm^2
$\bar{i}_{lim}$	average limiting current density, A/cm^2
j	$\sqrt{-1}$
J	dimensionless exchange current density
L	electrode length, cm
R	universal gas constant, 8.3143 J/mol-K
T	absolute temperature, K

t,v,w,z,z'	complex coordinates
V	electrode potential, V
x,y	cartesian coordinates, cm
x',y'	modified coordinate system for h/L = 0, cm
α_a,α_c	transfer coefficients
β	interior angle between insulator and electrode, radians
δ	dimensionless average current density
ϵ	ratio defined by equation (18)
η_s	surface overpotential, V
κ	specific conductivity, $\Omega^{-1}cm^{-1}$
π	3.141592654
Φ	solution potential, V
$\bar{\Phi}$	primary solution potential, V

Subscripts

app	apparent
avg	average
edge	electrode/insulator interface

References

[1] John Newman, "Current Distribution on a Rotating Disk below the Limiting Current," *J. Electrochem. Soc.*, 113, 1235 (1966).

[2] W. H. Tiedemann, J. Newman, and D. N. Bennion, "The Error in Measurements of Electrode Kinetics Caused by Nonuniform Ohmic-Potential Drop to a Disk Electrode," *J. Electrochem. Soc.*, 120, 256 (1973).

[3] Carl Wagner, "Theoretical Analysis of the Current Density Distribution in Electrolytic Cells," *J. Electrochem. Soc.*, **98**, 116 (1951).

[4] W. R. Parrish and John Newman, "Current Distributions on Plane, Parallel Electrodes in Channel Flow," *J. Electrochem. Soc.*, **117**, 43 (1970).

[5] Victoria Edwards and John Newman, "Design of Thin-Gap Channel Flow Cells," *J. Electrochem. Soc.*, **134**, 1181 (1987).

[6] John S. Newman, *Electrochemical Systems*, Prentice-Hall, Englewood Cliffs, N. J. (1973).

[7] John Newman, "Ohmic Potential Measured by Interrupter Techniques," *J. Electrochem. Soc.*, **117**, 507 (1970).

[8] William H. Smyrl and John Newman, "Current Distribution at Electrode Edges at High Current Densities," *J. Electrochem. Soc.*, **136**, 132 (1989).

[9] John Newman, "Engineering Design of Electrochemical Systems," *Ind. Eng. Chem.*, **60**, no. 4, 12 (1968).

[10] John Newman, "The Fundamental Principles of Current Distribution and Mass Transport in Electrochemical Systems," in *Electroanalytical Chemistry*, A. J. Bard, Editor, pp. 187-351, Marcel-Dekker, Inc., New York (1973).

CHAPTER 7
The Ohmic Resistance of a Recessed Disk Electrode

The primary current distribution and ohmic resistance are evaluated for a disk electrode recessed in an insulating plane (see figure 1). The analysis can also be used to determine the ohmic resistance to flow of current through a pore of a separator. Additionally, the errors that might occur by approximating an axisymmetric geometry by its two-dimensional analog are elucidated.

For steady-state diffusion relevant in biological systems, Kelman [1,2] investigated the mathematically identical problem. He used a separation of variables technique that utilizes Bessel functions in the "pore" and Legendre polynomials in the region outside the pore. The coefficients of the two series are determined by matching everywhere along the pore mouth the potential and the z derivative of the potential. He gave a formal solution that is complicated and difficult to use. Furthermore, he does not present his solution in a graphical manner, so it is difficult to evaluate the validity of his solution. We compare his solution for the ohmic resistance of this cell with our calculations, obtained from axisymmetric boundary integral equations.

Analysis

The primary current distribution is valid when concentration variations are negligible and when the resistance of the interfacial reaction is zero. For these conditions, the distribution of current

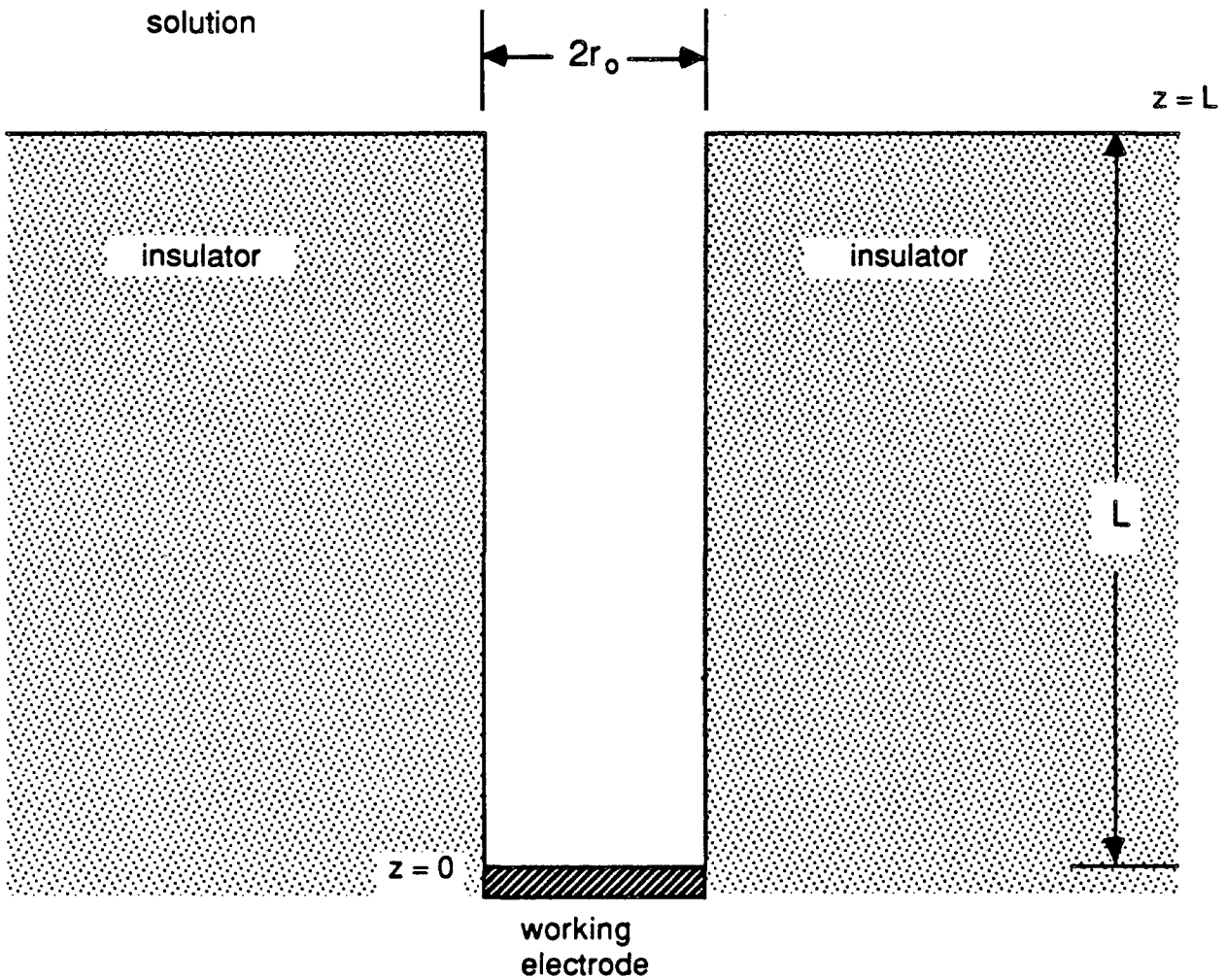

Figure 1. Schematic diagram of a recessed disk electrode.

density and potential is given by Laplace's equation. The boundary conditions are

$$\Phi = 0 \quad \text{as} \quad z^2 + r^2 \longrightarrow \infty, \tag{1}$$

$$\Phi = V \quad \text{at} \quad z = 0 \text{ and } r < r_o, \tag{2}$$

$$\frac{\partial \Phi}{\partial z} = 0 \quad \text{at} \quad z = L \text{ and } r > r_o, \tag{3}$$

and

$$\frac{\partial \Phi}{\partial r} = 0 \quad \text{at} \quad r = r_o \text{ and } 0 < z < L. \tag{4}$$

The outer radius of the insulating plane (at $z = L$) is assumed to be much larger than r_o.

Axisymmetric boundary integral equations were used to solve this problem for various values of the aspect ratio, L/r_o. A summary of the solution procedure is given in Appendix A. The solution for $L/r_o = 0$ is given by Newman [3]. As $L/r_o \longrightarrow \infty$, the current distribution on the electrode is uniform, and the ohmic resistance becomes infinite.

The resistance of this geometry can be approximated by the resistance of a disk electrode (when $L/r_o = 0$) plus the resistance to flow of current along the axis of a tube with insulating walls. The order of magnitude of the correction to this approximation is expected to be the same order of magnitude as the resistance of a disk electrode.

Results and Discussion

The distribution of current density on the electrode is shown in figure 2 for various aspect ratios. Except for the undulations, the current distribution for $L/r_o = 0.01$ might appear to be approximately correct, but an asymptotic analysis, given in Appendix C, indicates that the calculated current density near the edge is likely to be in error by nearly 100 percent. The difficulties in calculating the distribution for small aspect ratios are discussed in Appendix A.

The ohmic resistance R for current flow from the recessed disk to a counterelectrode at infinity can be given by

$$R\kappa r_o = \frac{1}{4} + \frac{L}{\pi r_o} + h(L/r_o). \tag{5}$$

$h(L/r_o)$ is the explicit correction to the estimate of the resistance given by the other two terms. Maxwell [4] estimated an upper bound for $h(L/r_o)$ to be 0.02019, and Rayleigh [5] gave a refined maximum estimate of 0.01235.

Kelman [1,2] gave three asymptotic formulae, valid for different ranges of L/r_o, that can be used to estimate the resistance of the cell. These formulae, when expanded, predict that $h(L/r_o) \longrightarrow 0.011$ as $L/r_o \longrightarrow \infty$, and $h(L/r_o) \longrightarrow 0.067\ L/r_o \ln(L/r_o)$ as $L/r_o \longrightarrow 0$. A preliminary analysis, discussed briefly in Appendix C, also suggests the same relation for small aspect ratios, but the coefficient has yet to be determined. The formulae are shown by the solid line of figure 3.

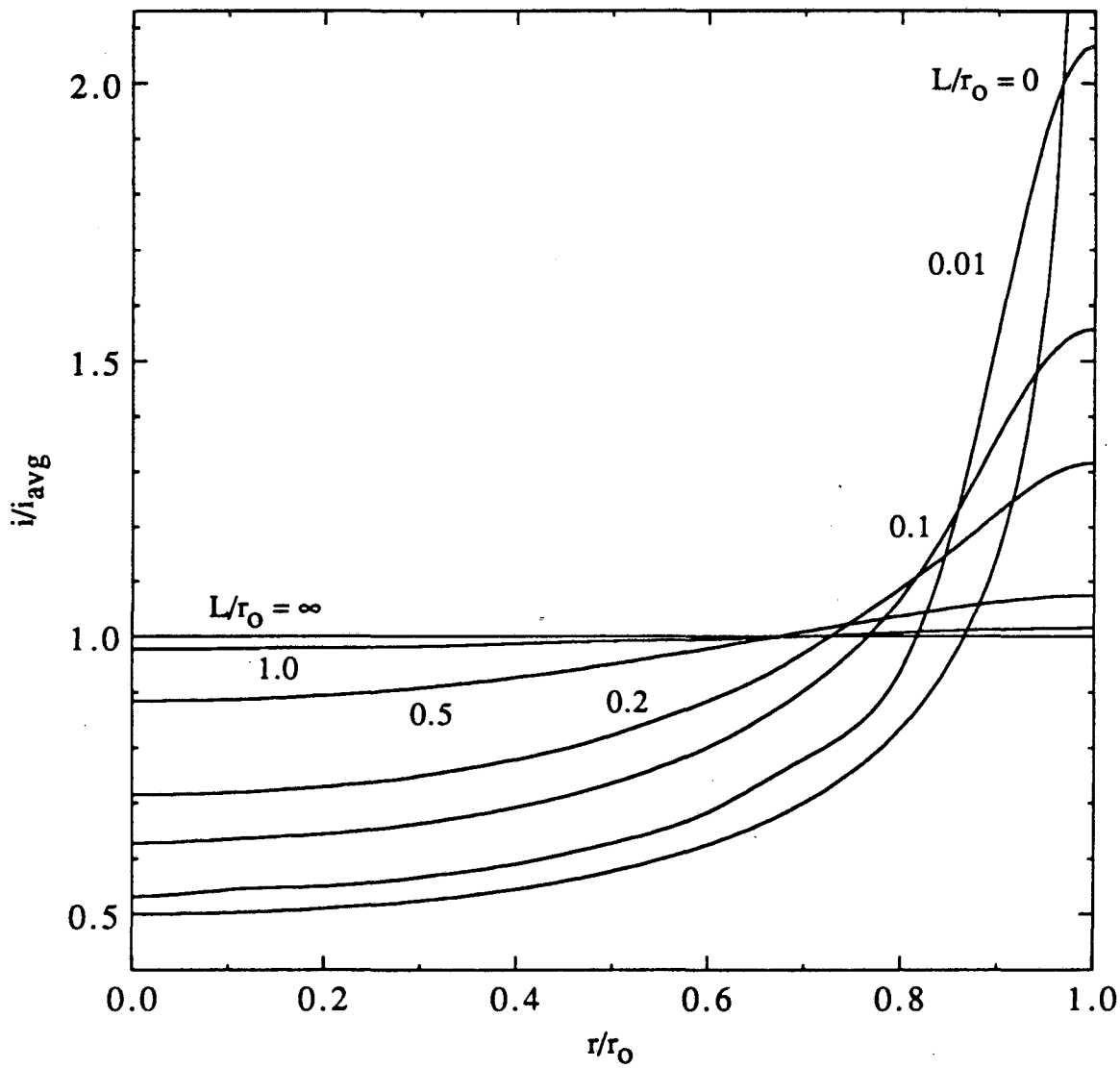

Figure 2. The primary current distribution on a recessed disk electrode for various values of the aspect ratio.

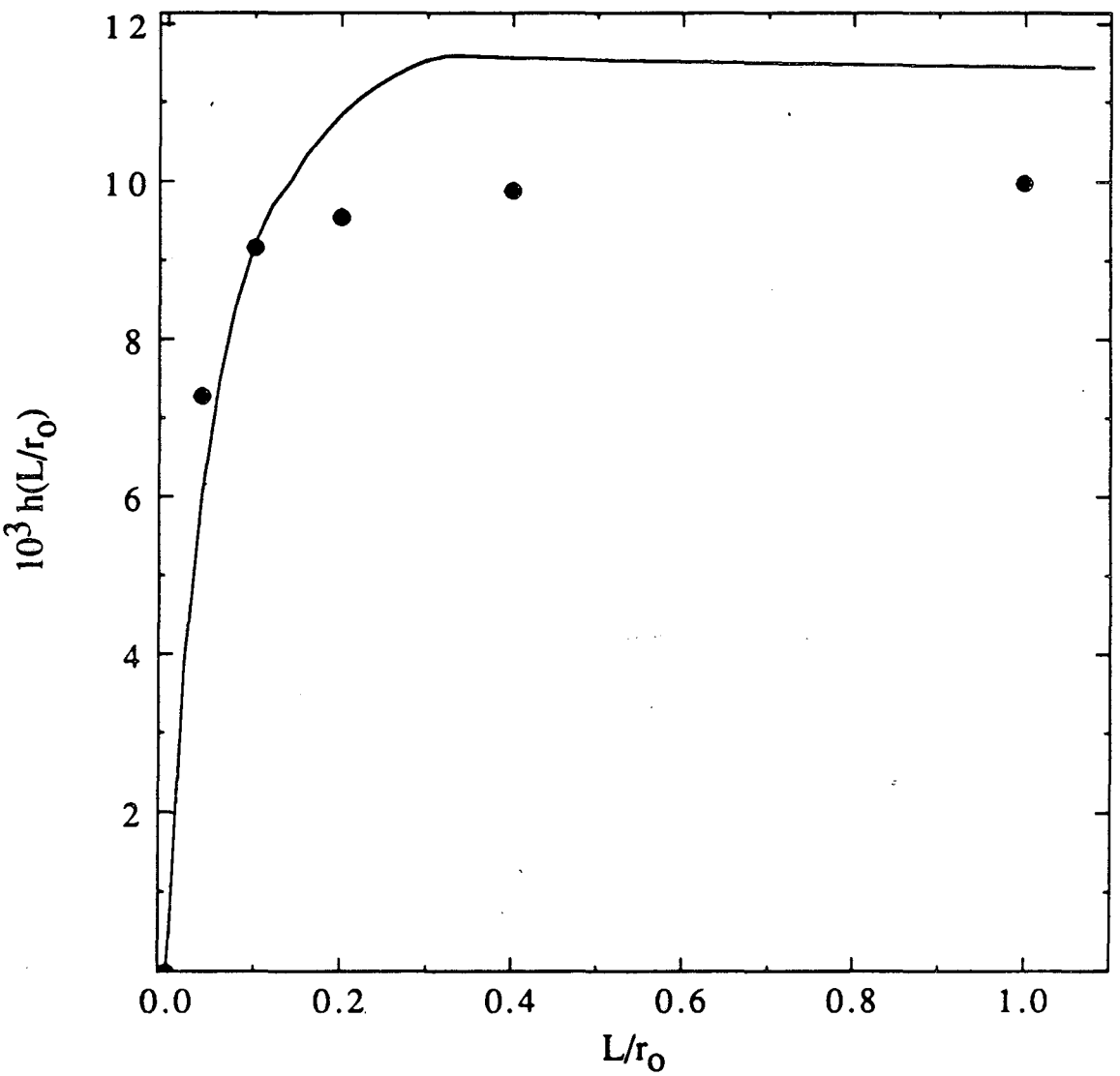

Figure 3. A correction to an estimation of the ohmic resistance of a recessed disk electrode as calculated by Kelman's formulae [1,2] and by the numerical procedure described in Appendix A.

Kelman estimated that these formulae for the resistance give a maximum relative error of 0.0341 in the total current for a set potential difference between the counter and working electrodes. Kelman's estimated error translates into an absolute error for $h(L/r_o)$ of at least 0.0085, larger than or nearly as large as $h(L/r_o)$ itself. The points shown in figure 3 are our numerical results. We calculate that, for $L/r_o = 10$, $h(L/r_o) = 0.011$. Because this problem is relatively expensive to solve, we have not tested thoroughly the validity of our results. For the reasons outlined in Appendix B, one might also be suspicious of Kelman's results. Further work is necessary if more definite conclusions are required. We estimate that the maximum relative error in the resistance, when predicted by the first two terms of equation (5), is 0.03 and occurs near $L/r_o = 0.1$.

Since two-dimensional geometries are often easier to solve (for example, because conformal mapping procedures might be possible), it may be tempting to approximate an axisymmetric geometry with its two-dimensional analog. Such approximations are often rationalized by noting that the current density has the same asymptotic behavior near the edge of an electrode because, in this region, curvature effects can justifiably be neglected. Quantitative agreement is unlikely since the average current density will usually be influenced by curvature.

To elaborate further, the results are compared with results for this geometry's two-dimensional analog, given by Diem *et al.* [6]. The geometry is shown in figure 4, where the geometric ratios held

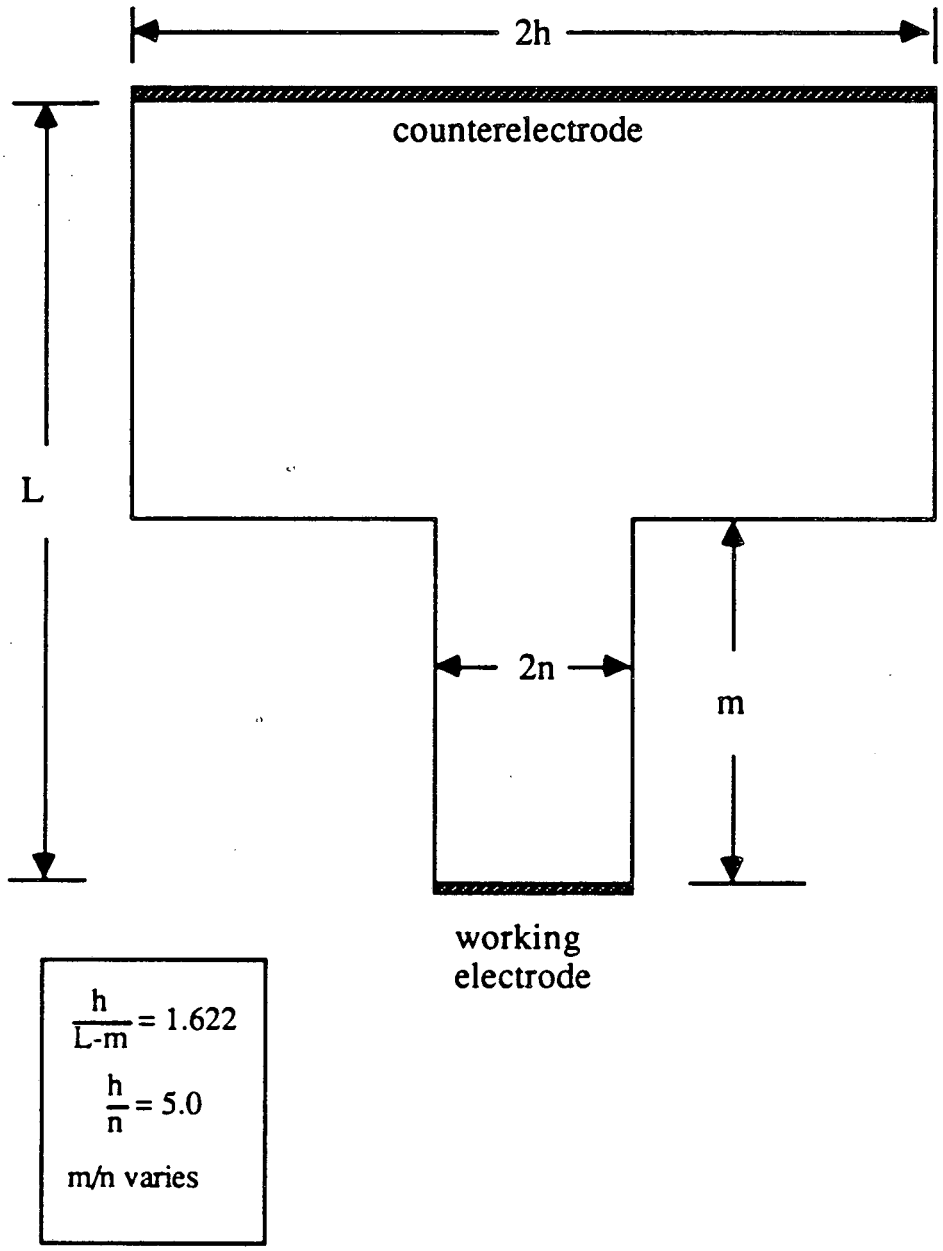

Figure 4. Two-dimensional analog to figure 1. Adapted from reference [6].

constant in their analysis are also given. The ratio m/n is analogous to L/r_o.

Since, in two dimensions, currents can not flow to infinity without an infinite potential drop, the counterelectrode is placed at a finite distance from the working electrode. Placing the counterelectrode too close to the working electrode distorts the current distribution on the supposedly "isolated working electrode." Here, the distortions are minimal, as is seen by comparing $i_{center}/i_{avg} = 0.66$ for $m/n = 0$ with $i_{center}/i_{avg} = 2/\pi$ for an isolated electrode. Comparisons between the two-dimensional and axisymmetric geometries are summarized in table 1. The reported values of $h(L/r_o)$ are based on our analysis. The correction to the ohmic resistance of the two-dimensional cell is given by Diem's Δ_1 and is similar to $h(L/r_o)$. The current distribution for $L/r_o = 0.04$ displayed similar undulations to the distribution shown for L/r_o; therefore, as Appendix C also indicates, the values given for $L/r_o = 0.04$ are suspicious.

A conclusion drawn from table 1 is that an axisymmetric geometry should generally not be approximated by a two-dimensional analog, if quantitative results are desired. If only qualitative results are required, numerical calculations may be unnecessary.

Conclusions

The primary current distribution and ohmic resistance for various aspect ratios are given. The results can be used to design a

Table 1. A comparison between results for two-dimensional and axisymmetric geometries.

$\frac{L}{r_o}$	i_{center}/i_{avg}		i_{edge}/i_{avg}		$h(L/r_o)$	
	2-D	axi	2-D	axi	2-D	axi
0.0	0.66	0.5	∞	∞	0.0	0.0
0.04	0.70	0.56	2.87	1.89	0.013	0.0059
0.2	0.79	0.71	1.47	1.32	0.031	0.0092
0.4	0.87	0.84	1.18	1.10	0.036	0.0099
2.5	1.0	1.0	1.0	1.0	0.037	0.011
∞	1.0	1.0	1.0	1.0	0.037	0.011

cell that would have an approximately uniform current distribution in the absence of concentration variations. With convection, the mass-transfer limited current distribution can be nonuniform.

Appendix A. The Solution Procedure

Equations (14) through (19) of chapter 2 give an expression for the potential on the boundary. Finite-difference approximations of these equations were solved with an iterative procedure. The problem was solved as one with a prescribed current distribution on the electrode. Corresponding distributions of potential on the working electrode were superimposed until the constant boundary condition was satisfied.

The current distributions that were superimposed are

$$\frac{\partial \Phi}{\partial z} = P_{2n}\left[\sin\left[\frac{\pi r}{2r_o}\right]\right], \tag{A.1}$$

where P_{2n} are the even Legendre polynomials. It was found that the polynomials from $2n = 0$ to $2n = 24$ were sufficient. Additional polynomials did not change appreciably the distribution. The argument for the polynomials is chosen so that the radial derivative of the current density is zero at the center and edge of the electrode. The recurrence formula used to evaluate the polynomials is given in Hildebrand [7] and Abramowitz and Stegun [8].

The undulations in the current distribution for $L/r_o = 0.01$ are caused by inaccuracies in the numerical procedure. A more natural set of functions to describe the current density is suggested by Kelman [1,2]:

$$\frac{\partial \Phi}{\partial z} = A_o + \sum_{n=1}^{N} A_n J_o(\alpha_n r/r_o) \ , \tag{A.2}$$

where $J_o(x)$ is the Bessel function of the first kind of order zero, and α_n is the n^{th} root of $J_1(x)$. By letting $N = 12$, we determined the current distribution for $L/r_o = 0.01$. Abramowitz and Stegun [9] gave approximations for $J_o(x)$. The resulting current distribution is nearly identical (including the undulations) to the distribution shown in figure 2. This indicates that the inaccuracy is not caused by the choice of current functions. The reason that such inaccuracies exist is suggested by chapters 2 and 3. For such small aspect ratios, the *edge* regions are not completely isolated, and it is not

obvious where the asymptotic behavior dictated by one angle of intersection ends and the other begins. We did not pursue this problem in greater detail because it is relatively expensive to solve. Appendix C provides a starting point for a more involved investigation of the behavior of the current distribution for small aspect ratios.

For this cell geometry, other techniques [10] for determining the current density on an electrode with a constant potential boundary condition might give accurate solutions. For cells with obtuse angles of intersection between the electrode and insulator, the infinite current densities that arise can not be calculated accurately unless the correct form of the singularity is imbedded into the problem. Miksis and Newman [11] and Pierini and Newman [12] followed this procedure.

One alternative to the solution procedure outlined above is to solve directly for the gradient of the potential. The gradient of equation (5) of chapter 2 is

$$-\alpha_3 \nabla_q \Phi = \int_{\partial V} \left[-\frac{\partial \Phi}{\partial n} \frac{1}{\xi_3^2} \nabla_q \xi_3 + \Phi \left[\frac{1}{\xi_3^2} \nabla_q \left[\frac{\partial \xi_3}{\partial n} \right] - \frac{2}{\xi_3^3} \frac{\partial \xi_3}{\partial n} \nabla_q \xi_3 \right] \right] dA, \qquad (A.3)$$

where ∇_q emphasizes that we are taking the gradient with respect to x_q, y_q, z_q.

A specific form of equation (A.3) was used to determine the current distribution on the counterelectrode in the slotted-electrode cell of chapter 4. The solution procedure worked, but the calculated current density near the edge was very sensitive to the placement of

the nodes.

For the recessed disk, after the θ dependence of equation (A.3) is eliminated, the z derivative of the potential along the disk can be described by

$$\frac{\partial \Phi}{\partial z_q} = \frac{2}{\pi} \int_{r_o}^{\infty} \frac{(\Phi - V) E(m) r dr}{((r-r_q)^2+L^2)((r+r_q)^2+L^2)^{1/2}} \tag{A.4}$$

$$- \frac{2}{\pi} \int_{r_o}^{\infty} \frac{(\Phi - V) r L^2}{((r+r_q)^2+L^2)^{3/2}((r-r_q)^2+L^2)} \left[\frac{4E(m)(r^2+r_q^2+L^2)}{(r-r_q)^2+L^2} - K(m) \right] dr$$

$$+ \frac{3}{\pi} \int_0^L \frac{(\Phi - V) E(m) z dz}{((r_o-r_q)^2+z^2)((r_o+r_q)^2+z^2)^{1/2}}$$

$$+ \frac{2}{\pi} \int_0^L \frac{(\Phi - V) z (r_o^2 - r_q^2 - z^2)}{((r_o-r_q)^2+z^2)((r_o+r_q)^2+z^2)^{3/2}} \left[\frac{2(r_o^2+r_q^2+z^2)E(m)}{(r_o-r_q)^2+z^2} - \frac{K(m)}{2} \right] dz$$

We did not have great success with equation (A.4). Away from $r = r_o$, the current distribution gave what appeared to be the correct behavior, but, near the edge, the current distribution was very sensitive to the node placement. Because this equation is relatively expensive to solve and other solution procedures were available, we did not investigate thoroughly why equation (A.4) caused difficulties. For the case of $L/r_o = 0$, equation (A.4) reduces to equation (23) of chapter 2, which, when integrated numerically, showed good agreement with the known, analytic solution.

A situation may arise where the procedure described here is the best method. We have, therefore, documented our efforts in the hope

that they may be useful.

Appendix B. A Discussion of Kelman's Analysis

Near $z = L$, $r = r_o$ (see figure 1), Laplace's equation can be solved to show that

$$\Phi(\rho,\theta) \propto \rho^{2/3}\cos(2\theta/3), \tag{B.1}$$

where ρ is the radial distance from the singular point and θ is the angular coordinate with $\theta = 0$ corresponding to $z = L$, $r > r_o$ and $\theta = \frac{3\pi}{2}$ corresponding to $r = r_o$, $z < L$. This implies that along the mouth of the pore,

$$\lim_{r \to r_o} \frac{\partial \Phi}{\partial z} \propto \rho^{-1/3}, \tag{B.2}$$

which is singular at $r = r_o$. A corresponding behavior for the radial derivative of potential prevails on the insulating plane near the opening.

We can ask whether Kelman's two series can give this behavior. Inside the pore, his expression for the current density at $z = L$ can be written as

$$\frac{\partial \Phi}{\partial z} = A_o + \sum_{n=1}^{\infty} A_n J_o(\alpha_n r/r_o). \tag{B.3}$$

Since the Bessel functions $J_o(x)$ are well-behaved, it is difficult for this series to converge for all $r \neq r_o$ and still to give the correct asymptotic behavior near $r = r_o$.

In the outer region, his expression for the current density can be written as

$$\frac{\partial \Phi}{\partial z} = \frac{1}{\eta} \sum_{n=0}^{\infty} B_n P_{2n}(\eta), \tag{B.4}$$

where $\eta = (1 - r^2/r_o^2)^{1/2}$. Since the $P_{2n}(\eta)$ are well-behaved, equation (B.4) is also unlikely to converge for all $r \neq r_o$ and to give the correct asymptotic behavior near $r = r_o$. Note that, when $L/r_o = 0$, the nature of the singularity changes, and the solution is valid because the term multiplying the summation goes to infinity in the correct manner as $r \longrightarrow r_o$.

In summary, we indicate that the "solution" given by Kelman is not reasonable because the series represented by equations (B.3) and (B.4) do not have the correct asymptotic behavior. This does not imply that Kelman's results should be completely disregarded because numerical solutions that are clearly in error near a singular point have been observed to be approximately correct over the remainder of the domain.

Appendix C. Small Aspect Ratios

Away from the electrode edge, for very small aspect ratios, the current distribution is indistinguishable from the current distribution for $L/r_o = 0$. Near the edge, the deviation from a zero aspect ratio has a major influence on the distribution. In this region, the curvature of the axisymmetric geometry can be neglected, and the problem can be considered two dimensional. Hence, the treatment given here is applicable for both the recessed disk and the two-dimensional analog, shown in figure 4.

To investigate the region near the edge, we used conformal mapping to obtain a solution to Laplace's equation. The current distribution on the electrode is described by

$$-\kappa \frac{\partial \Phi}{\partial \bar{y}} = \frac{\sqrt{\pi L/2}\ P_o}{\sqrt{1-u}}, \tag{C.1}$$

where the coordinates are shown in figure 5, and w and z are related through

$$\bar{z} = \frac{z}{L} = \frac{2}{\pi} \frac{w\sqrt{w-1}}{\sqrt{w}} + \frac{1}{\pi} \ln\left[\frac{\sqrt{w-1} - \sqrt{w}}{\sqrt{w-1} + \sqrt{w}}\right], \tag{C.2}$$

P_o is the parameter introduced by Smyrl and Newman [13] and generalized in chapter 3. To apply equations (C.1) and (C.2) to the two-dimensional analog, L should be replaced with m. For the recessed disk,

$$P_o = \sqrt{r_o/8}\ i_{avg}. \tag{C.3}$$

and, for the two-dimensional analog in the case where $L - m \gg n$,

$$P_o = \frac{\sqrt{2n}}{\pi}\ i_{avg}. \tag{C.4}$$

Equations (C.1), (C.3), and (C.4) show that the current distribution near the edge is inversely proportional to the square root of the aspect ratio. When evaluated at $u = 0$, equation (C.1), with P_o given by equation (C.4), is in good agreement with the result for $m/n = 0.04$. Equations (C.1) and (C.3) cast serious doubt on the current distribution calculated for $L/r_o = 0.01$. Current distributions, as given by equations (C.1) through (C.3), are shown in figure 6 for various, small aspect ratios.

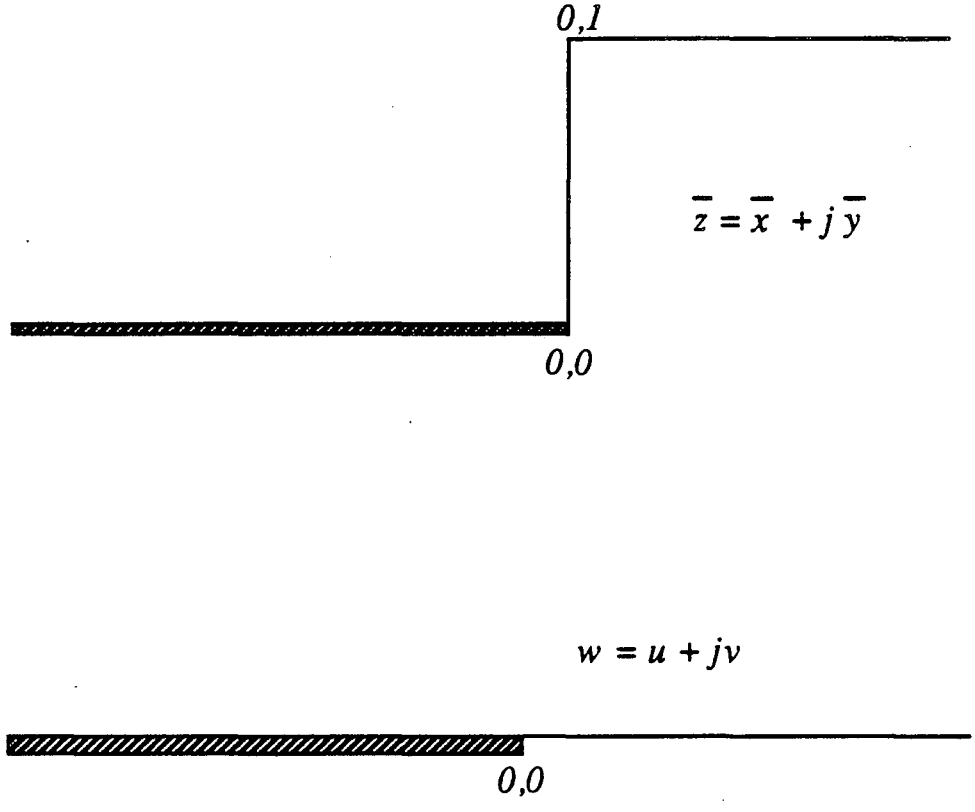

Figure 5. The original and transformed coordinate systems used to elucidate the current distribution near the edge of a recessed disk for small aspect ratios. The mapping is achieved by requiring that

$$\frac{d\bar{z}}{dw} = \frac{2}{\pi}\frac{\sqrt{w-1}}{\sqrt{w}}.$$

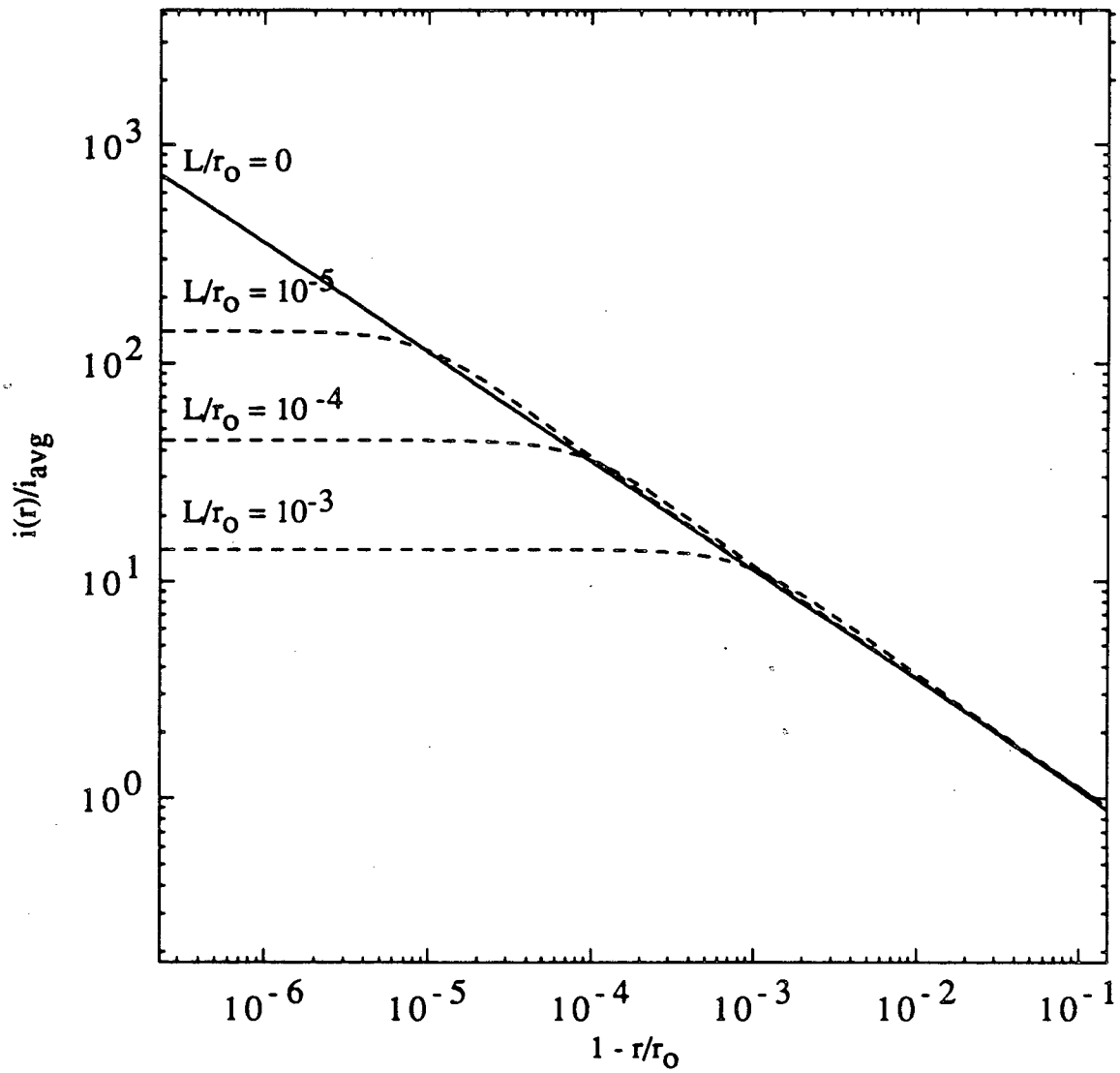

Figure 6. The distribution of current density, valid for small aspect ratios, near the edge of a recessed disk. The dashed lines were obtained from equations (C.1) (C.2), and (C.3), and the solid line is the primary current distribution for a disk electrode, as given by Newman [3].

To design an accurate, boundary-integral procedure for a complete study of the current distribution on a recessed disk, it is important to have an *a priori* estimate of the potential distribution along the insulating wall and plane near the pore mouth. This analysis gives

$$\frac{\kappa(V - \Phi)}{r_o i_{avg}} = \sqrt{u/\pi}, \tag{C.5}$$

where, on the insulating wall, u and $\bar{y}$ are related through

$$\frac{y}{L} = \frac{2}{\pi}(u - u^2)^{1/2} + \frac{1}{\pi}\tan^{-1}\left[\frac{2(u - u^2)^{1/2}}{1 - 2u}\right]. \tag{C.6}$$

Along the insulating plane, $\bar{x}$ and u are related through

$$\frac{x}{L} = \frac{2}{\pi}(u^2 - u)^{1/2} + \frac{1}{\pi}\ln\left[\frac{\sqrt{u} - \sqrt{u-1}}{\sqrt{u} + \sqrt{u-1}}\right]. \tag{C.7}$$

These equations can be expanded to show that the tangential gradients of potential satisfy the proportionality (B.2) near the singular point.

We should also be able to determine, in general, the order of magnitude of the correction to the resistance, but, to date, we have been unsuccessful. The evidence, though, strongly suggests

$$\lim_{L/r_o \to 0} h(L/r_o) \propto L/r_o \ln(L/r_o). \tag{6}$$

This result agrees with Kelman's analysis and is partly arrived at by determining the ohmic resistance of a recessed, planar electrode, similar to the cell in figure 4, with the counterelectrode replaced with a hemicylinder at a distance very far from the counterelectrode.

To determine the correction to the ohmic resistance for this cell, the mappings shown in figure 7 are useful. When the constants a and C are related to m and n, the ohmic resistance of the cell can be determined. For small m/n, these constants are given by

$$m = \frac{\pi}{2} aC \tag{C.8}$$

and

$$n = C\ (1 - \frac{a}{2} \ln a\ ). \tag{C.9}$$

With these relations it can be shown that

$$\lim_{m/n \longrightarrow 0} h(m/n) = -\frac{1}{\pi^2} \frac{m}{n} \ln(m/n), \tag{C.10}$$

which is in good agreement with the results given by Diem *et al.* [6].

List of Symbols

A_n, B_n	coefficients in a series
$h(L/r_o)$	correction to estimate of cell resistance
i	current density, A/cm^2
J_o	Bessel function of the first kind of order zero
L	wall length, cm
m/n	ratio of lengths, given by figure 4
P_{2n}	even Legendre polynomials
r, z	cylindrical coordinates
r_o	radius of the disk electrode, cm
R	cell resistance, ohm
V	electrode potential, V

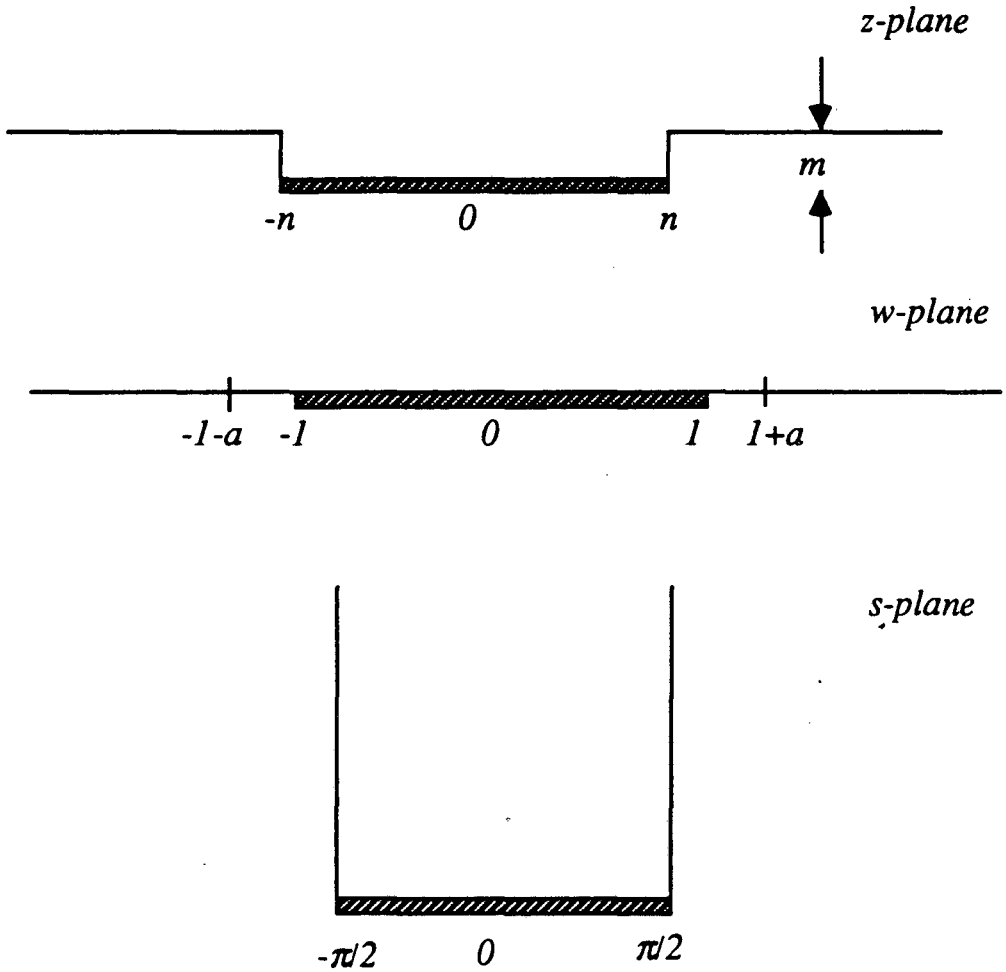

$$\frac{dz}{dw} = C\,\frac{\sqrt{w\text{-}1\text{-}a}\,\sqrt{w+1+a}}{\sqrt{w\text{-}1}\,\sqrt{w+1}}$$

$$w = \sin(s)$$

Figure 7. A schematic of the mappings used to determine the ohmic resistance of a recessed, planar electrode, with a counterelectrode placed at a distance very far from the working electrode. Also shown are the coordinate transformations that provide the mappings.

η	rotational elliptic coordinate used in equation (B.4)
κ	specific conductivity, $\Omega^{-1}cm^{-1}$
π	3.141592654
ρ, θ	cylindrical coordinates used near $r = r_o$, $z = L$
Φ	solution potential, V

Subscripts

avg	average
center	center
edge	edge
q	denotes a point at which the potential is solved

References

[1] R. B. Kelman, "Axisymmetric Potentials in Composite Geometries: Finite Cylinder and Half Space," *Contr. Diff. Eqs.*, 2, 421 (1963).

[2] R. B. Kelman, "Steady-State Diffusion Through a Finite Pore into an Infinite Reservoir: An Exact Solution," *Bull. Math. Biophysics*, 27, 57 (1965).

[3] John Newman, "Resistance for Flow of Current to a Disk," *J. Electrochem. Soc.*, 113, 501 (1966).

[4] James Clerk Maxwell, *A Treatise on Electricity and Magnetism*, vol. 1, pp 431-434, 3rd edition, Clarendon Press, Oxford (1904).

[5] John William Strutt Rayleigh, *Theory of Sound*, vol. 2, pp. 487-491, republication of the 2nd edition, Dover, New York (1926).

[6] Conrad B. Diem, Bernard Newman, and Mark E. Orazem, "The Influence of Small Machining Errors on the Primary Current Distribution at a Recessed Electrode," *J. Electrochem. Soc.*, 135, 2524 (1988).

[7] Francis B. Hildebrand, *Advanced Calculus for Applications*, p. 158, Prentice-Hall, Inc., Englewood Cliffs, N. J. (1976).

[8] M. Abramowitz and I. Stegun, *Handbook of Mathematical Functions*, p. 333, National Bureau of Standards, Washington (1964).

[9] M. Abramowitz and I. Stegun, *ibid.*, p. 369.

[10] B. D. Cahan, Daniel Scherson, and Margaret A. Reid, "I-BIEM. An Iterative Boundary Integral Equation Method for Computer Solutions of Current Distribution Problems with Complex Boundaries—A New Algorithm," *J. Electrochem. Soc.*, 135, 285 (1988).

[11] Joseph J. Miksis, Jr., and John Newman, "Primary Resistances for Ring-Disk Electrodes," *J. Electrochem. Soc.*, 123, 1030 (1976).

[12] Peter Pierini and John Newman, "Potential Distribution for Disk Electrodes in Axisymmetric Cylindrical Cells," *J. Electrochem. Soc.*, 122, 1348 (1979).

[13] William H. Smyrl and John Newman, "Current Distributions at Electrode Edges at High Current Densities," *J. Electrochem. Soc.*, 136, 132 (1989).

CHAPTER 8
The Dissolution Kinetics of $FeSO_4$ Films

Introduction

The dissolution of iron in sulfuric acid has been extensively investigated. Russell [1], [2] and Haili [3] recently reviewed these studies. The most significant development that has arisen since their reviews is the recognition of the importance of certain, universal phenomena observed in nonlinear systems. These lines of inquiry may provide the means to analyze data and to compare quantitatively experiments with numerical simulations. Papers that are relevant to iron dissolution include [4], [5], and [6].

Sustained periodic and aperiodic dynamic behavior, which occurs in a potential range within the limiting current plateau which is presumably caused by a ferrous-sulfate film, is one of the more interesting phenomena observed in this system. Russell and Newman [1], [2] attempted to explain this behavior. Their work is probably the most complete theoretical investigation of such problems. Coupled transport equations within the ferrous-sulfate film and in the bulk electrolyte were used. One assumption in their model is that the concentration of ferrous ions at the solution/salt-film interface is equal to the saturation value. The goal of the experiments discussed here is to test the validity of this assumption. If it is not valid, a kinetic rate constant that could be used to describe the rate of dissolution might be determined. If the results indicate that it is necessary, a rather minor modification of Russell and

Newman's model could be made, and better agreement between experiments and theory might be possible. Otherwise, more extensive modifications to the model are necessary.

We use a ring-disk electrode system, where ferrous ions produced by the dissolution of the iron disk electrode or by the dissolution of the $FeSO_4$ film are oxidized on a plat-inum ring. After the inter--ruption of current on the disk, the ferrous-sulfate film dissolves and is the only source of Fe^{2+}. Through the collection efficiency, the rate of dissolution of the salt film might be estimated. Previously, Okinaka [7] used a similar procedure to estimate the dissolution kinetics of a cadmium-hydroxide film in concentrated, alkaline solution. For the conditions that he investigated, the films dissolved over a time of the magnitude of hundreds of seconds. Prater and Bard [8] modeled the transient response of the ring current after a step change in the disk current. They showed that, after the interruption of disk current, the ring current, if the only available reactant is produced at the disk, will decay to zero in a time of roughly

$$t \approx 5.0\ Sc^{1/3}\ \omega^{-1}, \tag{1}$$

where Sc is the Schmidt number and ω is the rotation speed of the disk. Hence, if the rate of dissolution of the $FeSO_4$ film is to be determined with this experiment, its time constant for dissolution should be greater than a second.

When these experiments were carried out at room temperature, the current on the ring decayed to zero within a time consistent with the

model of Prater and Bard. It is, therefore, not possible to deduce from these experiments any quantitative information about the dissolution kinetics of the ferrous-sulfate film. Since the rate of a reaction is expected to decrease significantly with temperature, we repeated the experiments at 0°C, and we, again, obtained no quantitative information about the dissolution kinetics. In the remainder of the chapter, we describe the experimental procedure and briefly discuss the implications that these results have on further modeling efforts.

Experimental Procedure

The rotating ring-disk electrode consisted of an iron disk with a 0.4 cm diameter and a platinum ring with an inner diameter of 0.75 cm and an outer diameter of 0.85 cm. All experiments used 1 M sulfuric acid solutions. The glass cell that was used was shown and described by Russell and Newman [9]. The temperature was controlled with a constant-temperature bath at 25.0±0.1°C or 0.0±0.3°C. Before each experiment, N_2 was bubbled through the electrolyte for 1 to 2 hours, and the ring-disk electrode system was polished with 9, 3, and 1 micron diamond paste.

All experiments used a Hg/Hg_2SO_4 reference electrode and a platinum counterelectrode, both placed at distances very far from the working electrode. The ring-disk rotation speed was set at either 83.8 or 41.9 sec^{-1}. The potential of the disk was slowly swept until current oscillations were observed. The potential was then slowly decreased until the oscillations stopped. The ring electrode was set

at a potential so that the oxidation of the ferrous ions was clearly at a limiting current. Once the disk and ring currents were steady, the potential of the disk was stepped to a potential near -1.0 V. The ring and disk currents were recorded with a Nicolet digital oscilloscope.

Results and Discussion

The theoretical collection efficiency, when it is taken into consideration that the disk electrode reaction involves two electrons and the ring electrode reaction involves one, is 0.108 [10]. As was briefly discussed in the Introduction, the time constant for dissolution of the film was found to be at least as small as the time constant described by Prater and Bard [8]. The experiments were therefore repeated at 0°C. Polarization curves obtained at two different sweep rates with the ring at open circuit are shown in figure 1. The behavior was qualitatively the same as that observed at room temperature. Complicated dynamic behavior appeared at the slower sweep rate, and, if the potential was held constant in this range, sustained unsteady behavior was observed.

Figure 2 shows a typical ring-disk experiment. The time lag observed on the ring electrode is consistent with the predictions of Prater and Bard [8]. Prater and Bard showed the effects of varying the ratios of the three characteristic radii of a ring-disk system. It can be seen that, even with a very small gap between the disk and ring, the time constant is probably too large to obtain information about the dissolution kinetics of $FeSO_4$.

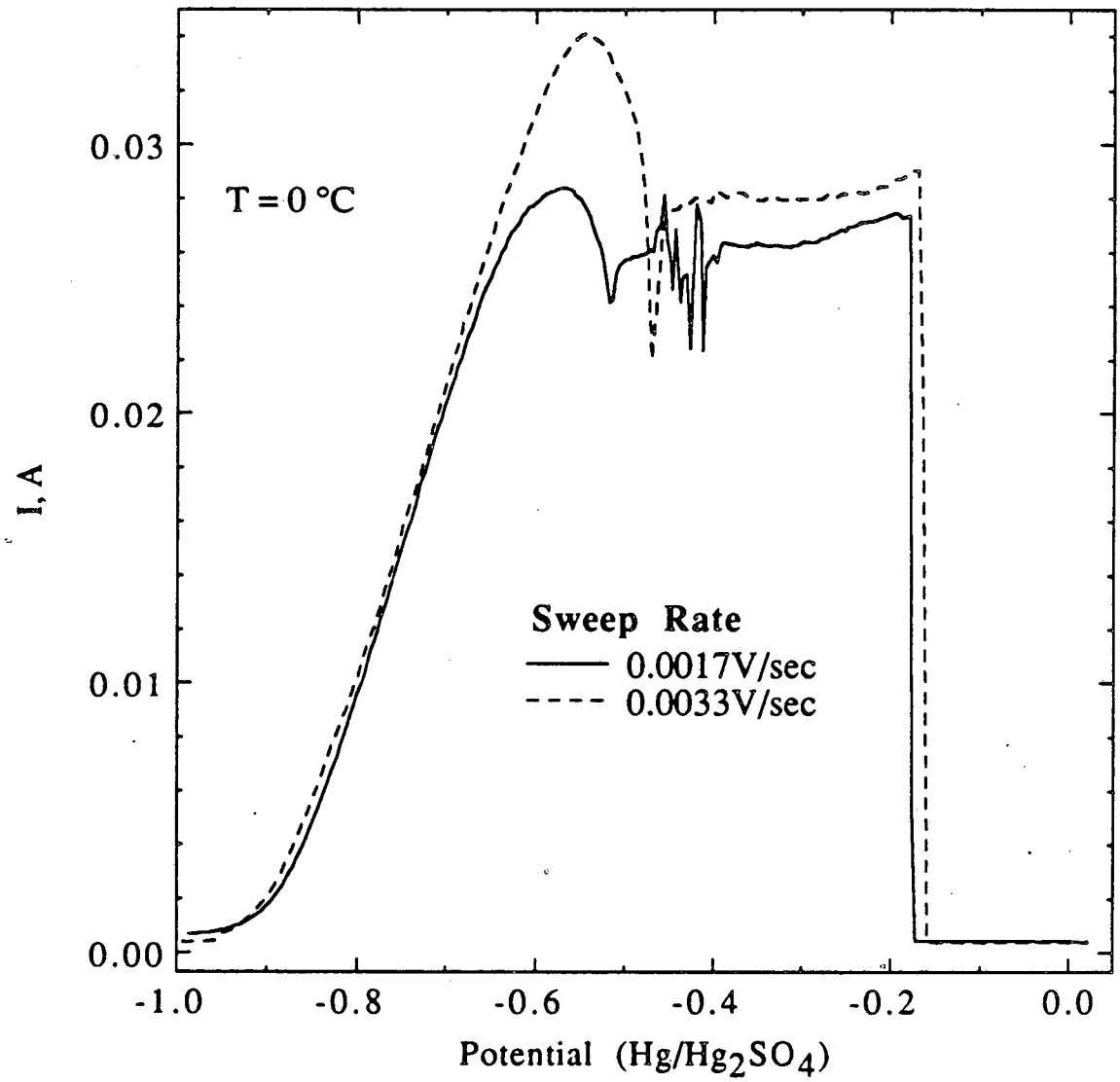

Figure 1. Polarization curves for iron dissolution at a rotation speed of 41.9 sec^{-1}.

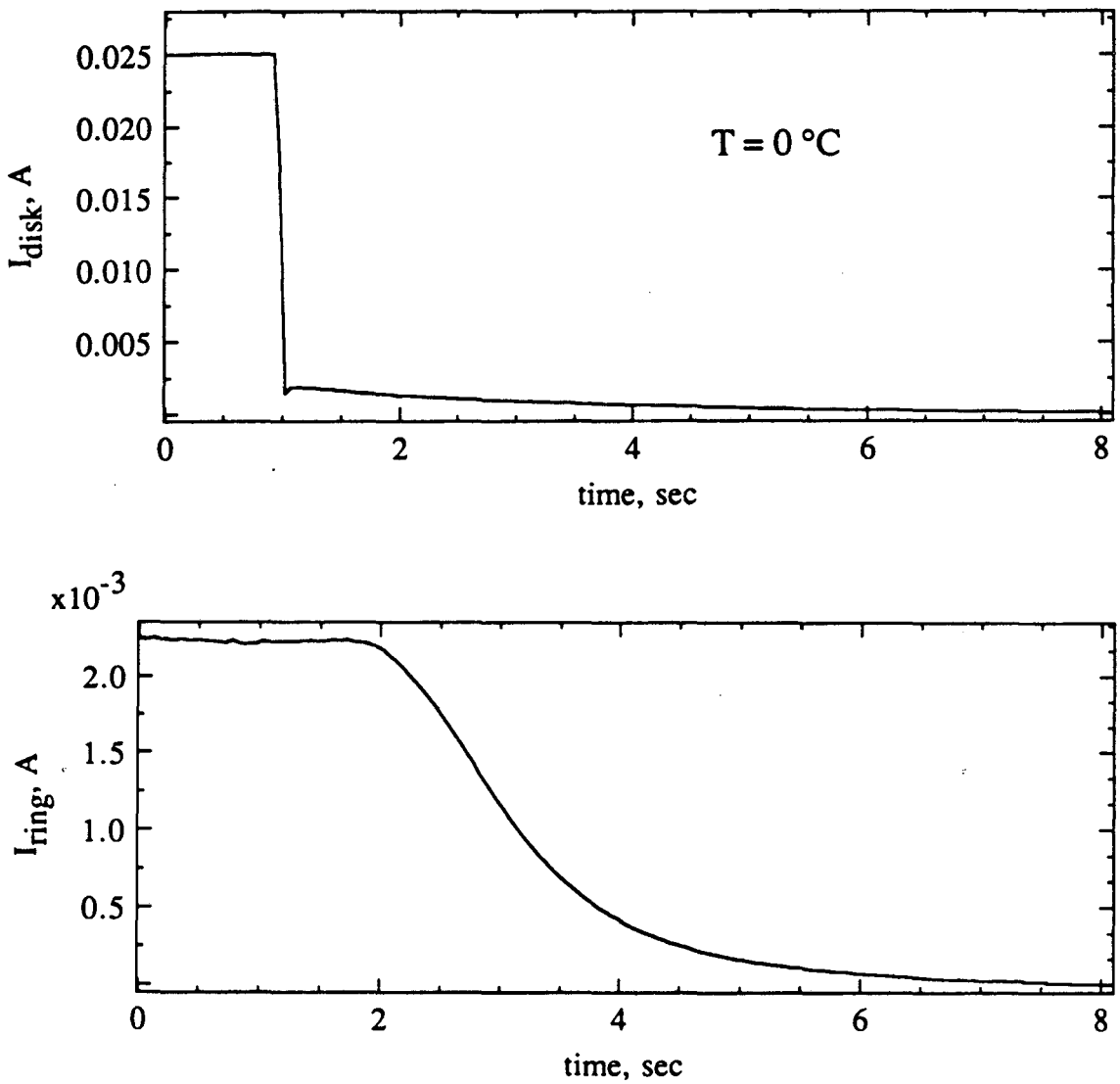

Figure 2. A typical ring-disk experiment at a rotation speed of 41.9 sec^{-1}.

Any attempt to estimate a rate constant from these experiments would be meaningless. The rate of dissolution of a salt film can often be described by [11]

$$N_{Fe^{2+}} = k_d(c_{sat} - c_o), \tag{2}$$

where c_o is the concentration of ferrous ions at the film/solution interface and c_{sat} is the equilibrium concentration of Fe^{2+}. If k_d is very large, this reaction can be considered mass-transfer limited. More specifically, for the rotating-disk electrode, if $\frac{D}{\delta k_d}$ is very small, the kinetics of dissolution can be neglected. D is the diffusion coefficent of Fe^{2+}, and δ provides an estimate of the size of the mass-transfer boundary layer and is given by [12]

$$\delta = 1.61\ Sc^{-1/3}\sqrt{\nu/\omega}\ . \tag{3}$$

Since even at 0°C the rate of dissolution of the $FeSO_4$ is fast enough that it could not be measured, it is unlikely that the simplified boundary condition used by Russell and Newman is a major source of discrepancy between theory and experiment. More complicated changes, therefore, are necessary to obtain agreement. For example, radial variations in the potential and surface concentration might need to be accounted for more accurately, or perhaps it may be necessary to account more explicitly for changing film porosity.

As a further check on the rate of dissolution of the salt film, the concentration of the Fe^{2+} at the film/solution interface could be estimated from the ring current and the theoretical collection efficiency. The surface concentration c_o, using the theoretical

collection efficiency, would be estimated by

$$c_o = \frac{\delta}{2FDA} \frac{I_{ring}}{0.108}, \tag{4}$$

where A is the surface area of the disk and F is Faraday's constant. Using Russell and Newman's [13] estimates of D and ν, we estimate for the experiments at 25°C that $c_o = 3.3 \pm 0.1$ M for $\omega = 83.8$ sec^{-1} and that $c_o = 3.4 \pm 0.1$ M for $\omega = 41.9$ sec^{-1}. These concentrations are greater than 1.88 M, the estimated saturation value.

This discrepancy is explained by figure 5 of Russell and Newman. It shows that the pH increases significantly in the mass-transfer boundary layer and that the concentration of Fe^{2+} is around an order of magnitude greater than the concentration of H^+. Hence, a term accounting for migration must be included in equation (4). Using the physical property data given by Russell and Newman [13], the surface concentration of the ferrous species was determined with a modified version of program MIGR [14]. In the first case, it was assumed that the H_2SO_4 dissociated into H^+ and SO_4^{2-}, and in the second case, the supporting ionic species were assumed to be H^+ and HSO_4^-. For the first case, the surface concentration was found to be 2.3 M, and, for the second case, the surface concentration was found to be 1.6 M. The actual concentration at the surface should be intermediate between these two values.

Because of the complexity of the solution chemistry and limited physical property data, it is not possible to determine precisely the surface concentration of Fe^{2+}. Consequently, the most important con-

clusion from these results is that the concentrations obtained from the two different rotation speeds are the same to within the experimental uncertainty. This confirms that the rate of dissolution of $FeSO_4$ can be considered mass-transfer limited.

Conclusions

The kinetics of dissolution of ferrous-sulfate films in a sulfuric acid medium is sufficiently fast that it can be considered mass-transfer limited. It is valid in most models to assume that the concentration of ferrous ions adjacent to the salt film is given by its saturation value. Thus, for Russell and Newman's model to show better agreement with experiments, it is most likely necessary to switch to a two-dimensional model. Simulations of dynamic behavior may, therefore, be quite expensive.

List of Symbols

A	surface area of the disk electrode, cm^2
c_o	concentration of Fe^{2+} at the film/solution interface, mol/cm3
c_{sat}	saturation concentration of Fe^{2+}, mol/cm^3
D	diffusion coefficient, cm^2/sec
F	Faraday's constant, 96487 C/equiv
I	current, A
k_d	dissolution rate constant, cm/sec
$N_{Fe^{2+}}$	flux of ferrous ions, mol sec^{-1} cm^{-2}

Sc	Schmidt number
t	time, sec
δ	mass-transfer boundary layer thickness, cm
ν	kinematic viscosity, cm^2/sec
ω	disk rotation speed, sec^{-1}

References

[1] Philip Paul Russell, *Corrosion of Iron: The Active-Passive Transition and Sustained Electrochemical Oscillations*, Ph. D. Thesis, Univeristy of California, Berkeley (February, 1984).

[2] Philip Russell and John Newman, "Anodic Dissolution of Iron in Acidic Sulfate Electrolytes. II. Mathematical Model of Current Oscillations Observed under Potentiostatic Conditions," *J. Electrochem. Soc.*, 134, 1051 (1987).

[3] Chrystalla C. Haili, *The Corrosion of Iron Rotating Hemispheres in 1M Sulfuric Acid: An Electrochemical Impedance Study*, M. S. Thesis, University of California, Berkeley (June, 1987), LBL-23776.

[4] C. B. Diem and J. L. Hudson, "Chaos During the Dissolution of Iron," *AIChE Journal*, 33, 218 (1987).

[5] S. M. Sharland, C. M. Bishop, P. H. Balkwill, and J. Stewart, "The Initiation of Localised Corrosion: A Process Governed by a Strange Attractor?" *International Conference on Localized*

Corrosion, Orlando, FL (June 1, 1987).

[6] G. Beni and S. Hackwood, "Intermittent Turbulence and Period Doubling at the Corrosion-Passivity Transition in Iron," *J. Appl. Electrochem*, 14, 623 (1984).

[7] Yutaka Okinaka, "On the Oxidation-Reduction Mechanism of the Cadmium Metal-Cadmium Hydroxide," *J. Electrochem. Soc.*, 117, 289 (1970).

[8] Keith B. Prater and Allen J. Bard, "Rotating Ring-Disk Electrodes. 1. Fundamentals of the Digital Simulation Approach. Disk and Ring Transients and Collection Efficiencies," *J. Electrochem. Soc.*, 117, 207 (1970).

[9] Philip P. Russell and John Newman, "Experimental Determination of the Passive-Active Transition for Iron in 1M Sulfuric Acid," *J. Electrochem. Soc.*, 130, 547 (1983).

[10] W. J. Albery and S. Bruckenstein, "Ring-Disc Electrodes. Part 2.—Theoretical and Experimental Collection Efficiencies," *Trans. Faraday Soc.*, 62, 1920 (1966).

[11] Veniamin G. Levich, *Physichemical Hydrodynamics*, p. 41, Prentice-Hall Inc., Englewood Cliffs, N. J. (1962).

[12] Veniamin G. Levich, *ibid.*, p. 64.

[13] Philip Russell and John Newman, "Anodic Dissolution of Iron in Acidic Sulfate Electrolytes. I. Formation and Growth of a Porous

Salt Film," *J. Electrochem. Soc.*, **133**, 59 (1986).

[14] John S. Newman, *Electrochemical Systems*, p. 423, Prentice-Hall, Englewood Cliffs, N. J. (1973).

APPENDIX
Computer Programs

The following are program listings used for work presented in this thesis. The code which generates information used as input for *john.for* is given by Orazem.[†]

1. wedge.for (chapter 3)
2. john.for[‡] (chapter 4)
3. alan.for (chapter 4)
4. scchan.for (chapter 6)
5. scinf.for (chapter 6)
6. luggin.for (chapter 7)

[†]Mark E. Orazem, *Mathematical Modeling and Optimization of Liquid-Junction Photovoltaic Cells*, Ph. D. Thesis, University of California, Berkeley (June, 1983).

[‡]written by Johannes H. Sukamto

```
      program wedge
      implicit double precision(a-h,o-z)
      dimension x(201),s(201),phi(2,201),rl(2,2,201,201),phio(201),
     1r2(2,2,201,201),cdl(201),as(2,201)
      common x,phi,rl,r2,my,mx,cdl,xmax,as,pp,pi
c_____________________
      read*,angle
      print101,angle
101   format('beta=pi*',G10.4)
      pi=3.14159265358979d0
      beta=angle*pi
      damp=0.1d0
      read*,ikinet
      call tread
      call fillmat(beta)
      call asymp(beta)
333   iter=1
      if (ikinet.eq.1)then
           print*,'linear kinetics'
      else
           print*,'Tafel kinetics'
      end if
c_____________________
c   initial guess
      do 3 i=1,mx
3     phi(1,i)=-1.0d0
100   call current(1,ikinet,beta)
c_____________________
c   solve for phi1
      do 15 i=1,mx
       phio(i)=as(1,i)
      do 16 j=1,mx-1
         a1=fa(cdl(j),cdl(j+1),x(j),x(j+1))
         b1=fb(cdl(j),cdl(j+1),x(j),x(j+1))
16    phio(i)=phio(i)+a1*rl(1,1,i,j)+b1*rl(1,2,i,j)
15    phio(i)=phio(i)/pi/2.0d0
      if (ikinet.eq.1)then
         const=-xmax**(0.5d0-beta/pi)-phio(mx)
      else
         const=-dlog(xmax**(0.5d0-beta/pi))-phio(mx)
      end if
      do 555 i=1,mx
555   phio(i)=phio(i)+const
c_____________________
c  check for errors
      error=0.0d0
      do 30 i=2,mx
30    error=dmax1(error,dabs(phi(1,i)-phio(i)))
      if (error.gt.1.d-5) then
          do 35 i=1,mx
35        phi(1,i)=phi(1,i)+damp*(phio(i)-phi(1,i))
```

```
            iter=iter+1
            if (iter.ge.800) then
               print*,'greater than 300 iterations','error=',error
               goto 999
            end if
            goto 100
         end if
999      call tprint(iter,ikinet,beta)
         end
c_____________________________
         subroutine fillmat(beta)
         implicit double precision(a-h,o-z)
         dimension x(201),s(201),phi(2,201),r1(2,2,201,201),phio(201),
        1r2(2,2,201,201),cd1(201),as(2,201)
         common x,phi,r1,r2,my,mx,cd1,xmax,as,pp,pi
         en=beta/pi-1.0d0
         en1=en+1.0d0
         mm=100
         do 1 i=1,mx
         do 1 j=1,mx-1
            call integrate(x(j+1),x(j),x(i),en,mm)
            r1(1,1,i,j)=beta/pi*pp
            call integrate(x(j+1),x(j),x(i),en1,mm)
            r1(1,2,i,j)=beta/pi*pp
1        continue
         return
         end
c_____________________________
         subroutine current(ielec,ikinet,beta)
         implicit double precision(a-h,o-z)
         dimension x(201),s(201),phi(2,201),r1(2,2,201,201),phio(201),
        1r2(2,2,201,201),cd1(201),as(2,201)
         common x,phi,r1,r2,my,mx,cd1,xmax,as,pp,pi
         if (ikinet.eq.1)then
              do 1 i=1,mx
1             cd1(i)=phi(1,i)
         else
              do 3 i=1,mx
3             cd1(i)=-dexp(-phi(1,i))
         end if
         return
         end
c_____________________________
         function fa(p1,p2,z1,z2)
         implicit double precision(a-h,o-z)
         fa=p1-(p2-p1)*z1/(z2-z1)
         return
         end
c_____________________
         function fb(p1,p2,z1,z2)
         implicit double precision(a-h,o-z)
```

```
      fb=(p2-p1)/(z2-z1)
      return
      end
c_____________
      subroutine tread
      implicit double precision(a-h,o-z)
      dimension x(201),s(201),phi(2,201),r1(2,2,201,201),phio(201),
     1r2(2,2,201,201),cd1(201),as(2,201)
      common x,phi,r1,r2,my,mx,cd1,xmax,as,pp,pi
      read*,mx
      read*,xmax
      do 1 i=1,mx
1     x(i)=xmax*(dfloat(i-1)/dfloat(mx-1))**2
      return
      end
c_____________________
      subroutine tprint(iter,ikinet,beta)
      implicit double precision(a-h,o-z)
      dimension x(201),s(201),phi(2,201),r1(2,2,201,201),phio(201),
     1r2(2,2,201,201),cd1(201),as(2,201)
      common x,phi,r1,r2,my,mx,cd1,xmax,as,pp,pi
      print*,'Along electrode:'
       do 21 i=1,mx
21     print*,x(i)**(0.5d0),char(9),dabs(cd1(i))
      if (iter.ge.800)then
          print*,'The last run did not converge'
          stop
      end if
      return
      end
c_____________________
      subroutine asymp(beta)
      implicit double precision(a-h,o-z)
      dimension x(201),s(201),phi(2,201),r1(2,2,201,201),phio(201),
     1r2(2,2,201,201),cd1(201),as(2,201)
      common x,phi,r1,r2,my,mx,cd1,xmax,as,pp,pi
      en=-0.5d0
      mm=1000
      call integrate(xmax,0.0d0,0.0d0,en,mm)
      as(1,1)=beta/pi*pp
      do 3 i=2,mx-1
          call integrate(x(i),0.0d0,x(i),en,mm)
          temp=pp
          call integrate(xmax,x(i),x(i),en,mm)
          as(1,i)=(pp+temp)*beta/pi
3     continue
      call integrate(xmax,0.0d0,xmax,en,mm)
      as(1,mx)=pp*beta/pi
      return
      end
c_____________________
```

```
      subroutine integrate(b,a,xq,en,mm)
      implicit double precision(a-h,o-z)
      dimension x(201),s(201),phi(2,201),r1(2,2,201,201),phio(201),
     1 r2(2,2,201,201),cd1(201),as(2,201)
      common x,phi,r1,r2,my,mx,cd1,xmax,as,pp,pi
      if (dabs(xq).le.1.d-5)then
        if (a.ne.0.0d0)then
        pp=b**(en+1.0d0)/(en+1.0d0)*dlog(b**2)-2.0d0*b**(en+1.0d0)/
     1     (en+1.0d0)**2-
     1     (a**(en+1.0d0)/(en+1.0d0)*dlog(a**2)-2.0d0*a**(en+1.0d0)/
     1     (en+1.0d0)**2)
        else
        pp=b**(en+1.0d0)/(en+1.0d0)*dlog(b**2)-2.0d0*b**(en+1.0d0)/
     1     (en+1.0d0)**2
        end if
      else
        if (dabs(en).le.1.d-3)then
           pp=2.0d0*fln(b,a,xq)
        else if (en.gt.0.0d0)then
           eps=(b-a)/dfloat(mm-1)
           pp=xq**en*2.0d0*fln(b,a,xq)
           x1=a
           z1=f1(x1,xq,en)
           do 1 i=1,mm-1
             x2=x1+eps
             z2=f1(x2,xq,en)
             pp=pp+(z2+z1)*eps/2.0d0
             z1=z2
             x1=x2
1          continue
        else if (en.lt.0.0d0)then
           pp=xq**en*2.0d0*fln(b,a,xq)
           bns=b**(en+1.0d0)
           ans=a**(en+1.0d0)
           eps=(bns-ans)/dfloat(mm-1)
           x1=ans
           z1=f2(x1,xq,en)
           do 2 i=1,mm-1
             x2=x1+eps
             z2=f2(x2,xq,en)
             pp=pp+(z2+z1)*eps/2.0d0
             z1=z2
             x1=x2
2          continue
        end if
      end if
      return
      end
c_____________________
      function fln(b,a,xq)
      implicit double precision(a-h,o-z)
```

```
      if (a.eq.xq)then
           fa=0.0d0
      else
           fa=(a-xq)*(dlog(dabs(a-xq))-1.0d0)
      end if
      if (b.eq.xq)then
           fb=0.0d0
      else
           fb=(b-xq)*(dlog(dabs(b-xq))-1.0d0)
      end if
      fln=fb-fa
      return
      end
c_____________________
      function f1(z,xq,en)
      implicit double precision(a-h,o-z)
      if (z.eq.xq)then
          f1=0.0d0
      else
          f1=(z**en-xq**en)*dlog((z-xq)**2)
      end if
      return
      end
c_____________________
      function f2(z,xq,en)
      implicit double precision(a-h,o-z)
      x=z**(1.0d0/(en+1.0d0))
      if (x.eq.xq)then
           f2=0.0d0
      else
           f2=((1.0d0-xq**en*x**(-en))*dlog((x-xq)**2))/(en+1.0d0)
      end if
      return
      end
```

```
      program john
c _____________________
c   Written by Johannes H. Sukamto
c   The program calculates the relationships between the different
c   coordinates for the slotted-electrode cell.
c   Its input is obtained from a slightly modified version of
c   PROGRAM RCALC of Orazem.
c_____________________________________
      dimension fintga(100000),fintgc(100000),tta(100000),ttc(100000),
     +          xa(500),xc(500),ga(500),za(500),zc(500),gc(500)
      common/int/numint1,numint2,numint3,numint4,numint5,
     +           numint6,numint7,numx,dl,tg
      common/const/a,b,c,d,xmax,wimax,rescd
      common/limit/limit1,limit2
      common/points/fintga,fintgc,tta,ttc,xa,xc
      common/calc/ga,za,zc,gc
      complex za,zc
      call input
      call cxmax
      call cxcz
      call output
      stop
      end

      subroutine input
      common/int/numint1,numint2,numint3,numint4,numint5,
     +           numint6,numint7,numx,dl,tg
      common/const/a,b,c,d,xmax,wimax,rescd
c
c  a,b,c,d  - A,B,C,D in original geometry
c  wimax    - y-max
c  dl       - length of electrode
c  rescd    - ohmic resistance

c  numint's - Number of intervals for integration; they do not
c             require any changes unless 'max' and 'min' (look at
c             output) differ significantly.  Have the same number
c             for the first 4, and the same number for the last 2.
c  numx     - number of evenly spaced nodes, rectangular geometry
c
      read*, a,b,c,d
      read*, wimax
      read*, dl
      read*, rescd
      read*, numint1,numint2,numint3,numint4,numint5,numint6,numint7
      read*, numx
      return
      end

      subroutine cxmax
c calculate xmax
```

```
      dimension fintga(100000),fintgc(100000),tta(100000),ttc(100000),
     +          xa(500),xc(500),ga(500),za(500),zc(500),gc(500)
      common/int/numint1,numint2,numint3,numint4,numint5,
     +           numint6,numint7,numx,dl,tg
      common/const/a,b,c,d,xmax,wimax,rescd
      common/limit/limit1,limit2
      common/points/fintga,fintgc,tta,ttc,xa,xc
c a to I
      tta(1)=a
      width=sqrt((b-a)/2.)/float(numint1)
      beta=0.
      xmax=0.
      first=fax(tta(1))
      fintga(1)=0.
      do 10 i=2,numint1
         beta=beta+width
         tta(i)=a+beta**2
         second=fax(tta(i))
         fintga(i)=fintga(i-1)+.5*(first+second)*width
         first=second
 10   continue
      tta(numint1+1)=(a+b)/2.
      second=fax(tta(numint1+1))
      fintga(numint1+1)=fintga(numint1)+.5*(first+second)*width
c I to b
      limit=numint1+numint2
      beta=sqrt((b-a)/2.)
      width=(0.-sqrt((b-a)/2.))/float(numint2)
      first=fbx(tta(numint1+1))
      do 20 i=numint1+2,limit
         beta=beta+width
         tta(i)=b-beta**2
         second=fbx(tta(i))
         fintga(i)=fintga(i-1)+.5*(first+second)*width
         first=second
 20   continue
      tta(limit+1)=b
      second=fbx(tta(limit+1))
      fintga(limit+1)=fintga(limit)+.5*(first+second)*width
      limit1=limit+1
c -c to -I
      ttc(1)=-c
      width=sqrt((d-c)/2.)/float(numint3)
      beta=0.
      first=fcx(ttc(1))
      fintgc(1)=0.
      do 30 i=2,numint3
         beta=beta+width
         ttc(i)=-c-beta**2
         second=fcx(ttc(i))
         fintgc(i)=fintgc(i-1)+.5*(first+second)*width
```

```
         first=second
 30    continue
       ttc(numint3+1)=-(c+d)/2.
       second=fcx(ttc(numint3+1))
       fintgc(numint3+1)=fintgc(numint3)+.5*(first+second)*width
c -I to -d
       limit=numint3+numint4
       beta=sqrt((d-c)/2.)
       width=-sqrt((d-c)/2.)/float(numint4)
       first=fdx(ttc(numint3+1))
       do 40 i=numint3+2,limit
          beta=beta+width
          ttc(i)=beta**2-d
          second=fdx(ttc(i))
          fintgc(i)=fintgc(i-1)+.5*(first+second)*width
          first=second
 40    continue
       ttc(limit+1)=-d
       second=fdx(ttc(limit+1))
       fintgc(limit+1)=fintgc(limit)+.5*(first+second)*width
       limit2=limit+1
       xmax=(fintga(limit1)+fintgc(limit2))/2.
       return
       end

       subroutine cxcz
c calculate relations between derivatives of original and
c rectangular geometries
       dimension fintga(100000),fintgc(100000),tta(100000),ttc(100000),
      +          xa(500),xc(500),ga(500),za(500),zc(500),gc(500)
       common/int/numint1,numint2,numint3,numint4,numint5,
      +           numint6,numint7,numx,dl,tg
       common/const/a,b,c,d,xmax,wimax,rescd
       common/limit/limit1,limit2
       common/points/fintga,fintgc,tta,ttc,xa,xc
       common/calc/ga,za,zc,gc
       complex za,zc
       logical flag1,flag2
c integrate up to a
       temp=0.
 5.    sumr1=0.
       sumi1=0.
       widthz=a/float(numint5)
       t=0.
       first=fazr1(t)
       do 10 i=2,numint5
          t=t+widthz
          second=fazr1(t)
          sumr1=sumr1+.5*(first+second)*widthz
          first=second
 10.   continue
```

```
      second=0.
      sumr1=sumr1+.5*(first+second)*widthz
      del=abs(1.-temp/sumr1)
      if (del.gt.1.e-4) then
         if (numint5.gt.1000) then
            print*, 'PROBLEM WITH CONVERGENCE z-t, 0 to a'
            stop
         endif
         numint5=2*numint5
         temp=sumr1
         goto 5
      endif
      first=0.
      sumr2=sumr1
      za(1)=cmplx(sumr1,sumi1)
c integrate from a to b
      numint=2*(numint1+numint2)/numx
      width=xmax/float(numx-1)
      xa(1)=0.
      x=0.
      j=2
      temp=sqrt(b-a)
      first=0.
      ga(1)=gxa(tta(1))
      do 20 i=2,numx-1
         x=x+width
 30      if ((x.ge.fintga(j)).and.(j.lt.limit1)) then
            j=j+1
            goto 30
         endif
         if (j.eq.limit1) goto 300
         xa(i)=fintga(j)
         ga(i)=gxa(tta(j))
         widthz=(sqrt(b-tta(j))-temp)/float(numint)
         beta=temp
         temp=sqrt(b-tta(j))
         do 40 k=2,numint+1
            beta=beta+widthz
            t=b-beta**2
            second=fbzi1(t)
            sumi1=sumi1+.5*(first+second)*widthz
            first=second
 40      continue
         za(i)=cmplx(sumr1,sumi1)
 20   continue
 300  xa(numx)=xmax
      ga(numx)=gxa(tta(limit1))
      widthz=-temp/float(numint)
      beta=temp
      do 50 k=2,numint+1
         beta=beta+widthz
```

```
         t=b-beta**2
         second=fbzi1(t)
         sumi1=sumi1+.5*(first+second)*widthz
         first=second
 50    continue
       za(numx)=cmplx(sumr1,sumi1)
       sumi2=sumi1
c integrate from -b to -c
c integrate from -b to -I
       temp1=0.
 55    temp2=0.
       beta=0.
       widthz=sqrt((c-b)/2.)/float(numint6)
       t=-b
       first=fbzr2(t)
       do 60 i=2,numint6+1
          beta=beta+widthz
          t=-b-beta**2
          second=fbzr2(t)
          temp2=temp2+.5*(first+second)*widthz
          first=second
 60    continue
c integrate from -I to -c
       beta=sqrt((c-b)/2.)
       widthz=-beta/float(numint7)
       t=-(c+b)/2.
       first=fczr2(t)
       do 70 i=2,numint7
          beta=beta+widthz
          t=beta**2-c
          second=fczr2(t)
          temp2=temp2+.5*(first+second)*widthz
          first=second
 70    continue
       t=-c
       second=fczr2(t)
       temp2=temp2+.5*(first+second)*widthz
       del=abs(1.-temp1/temp2)
       if (del.gt.1.e-4) then
          if (numint6.gt.1000) then
             print*,'PROBLEM WITH CONVERGENCE, z-t, b to c'
             stop
          endif
          numint6=2*numint6
          numint7=2*numint7
          temp1=temp2
          goto 55
       endif
       sumr2=sumr2+temp2
       zc(1)=cmplx(sumr2,sumi2)
c integrate from -c to -d
```

```
      numint=2*(numint3+numint4)/numx
      xc(1)=0.
      gc(1)=gxc(ttc(1))
      x=0.
      j=2
      temp=0.
      beta=temp
      flag1=.true.
      flag2=.true.
      do 80 i=2,numx-1
         x=x+width
90       if ((x.ge.fintgc(j)).and.(j.le.limit2)) then
            j=j+1
            goto 90
         endif
         if (j.gt.limit2) then
            print*,'OUTSIDE OF REGION 2, c TO d'
            stop
         endif
         xc(i)=fintgc(j)
         gc(i)=gxc(ttc(j))
         if (abs(ttc(j)).lt.((c+d)/2.)) then
            widthz=(sqrt(-ttc(j)-c)-temp)/float(numint)
            beta=temp
            temp=sqrt(-ttc(j)-c)
            if (flag1) then
               t=-c
               first=fczi2(t)
               flag1=.false.
            endif
            do 100 k=2,numint+1
               beta=beta+widthz
               t=-c-beta**2
               second=fczi2(t)
               sumi2=sumi2+.5*(first+second)*widthz
               first=second
100         continue
            zc(i)=cmplx(sumr2,sumi2)
         else
            if (flag2) then
               t=-c-temp**2
               first=fdzi2(t)
               temp=sqrt(d+t)
               flag2=.false.
            endif
            widthz=(sqrt(d+ttc(j))-temp)/float(numint)
            beta=temp
            temp=sqrt(d+ttc(j))
            do 110 k=2,numint+1
               beta=beta+widthz
               t=beta**2-d
```

```
               second=fdzi2(t)
               sumi2=sumi2+.5*(first+second)*widthz
               first=second
110         continue
            zc(i)=cmplx(sumr2,sumi2)
         endif
80    continue
      xc(numx)=xmax
      gc(numx)=gxc(ttc(limit2))
      widthz=-temp/float(numint)
      do 120 k=2,numint+1
         beta=beta+widthz
         t=beta**2-d
         second=fdzi2(t)
         sumi2=sumi2+.5*(first+second)*widthz
         first=second
120   continue
      zc(numx)=cmplx(sumr2,sumi2)
      return
      end

      subroutine output
      dimension fintga(100000),fintgc(100000),tta(100000),ttc(100000),
     +          xa(500),xc(500),ga(500),za(500),zc(500),gc(500)
      common/int/numint1,numint2,numint3,numint4,numint5,
     +           numint6,numint7,numx,dl,tg
      common/const/a,b,c,d,xmax,wimax,rescd
      common/points/fintga,fintgc,tta,ttc,xa,xc
      common/calc/ga,za,zc,gc
      complex za,zc
      print100,xmax,wimax
100   format (2e17.8)
      print150,b,c,d
150   format (3e17.8)
      print160,dl
160   format (e17.8)
      print*,numx
      print160,rescd
      do 10 i=1,numx
         print200,xa(i),ga(i),xc(i),gc(i)
10    continue
200   format (4e17.8)
      do 20 i=1,numx
         print300,za(i),zc(i)
20    continue
300   format (4e17.8)
      error1=0.
      error2=1000.
      do 30 i=2,numx
         error1=amax1(error1,abs(xa(i)-xa(i-1)),abs(xc(i)-xc(i-1)))
         error2=amin1(error2,abs(xa(i)-xa(i-1)),abs(xc(i)-xc(i-1)))
```

```
30    continue
      print*, 'max. = ',error1
      print*, 'min. = ',error2
      return
      end

      function fax(t)
      common/const/a,b,c,d,xmax,wimax,rescd
      fax=2./sqrt(b-t)/sqrt(c+t)/sqrt(d+t)
      return
      end

      function fbx(t)
      common/const/a,b,c,d,xmax,wimax,rescd
      fbx=-2./sqrt(t-a)/sqrt(c+t)/sqrt(d+t)
      return
      end

      function fcx(t)
      common/const/a,b,c,d,xmax,wimax,rescd
      fcx=2./sqrt(a-t)/sqrt(b-t)/sqrt(d+t)
      return
      end

      function fdx(t)
      common/const/a,b,c,d,xmax,wimax,rescd
      fdx=-2./sqrt(a-t)/sqrt(b-t)/sqrt(-c-t)
      return
      end

      function fazr1(t)
      common/const/a,b,c,d,xmax,wimax,rescd
      if (t.eq.a) goto 10
      fazr1=-sqrt(a**2-t**2)/sqrt(b**2-t**2)/sqrt(c**2-t**2)/
     +     sqrt(d**2-t**2)
      return
10    fazr1=0.
      return
      end

      function fbzi1(t)
      common/const/a,b,c,d,xmax,wimax,rescd
      if (t.eq.a) goto 10
      fbzi1=-2.*sqrt(t**2-a**2)/sqrt(b+t)/sqrt(c**2-t**2)/
     +     sqrt(d**2-t**2)
      return
10    fbzi1=0.
      return
      end

      function fbzi2(t)
```

```
      common/const/a,b,c,d,xmax,wimax,rescd
      if (t.eq.a) goto 10
      fbzi2=-2.*sqrt(a-t)*sqrt(-a-t)/sqrt(b-t)/sqrt(c**2-t**2)/
     +      sqrt(d**2-t**2)
      return
10    fbzi2=0.
      return
      end

      function fbzr2(t)
      common/const/a,b,c,d,xmax,wimax,rescd
      fbzr2=2.*sqrt(a-t)*sqrt(-a-t)/sqrt(b-t)/sqrt(c**2-t**2)/
     +      sqrt(d**2-t**2)
      return
      end

      function fczr2(t)
      common/const/a,b,c,d,xmax,wimax,rescd
      fczr2=-2.*sqrt(a-t)*sqrt(-a-t)/sqrt(b-t)/sqrt(-b-t)/
     +     sqrt(c-t)/sqrt(d**2-t**2)
      return
      end

      function fczi2(t)
      common/const/a,b,c,d,xmax,wimax,rescd
      fczi2=fczr2(t)
      return
      end

      function fdzi2(t)
      common/const/a,b,c,d,xmax,wimax,rescd
      fdzi2=2.*sqrt(a-t)*sqrt(-a-t)/sqrt(b-t)/sqrt(-b-t)/
     +     sqrt(c-t)/sqrt(-c-t)/sqrt(d-t)
      return
      end

      function gxa(t)
      common/const/a,b,c,d,xmax,wimax,rescd
      gxa=(t-a)*sqrt(t+a)/sqrt(b+t)/sqrt(c-t)/sqrt(d-t)
      return
      end

      function gxc(t)
      common/const/a,b,c,d,xmax,wimax,rescd
      gxc=(a-t)*sqrt(-t-a)/sqrt(-t-b)/sqrt(c-t)/sqrt(d-t)
      return
      end
```

```
      program alan
      implicit double precision(a-h,o-z)
      character*72 11
      dimension x(51),y(51),phi(4,51),r1(4,2,51,51),phio(51),
     1 r2(4,2,51,51),r3(4,2,51,51),r4(4,2,51,51),cd(51),g(100),phio3(51)
     1 ,za(51),zc(51),x3(51),g3(100)
      common x,y,phi,r1,r2,r3,r4,my,mx,cd,xmax,ymax,g,xmaxi,za,zc,bj,
     1       dj
c_____________________
c   x,y  are the coordinates of the rectangle.
c   phi  stores the values of the unknowns on the four sides.
c   phi(3,i) is the current density on side 3.  phi(1,i), phi(2,i) and
c   phi(3,i) are the values of the potentials on the four sides.
c   r1, r2, r3, and r4 store the values of the integrand for each side.
c   cd(i) is used to store the current density on side 1.
c_____________________
      pi=3.14159265358979d0
      read*,iflag
      read*,imax,damp,dj,djinc,djmax
      tdamp=damp
      read*,mx,my
      read*,xmaxi,ymaxi
      read*,bt,ct,dt
      read*,dl,tg,dum
      read*,numpts
      read*,resis
      write(1,*),resis
      write(2,*),resis
      bj=dj*resis/dl
      ymax=ymaxi/xmaxi
      xmax=1.0d0
      read*,x(1),g(1),x3(1),g3(1)
      limit=(numpts-1)/(mx-1)-1
      do 78  i=2,mx
      do 77 j=1,limit
77    read*,dum,dum,dum,dum
78    read*,x(i),g(i),x3(i),g3(i)
      read*,dum,za(1),dum,zc(1)
      do 80 i=2,mx
      do 79 j=1,limit
79    read*,dum,dum,dum,dum
80    read*,dum,za(i),dum,zc(i)
      do 1 i=1,mx
1     x(i)=x(i)/xmaxi
      do 2 i=1,my
2     y(i)=ymax*dfloat(i-1)/dfloat(my-1)
      call fillmat
c_____________________
c   initial guess
      if (iflag.eq.1) then
           call readguess
```

```
      else
           do 3 i=1,mx
              phi(1,i)=ymax*xmaxi*g(i)
3             phi(3,i)=-1.0d0*xmaxi*g(i)
           do 4 i=1,my
              phi(2,i)=phi(1,1)*(ymax-y(i))/ymax
4             phi(4,i)=phi(1,mx)*(ymax-y(i))/ymax
      end if
c_____________________
100   call current
c_____________________
c   solve for phi2
      do 6 i=2,my-1
      phi(2,i)=0.0d0
      do 7 j=1,mx-1
         a2=fa(phi(1,j),phi(1,j+1),x(j),x(j+1))
         b2=fb(phi(1,j),phi(1,j+1),x(j),x(j+1))
         a1=fa(cd(j),cd(j+1),x(j),x(j+1))
         b1=fb(cd(j),cd(j+1),x(j),x(j+1))
         a3=fa(phi(3,j),phi(3,j+1),x(j),x(j+1))
         b3=fb(phi(3,j),phi(3,j+1),x(j),x(j+1))
7     phi(2,i)=phi(2,i)+a1*r2(1,1,i,j)+b1*r2(1,2,i,j)+
     1 a2*r2(2,1,i,j)+b2*r2(2,2,i,j)+a3*r2(3,1,i,j)+b3*r2(3,2,i,j)
      do 8 j=1,my-1
         a=fa(phi(4,j),phi(4,j+1),y(j),y(j+1))
         b=fb(phi(4,j),phi(4,j+1),y(j),y(j+1))
8     phi(2,i)=phi(2,i)+a*r2(4,1,i,j)+b*r2(4,2,i,j)
6     phi(2,i)=phi(2,i)/pi
      phi(2,1)=phi(1,1)
      phi(2,my)=0.0d0
c_____________________
c   solve for phi4
      do 9 i=2,my-1
      phi(4,i)=0.0d0
      do 10 j=1,mx-1
         a2=fa(phi(1,j),phi(1,j+1),x(j),x(j+1))
         b2=fb(phi(1,j),phi(1,j+1),x(j),x(j+1))
         a1=fa(cd(j),cd(j+1),x(j),x(j+1))
         b1=fb(cd(j),cd(j+1),x(j),x(j+1))
         a3=fa(phi(3,j),phi(3,j+1),x(j),x(j+1))
         b3=fb(phi(3,j),phi(3,j+1),x(j),x(j+1))
10    phi(4,i)=phi(4,i)+a1*r4(1,1,i,j)+b1*r4(1,2,i,j)+
     1 a2*r4(2,1,i,j)+b2*r4(2,2,i,j)+a3*r4(3,1,i,j)+b3*r4(3,2,i,j)
      do 11 j=1,my-1
         a=fa(phi(2,j),phi(2,j+1),y(j),y(j+1))
         b=fb(phi(2,j),phi(2,j+1),y(j),y(j+1))
11    phi(4,i)=phi(4,i)+a*r4(4,1,i,j)+b*r4(4,2,i,j)
9     phi(4,i)=phi(4,i)/pi
      phi(4,1)=phi(1,mx)
      phi(4,my)=0.0d0
c_____________________
```

```
c   solve for i3
      do 12 i=1,mx
      phio3(i)=phi(3,i)
      phi(3,i)=0.0d0
      do 13 j=1,mx-1
         a1=fa(phi(1,j),phi(1,j+1),x(j),x(j+1))
         b1=fb(phi(1,j),phi(1,j+1),x(j),x(j+1))
         a2=fa(cd(j),cd(j+1),x(j),x(j+1))
         b2=fb(cd(j),cd(j+1),x(j),x(j+1))
13    phi(3,i)=phi(3,i)+a1*r3(1,1,i,j)+b1*r3(1,2,i,j)+
     1 a2*r3(2,1,i,j)+b2*r3(2,2,i,j)
      do 14 j=1,my-1
         a1=fa(phi(2,j),phi(2,j+1),y(j),y(j+1))
         b1=fb(phi(2,j),phi(2,j+1),y(j),y(j+1))
         a2=fa(phi(4,j),phi(4,j+1),y(j),y(j+1))
         b2=fb(phi(4,j),phi(4,j+1),y(j),y(j+1))
14    phi(3,i)=phi(3,i)+a1*r3(3,1,i,j)+b1*r3(3,2,i,j)+
     1 a2*r3(4,1,i,j)+b2*r3(4,2,i,j)
      phi(3,i)=phi(3,i)/pi
12    phi(3,i)=phio3(i)-damp*(phio3(i)-phi(3,i))
c_____________________
c   solve for phi1
      do 15 i=1,mx
      phio(i)=0.0d0
      do 16 j=1,mx-1
         a2=fa(phi(3,j),phi(3,j+1),x(j),x(j+1))
         b2=fb(phi(3,j),phi(3,j+1),x(j),x(j+1))
         a1=fa(cd(j),cd(j+1),x(j),x(j+1))
         b1=fb(cd(j),cd(j+1),x(j),x(j+1))
16    phio(i)=phio(i)+a1*r1(1,1,i,j)+b1*r1(1,2,i,j)+
     1 a2*r1(3,1,i,j)+b2*r1(3,2,i,j)
      do 17 j=1,my-1
         a1=fa(phi(2,j),phi(2,j+1),y(j),y(j+1))
         b1=fb(phi(2,j),phi(2,j+1),y(j),y(j+1))
         a2=fa(phi(4,j),phi(4,j+1),y(j),y(j+1))
         b2=fb(phi(4,j),phi(4,j+1),y(j),y(j+1))
17    phio(i)=phio(i)+a1*r1(2,1,i,j)+b1*r1(2,2,i,j)+
     1 a2*r1(4,1,i,j)+b2*r1(4,2,i,j)
15    phio(i)=phio(i)/pi
c_____________________
c  check for errors
      error=0.0d0
      do 30 i=2,mx
30    error=dmax1(error,dabs(1.0d0-phio(i)/phi(1,i)))
      if (error.gt.1.d-4) then
          do 35 i=1,mx
35        phi(1,i)=phi(1,i)+damp*(phio(i)-phi(1,i))
          iter=iter+1
          if (iter.ge.imax) then
             print*,'the number of iterations exceeds  ',imax
             print*,'error.   =  ',error
```

```
            goto 999
          end if
          goto 100
        end if
c_____________________
c   Print results
        print*, ' '
        print*, ' '
        print*, 'J = ',dj
        print*, 'resis. = ',resis
999     print*,'Number of iterations:',iter
c_____________________
c average current
        cd(1)=-bj*(1.0d0-phi(1,1))
        sum=0.0d0
        do 250 i=2,mx
           cd(i)=-bj*(1.0d0-phi(1,i))
250        sum=sum+.5d0*(cd(i)+cd(i-1))*(za(i)-za(i-1))
        sum=sum/(za(mx)-za(1))
        do 300 i=1,mx
           za(i)=(za(i)-za(1))/(za(mx)-za(1))
300        cd(i)=cd(i)/sum
        eta=sum/bj
        phimax=dabs(phi(1,1)-phi(1,mx))
        write(1,*),dj,eta,phimax
        if ((dj.eq.5.).or.(dj.eq.10.).or.(dj.eq.20.).or.(dj.eq.50.)
     + .or.(dj.eq.100.)) then
           write(2,*),dj
           do 500 i=1,mx
 500          write(2,*),za(i),char(9),cd(i)
        endif
        write(3,*),'J  = ',dj
        do 8000 nni=1,mx
8000    write(3,*),phi(1,nni),phi(2,nni),phi(3,nni),phi(4,nni)
c increment dj
        if (dj.lt.djmax) then
           dj=dj+djinc
           bj=dj*resis/dl
           iter=0
           damp=tdamp
           goto 100
        endif
        end
c_____________________
        subroutine fillmat
        implicit double precision(a-h,o-z)
        dimension x(51),y(51),phi(4,51),r1(4,2,51,51),phio(51),
     1 r2(4,2,51,51),r3(4,2,51,51),r4(4,2,51,51),cd(51),g(100),
     1 za(51),zc(51),x3(51),g3(100)
        common x,y,phi,r1,r2,r3,r4,my,mx,cd,xmax,ymax,g,xmaxi,za,zc,bj,
     1         dj
```

```
      do 1 i=1,mx
      do 1 j=1,mx-1
         r1(1,1,i,j)=f1(x(j+1),x(i))-f1(x(j),x(i))
         r1(1,2,i,j)=f2(x(j+1),x(i))-f2(x(j),x(i))
         r1(3,1,i,j)=-0.5d0*(f3(x(j+1)-x(i),ymax)-f3(x(j)-x(i),ymax))
         r1(3,2,i,j)=x(i)*r1(3,1,i,j)-
     1   (f4(x(j+1)-x(i),ymax)-f4(x(j)-x(i),ymax))*0.5d0
         r3(1,1,i,j)=-(f5(x(j+1)-x(i),ymax)-f5(x(j)-x(i),ymax)+2.0d0*
     1   ymax**2*(f7(x(j+1)-x(i),ymax)-f7(x(j)-x(i),ymax)))
         r3(1,2,i,j)=x(i)*r3(1,1,i,j)+
     1   2.0d0*ymax**2*(f8(x(j+1)-x(i),ymax)-
     1   f8(x(j)-x(i),ymax))-(f6(x(j+1)-x(i),ymax)-f6(x(j)-x(i),ymax))
         r3(2,1,i,j)=ymax*(f5(x(j+1)-x(i),ymax)-f5(x(j)-x(i),ymax))
         r3(2,2,i,j)=x(i)*r3(2,1,i,j)+
     1   ymax*(f6(x(j+1)-x(i),ymax)-f6(x(j)-x(i),ymax))
1     continue
      do 2 i=1,mx
      do 2 j=1,my-1
         if (i.eq.1) then
              r1(2,1,i,j)=0.0d0
              r1(2,2,i,j)=0.0d0
              r3(3,1,i,j)=0.0d0
              r3(3,2,i,j)=0.0d0
         else
              r1(2,1,i,j)=x(i)*(f5(y(j+1),x(i))-f5(y(j),x(i)))
              r1(2,2,i,j)=x(i)*(f6(y(j+1),x(i))-f6(y(j),x(i)))
              r3(3,1,i,j)=2.0d0*x(i)*(f8(y(j+1)-ymax,x(i))-
     1        f8(y(j)-ymax,x(i)))
              r3(3,2,i,j)=ymax*r3(3,1,i,j)+2.0d0*x(i)*
     1        (f9(y(j+1)-ymax,x(i))-f9(y(j)-ymax,x(i)))
         end if
         if (i.eq.mx) then
              r1(4,1,i,j)=0.0d0
              r1(4,2,i,j)=0.0d0
              r3(4,1,i,j)=0.0d0
              r3(4,2,i,j)=0.0d0
         else
              r1(4,1,i,j)=(xmax-x(i))*(f5(y(j+1),xmax-x(i))-
     1        f5(y(j),xmax-x(i)))
              r1(4,2,i,j)=(xmax-x(i))*(f6(y(j+1),xmax-x(i))-
     1        f6(y(j),xmax-x(i)))
              r3(4,1,i,j)=2.0d0*(xmax-x(i))*(f8(y(j+1)-ymax,
     1        x(i)-xmax)-f8(y(j)-ymax,xmax-x(i)))
              r3(4,2,i,j)=ymax*r3(4,1,i,j)+2.0d0*(xmax-x(i))*
     1        (f9(y(j+1)-ymax,xmax-x(i))-f9(y(j)-ymax,xmax-x(i)))
         end if
2     continue
      do 3 i=2,my-1
      do 3 j=1,mx-1
         r2(1,1,i,j)=0.5d0*(f3(x(j+1),y(i))-f3(x(j),y(i)))
         r2(1,2,i,j)=0.5d0*(f4(x(j+1),y(i))-f4(x(j),y(i)))
```

```
            r2(2,1,i,j)=y(i)*(f5(x(j+1),y(i))-f5(x(j),y(i)))
            r2(2,2,i,j)=y(i)*(f6(x(j+1),y(i))-f6(x(j),y(i)))
            r2(3,1,i,j)=-0.5d0*(f3(x(j+1),ymax-y(i))-
     1      f3(x(j),ymax-y(i)))
            r2(3,2,i,j)=-0.5d0*(f4(x(j+1),ymax-y(i))-
     1      f4(x(j),ymax-y(i)))+y(i)*r2(3,1,i,j)
            r4(1,1,i,j)=0.5d0*(f3(x(j+1)-xmax,y(i))-
     1      f3(x(j)-xmax,y(i)))
            r4(1,2,i,j)=0.5d0*(f4(x(j+1)-xmax,y(i))-
     1      f4(x(j)-xmax,y(i)))+r4(1,1,i,j)*xmax
            r4(2,1,i,j)=y(i)*(f5(x(j+1)-xmax,y(i))-
     1      f5(x(j)-xmax,y(i)))
            r4(2,2,i,j)=y(i)*(f6(x(j+1)-xmax,y(i))-
     1      f6(x(j)-xmax,y(i)))+xmax*r4(2,1,i,j)
            r4(3,1,i,j)=-0.5d0*(f3(x(j+1)-xmax,y(i)-ymax)-
     1      f3(x(j)-xmax,y(i)-ymax))
3           r4(3,2,i,j)=-0.5d0*(f4(x(j+1)-xmax,y(i)-ymax)-
     1      f4(x(j)-xmax,y(i)-ymax))+xmax*r4(3,1,i,j)
          do 4 i=2,my-1
          do 4 j=1,my-1
            r2(4,1,i,j)=xmax*(f5(y(j+1)-y(i),xmax)-
     1      f5(y(j)-y(i),xmax))
            r2(4,2,i,j)=y(i)*r2(4,1,i,j)+xmax*(f6(y(j+1)-y(i),xmax)-
     1      f6(y(j)-y(i),xmax))
            r4(4,1,i,j)=r2(4,1,i,j)
4           r4(4,2,i,j)=r2(4,2,i,j)
c_____________________
c  The two following do loops account for the fact the interior
c  angles at the corners are twice as small.
c_____________________
          do 5 j=1,mx-1
            r3(1,1,1,j)=2.0d0*r3(1,1,1,j)
            r3(1,2,1,j)=2.0d0*r3(1,2,1,j)
            r3(2,1,1,j)=2.0d0*r3(2,1,1,j)
            r3(2,2,1,j)=2.0d0*r3(2,2,1,j)
            r3(1,1,mx,j)=2.0d0*r3(1,1,mx,j)
            r3(1,2,mx,j)=2.0d0*r3(1,2,mx,j)
            r3(2,1,mx,j)=2.0d0*r3(2,1,mx,j)
            r3(2,2,mx,j)=2.0d0*r3(2,2,mx,j)
            r1(1,1,1,j)=2.0d0*r1(1,1,1,j)
            r1(1,2,1,j)=2.0d0*r1(1,2,1,j)
            r1(3,1,1,j)=2.0d0*r1(3,1,1,j)
            r1(3,2,1,j)=2.0d0*r1(3,2,1,j)
            r1(1,1,mx,j)=2.0d0*r1(1,1,mx,j)
            r1(1,2,mx,j)=2.0d0*r1(1,2,mx,j)
            r1(3,1,mx,j)=2.0d0*r1(3,1,mx,j)
5           r1(3,2,mx,j)=2.0d0*r1(3,2,mx,j)
          do 6 j=1,my-1
            r3(3,1,mx,j)=2.0d0*r3(3,1,mx,j)
            r3(3,2,mx,j)=2.0d0*r3(3,2,mx,j)
            r3(4,1,1,j)=2.0d0*r3(4,1,1,j)
```

```
            r3(4,2,1,j)=2.0d0*r3(4,2,1,j)
            r1(2,1,mx,j)=2.0d0*r1(2,1,mx,j)
            r1(2,2,mx,j)=2.0d0*r1(2,2,mx,j)
            r1(4,1,1,j)=2.0d0*r1(4,1,1,j)
6           r1(4,2,1,j)=2.0d0*r1(4,2,1,j)
      return
      end
c_____________________
c   SUBROUTINE CURRENT IS WHERE THE KINETICS AND THE INFORMATION
c   FROM THE SCHWARZ-CHRISTOFFEL TRANSFORMATION ARE INPUT
c_____________________
      subroutine current
      implicit double precision(a-h,o-z)
      dimension x(51),y(51),phi(4,51),r1(4,2,51,51),phio(51),
     1 r2(4,2,51,51),r3(4,2,51,51),r4(4,2,51,51),cd(51),g(100),
     1 za(51),zc(51),x3(51),g3(100)
      common x,y,phi,r1,r2,r3,r4,my,mx,cd,xmax,ymax,g,xmaxi,za,zc,bj,
     1       dj
      do 1 i=1,mx
1     cd(i)=-bj*(1.0d0-phi(1,i))*g(i)*xmaxi
      return
      end

c_____________________
c   THE FOLLOWING FUNCTIONS ARE INTEGRALS TO BE USED IN 2-D PROBLEMS.
c   THEY ARE CALLED IN SUBROUTINE FILLMAT.
c_____________________
      function f1(b,a)
      implicit double precision(a-h,o-z)
      if (a.eq.b) then
         f1=0.0d0
      else
         f1=(b-a)*(dlog(dabs(a-b))-1.0d0)
      end if
      return
      end
c_____________________
      function f2(b,a)
      implicit double precision(a-h,o-z)
      if (a.eq.b) then
          f2=0.0d0
      else
          te=(a-b)**2/2.0d0*(dlog(dabs(b-a))-0.5d0)
          f2=a*(b-a)*(dlog(dabs(b-a))-1.0d0)+te
      end if
      return
      end
c_____________________
      function f3(b,a)
      implicit double precision(a-h,o-z)
      f3=b*dlog(b**2+a**2)-2.0d0*b+2.0d0*a*datan(b/a)
```

```
      return
      end
c_____________
      function f4(b,a)
      implicit double precision(a-h,o-z)
      f4=0.5d0*(b**2+a**2)*dlog(b**2+a**2)-0.5d0*b**2
      return
      end
c_____________
      function f5(b,a)
      implicit double precision(a-h,o-z)
      f5=datan(b/a)/a
      return
      end
c_____________
      function f6(b,a)
      implicit double precision(a-h,o-z)
      f6=0.5d0*dlog(a**2+b**2)
      return
      end
c_____________
      function f7(b,a)
      implicit double precision (a-h,o-z)
      f7=(b/(a**2+b**2)-datan(b/a)/a)/2.0d0/a**2
      return
      end
c_____________
      function f8(b,a)
      implicit double precision(a-h,o-z)
      f8=-0.5d0/(b**2+a**2)
      return
      end
c_____________
      function f9(b,a)
      implicit double precision(a-h,o-z)
      f9=-b/(b**2+a**2)/2.0d0+datan(b/a)/a/2.0d0
      return
      end
c_____________
      function fa(p1,p2,z1,z2)
      implicit double precision(a-h,o-z)
      fa=p1-(p2-p1)*z1/(z2-z1)
      return
      end
c_____________
      function fb(p1,p2,z1,z2)
      implicit double precision(a-h,o-z)
      fb=(p2-p1)/(z2-z1)
      return
      end
c_____________
```

```
      subroutine readguess
      implicit double precision(a-h,o-z)
      dimension x(51),y(51),phi(4,51),r1(4,2,51,51),phio(51),
     1 r2(4,2,51,51),r3(4,2,51,51),r4(4,2,51,51),cd(51),g(100),
     1 za(51),zc(51),x3(51),g3(100)
      common x,y,phi,r1,r2,r3,r4,my,mx,cd,xmax,ymax,g,xmaxi,za,zc,bj,
     1       dj
      do 1 i=1,mx
      read*,phi(1,i),phi(2,i),phi(3,i)
1     read*,phi(4,i)
      return
      end
```

```
      program scchan
      implicit double precision(a-h,o-z)
      character*72 ll
      dimension x(51),y(51),phi(4,51),rl(5,2,51,51),phio(51),
     1r2(5,2,51,51),r3(5,2,51,51),r4(5,2,51,51),cdl(51),g(100),phio3(51)
     1,vj(200),vr(200),wins(200),wele(200),xins(200),xele(200),cd3(51)
      common x,y,phi,rl,r2,r3,r4,my,mx,cdl,xmax,ymax,g,xmaxi
     1,vj,vr,wins,wele,xins,xele,cd3,hl
c_____________________
      read*,djint
      dj=djint
      pi=3.14159265358979d0
      damp=0.5d0
      read*,ikinet
      if (ikinet.eq.1)then
           print*,'linear kinetics'
      ll='J           i(L)/iavg            Bl'
      print*,ll
      else if (ikinet.eq.2) then
      print*,'Tafel kinetics'
      ll='delta        i(L)/iavg         ln(Ec)              ln(g)'
      print*,ll
      else
      print*,'constant current'
      ll='delta        i(L)/iavg         ln(Ec)              ln(g)'
      print*,ll
      ll='J           i(L)/iavg            Bl'
      print*,ll
      end if
      call tread
      call fillmat
      iter=1
c_____________________
c   initial guess
      iflag=0
      if (iflag.eq.1) then
           call readguess
      else
           do 3 i=1,mx
              phi(1,i)=ymax*g(i)
3          phi(3,i)=0.1d0
      end if
      call current(3,ikinet,dj)
      do 4 i=1,my
      phi(2,i)=(phi(1,1)-phi(3,1))*(ymax-y(i))/ymax+phi(3,1)
4     phi(4,i)=(phi(1,mx)-phi(3,mx))*(ymax-y(i))/ymax+phi(3,mx)
c_____________________
100   call current(1,ikinet,dj)
c_____________________
c   solve for phi2
      do 6 i=2,my-1
```

```
      phi(2,i)=0.0d0
      do 7 j=1,mx-1
         a2=fa(phi(1,j),phi(1,j+1),x(j),x(j+1))
         b2=fb(phi(1,j),phi(1,j+1),x(j),x(j+1))
         a1=fa(cd1(j),cd1(j+1),x(j),x(j+1))
         b1=fb(cd1(j),cd1(j+1),x(j),x(j+1))
         a3=fa(cd3(j),cd3(j+1),x(j),x(j+1))
         b3=fb(cd3(j),cd3(j+1),x(j),x(j+1))
         a4=fa(phi(3,j),phi(3,j+1),x(j),x(j+1))
         b4=fb(phi(3,j),phi(3,j+1),x(j),x(j+1))
7     phi(2,i)=phi(2,i)+a1*r2(1,1,i,j)+b1*r2(1,2,i,j)+
     1 a2*r2(2,1,i,j)+b2*r2(2,2,i,j)+a3*r2(3,1,i,j)+b3*r2(3,2,i,j)
     1+a4*r2(5,1,i,j)+b4*r2(5,2,i,j)
      do 8 j=1,my-1
         a=fa(phi(4,j),phi(4,j+1),y(j),y(j+1))
         b=fb(phi(4,j),phi(4,j+1),y(j),y(j+1))
8     phi(2,i)=phi(2,i)+a*r2(4,1,i,j)+b*r2(4,2,i,j)
6     phi(2,i)=phi(2,i)/pi
      phi(2,1)=phi(1,1)
      phi(2,my)=phi(3,1)
c_____________________
c   solve for phi4
      do 9 i=2,my-1
      phi(4,i)=0.0d0
      do 10 j=1,mx-1
         a2=fa(phi(1,j),phi(1,j+1),x(j),x(j+1))
         b2=fb(phi(1,j),phi(1,j+1),x(j),x(j+1))
         a1=fa(cd1(j),cd1(j+1),x(j),x(j+1))
         b1=fb(cd1(j),cd1(j+1),x(j),x(j+1))
         a3=fa(cd3(j),cd3(j+1),x(j),x(j+1))
         b3=fb(cd3(j),cd3(j+1),x(j),x(j+1))
         a4=fa(phi(3,j),phi(3,j+1),x(j),x(j+1))
         b4=fb(phi(3,j),phi(3,j+1),x(j),x(j+1))
10    phi(4,i)=phi(4,i)+a1*r4(1,1,i,j)+b1*r4(1,2,i,j)+
     1 a2*r4(2,1,i,j)+b2*r4(2,2,i,j)+a3*r4(3,1,i,j)+b3*r4(3,2,i,j)
     1+a4*r4(5,1,i,j)+b4*r4(5,2,i,j)
      do 11 j=1,my-1
         a=fa(phi(2,j),phi(2,j+1),y(j),y(j+1))
         b=fb(phi(2,j),phi(2,j+1),y(j),y(j+1))
11    phi(4,i)=phi(4,i)+a*r4(4,1,i,j)+b*r4(4,2,i,j)
9     phi(4,i)=phi(4,i)/pi
      phi(4,1)=phi(1,mx)
      phi(4,my)=phi(3,mx)
c_____________________
c   solve for phi3
      do 12 i=1,mx
      phio3(i)=phi(3,i)
      phi(3,i)=0.0d0
      do 13 j=1,mx-1
         a1=fa(phi(1,j),phi(1,j+1),x(j),x(j+1))
         b1=fb(phi(1,j),phi(1,j+1),x(j),x(j+1))
```

```
            a2=fa(cd1(j),cd1(j+1),x(j),x(j+1))
            b2=fb(cd1(j),cd1(j+1),x(j),x(j+1))
            a3=fa(cd3(j),cd3(j+1),x(j),x(j+1))
            b3=fb(cd3(j),cd3(j+1),x(j),x(j+1))
13        phi(3,i)=phi(3,i)+a3*r3(1,1,i,j)+b3*r3(1,2,i,j)+
     1  a2*r3(3,1,i,j)+b2*r3(3,2,i,j)+a1*r3(5,1,i,j)+b1*r3(5,2,i,j)
          do 14 j=1,my-1
            a1=fa(phi(2,j),phi(2,j+1),y(j),y(j+1))
            b1=fb(phi(2,j),phi(2,j+1),y(j),y(j+1))
            a2=fa(phi(4,j),phi(4,j+1),y(j),y(j+1))
            b2=fb(phi(4,j),phi(4,j+1),y(j),y(j+1))
14        phi(3,i)=phi(3,i)+a1*r3(2,1,i,j)+b1*r3(2,2,i,j)+
     1  a2*r3(4,1,i,j)+b2*r3(4,2,i,j)
          phi(3,i)=phi(3,i)/pi
12        phi(3,i)=phio3(i)-damp*(phio3(i)-phi(3,i))
          call current(3,ikinet,dj)
c_____________________
c   solve for phi1
          do 15 i=1,mx
          phio(i)=0.0d0
          do 16 j=1,mx-1
            a2=fa(cd3(j),cd3(j+1),x(j),x(j+1))
            b2=fb(cd3(j),cd3(j+1),x(j),x(j+1))
            a3=fa(phi(3,j),phi(3,j+1),x(j),x(j+1))
            b3=fb(phi(3,j),phi(3,j+1),x(j),x(j+1))
            a1=fa(cd1(j),cd1(j+1),x(j),x(j+1))
            b1=fb(cd1(j),cd1(j+1),x(j),x(j+1))
16        phio(i)=phio(i)+a1*r1(1,1,i,j)+b1*r1(1,2,i,j)+
     1  a2*r1(3,1,i,j)+b2*r1(3,2,i,j)+a3*r1(5,1,i,j)+b3*r1(5,2,i,j)
          do 17 j=1,my-1
            a1=fa(phi(2,j),phi(2,j+1),y(j),y(j+1))
            b1=fb(phi(2,j),phi(2,j+1),y(j),y(j+1))
            a2=fa(phi(4,j),phi(4,j+1),y(j),y(j+1))
            b2=fb(phi(4,j),phi(4,j+1),y(j),y(j+1))
17        phio(i)=phio(i)+a1*r1(2,1,i,j)+b1*r1(2,2,i,j)+
     1  a2*r1(4,1,i,j)+b2*r1(4,2,i,j)
15        phio(i)=phio(i)/pi
c_____________________
c  check for errors
          error=0.0d0
          do 30 i=2,mx
30        if (phi(1,i).ne.0.0d0)
     1  error=dmax1(error,dabs(1.0d0-phio(i)/phi(1,i)))
          if (error.gt.1.d-4) then
              do 35 i=1,mx
35            phi(1,i)=phi(1,i)+damp*(phio(i)-phi(1,i))
              iter=iter+1
              if (iter.ge.500) then
                 print*,'greater than 300 iterations','error=',error
                 goto 999
              end if
```

```
          goto 100
        end if
999     call tprint(iter,ikinet,dj)
        dj=dj+djint
        if (dj.lt.10.0d0*djint) then
           if (dj.ge.9.0d0)damp=0.1d0
           iter=1
           goto 100
        end if
        end
c_____________________
        subroutine fillmat
        implicit double precision(a-h,o-z)
        dimension x(51),y(51),phi(4,51),r1(5,2,51,51),phio(51),
     1 r2(5,2,51,51),r3(5,2,51,51),r4(5,2,51,51),cd1(51),g(100),cd3(51)
        common x,y,phi,r1,r2,r3,r4,my,mx,cd1,xmax,ymax,g,xmaxi
     1,vj(200),vr(200),wins(200),wele(200),xins(200),xele(200),cd3,hl
        do 1 i=1,mx
        do 1 j=1,mx-1
           r1(1,1,i,j)=f1(x(j+1),x(i))-f1(x(j),x(i))
           r1(1,2,i,j)=f2(x(j+1),x(i))-f2(x(j),x(i))
           r1(3,1,i,j)=-0.5d0*(f3(x(j+1)-x(i),ymax)-f3(x(j)-x(i),ymax))
           r1(3,2,i,j)=x(i)*r1(3,1,i,j)-
     1     (f4(x(j+1)-x(i),ymax)-f4(x(j)-x(i),ymax))*0.5d0
           r1(5,1,i,j)=ymax*(f5(x(j+1)-x(i),ymax)-f5(x(j)-x(i),ymax))
           r1(5,2,i,j)=x(i)*r1(5,1,i,j)+ymax*(f6(x(j+1)-x(i),ymax)-
     1     f6(x(j)-x(i),ymax))
           r3(1,1,i,j)=-r1(1,1,i,j)
           r3(1,2,i,j)=-r1(1,2,i,j)
           r3(5,1,i,j)=r1(5,1,i,j)
           r3(5,2,i,j)=r1(5,2,i,j)
           r3(3,1,i,j)=-r1(3,1,i,j)
           r3(3,2,i,j)=-r1(3,2,i,j)
1       continue
        do 2 i=1,mx
        do 2 j=1,my-1
           if (i.eq.1) then
                r1(2,1,i,j)=0.0d0
                r1(2,2,i,j)=0.0d0
                r3(2,1,i,j)=0.0d0
                r3(2,2,i,j)=0.0d0
           else
                r1(2,1,i,j)=x(i)*(f5(y(j+1),x(i))-f5(y(j),x(i)))
                r1(2,2,i,j)=x(i)*(f6(y(j+1),x(i))-f6(y(j),x(i)))
                r3(2,1,i,j)=-x(i)*(f5(ymax-y(j+1),x(i))-
     1          f5(ymax-y(j),x(i)))
                r3(2,2,i,j)=ymax*r3(2,1,i,j)+
     1          x(i)*(f6(ymax-y(j+1),x(i))-f6(ymax-y(j),x(i)))
           end if
           if (i.eq.mx) then
                r1(4,1,i,j)=0.0d0
```

```
                r1(4,2,i,j)=0.0d0
                r3(4,1,i,j)=0.0d0
                r3(4,2,i,j)=0.0d0
           else
                r1(4,1,i,j)=(xmax-x(i))*(f5(y(j+1),xmax-x(i))-
     1          f5(y(j),xmax-x(i)))
                r1(4,2,i,j)=(xmax-x(i))*(f6(y(j+1),xmax-x(i))-
     1.         f6(y(j),xmax-x(i)))
                r3(4,1,i,j)=-(xmax-x(i))*(f5(ymax-y(j+1),xmax-x(i))-
     1          f5(ymax-y(j),xmax-x(i)))
                r3(4,2,i,j)=ymax*r3(4,1,i,j)+
     1          (xmax-x(i))*(f6(ymax-y(j+1),xmax-x(i))-
     1          f6(ymax-y(j),xmax-x(i)))
           end if
2        continue
         do 3 i=2,my-1
         do 3 j=1,mx-1
            r2(1,1,i,j)=0.5d0*(f3(x(j+1),y(i))-f3(x(j),y(i)))
            r2(1,2,i,j)=0.5d0*(f4(x(j+1),y(i))-f4(x(j),y(i)))
            r2(2,1,i,j)=y(i)*(f5(x(j+1),y(i))-f5(x(j),y(i)))
            r2(2,2,i,j)=y(i)*(f6(x(j+1),y(i))-f6(x(j),y(i)))
            r2(3,1,i,j)=-0.5d0*(f3(x(j+1),ymax-y(i))-
     1      f3(x(j),ymax-y(i)))
            r2(3,2,i,j)=-0.5d0*(f4(x(j+1),ymax-y(i))-
     1      f4(x(j),ymax-y(i)))
            r2(5,1,i,j)=-(y(i)-ymax)*(f5(x(j+1),ymax-y(i))-f5(x(j),ymax-y(i)))
            r2(5,2,i,j)=-(y(i)-ymax)*(f6(x(j+1),ymax-y(i))-f6(x(j),ymax-y(i)))
            r4(1,1,i,j)=-0.5d0*(f3(xmax-x(j+1),y(i))-
     1      f3(xmax-x(j),y(i)))
            r4(1,2,i,j)=0.5d0*(f4(xmax-x(j+1),y(i))-
     1      f4(xmax-x(j),y(i)))+r4(1,1,i,j)*xmax
            r4(2,1,i,j)=-y(i)*(f5(xmax-x(j+1),y(i))-
     1      f5(xmax-x(j),y(i)))
            r4(2,2,i,j)=y(i)*(f6(xmax-x(j+1),y(i))-
     1      f6(xmax-x(j),y(i)))+xmax*r4(2,1,i,j)
            r4(5,1,i,j)=-(ymax-y(i))*(f5(xmax-x(j+1),ymax-y(i))-
     1      f5(xmax-x(j),ymax-y(i)))
            r4(5,2,i,j)=xmax*r4(5,1,i,j)+
     1     (ymax-y(i))*(f6(xmax-x(j+1),ymax-y(i))-f6(xmax-x(j),ymax-y(i)))
            r4(3,1,i,j)=0.5d0*(f3(xmax-x(j+1),ymax-y(i))-
     1      f3(xmax-x(j),ymax-y(i)))
3           r4(3,2,i,j)=-0.5d0*(f4(xmax-x(j+1),ymax-y(i))-
     1      f4(xmax-x(j),ymax-y(i)))+xmax*r4(3,1,i,j)
         do 4 i=2,my-1
         do 4 j=1,my-1
            r2(4,1,i,j)=xmax*(f5(y(j+1)-y(i),xmax)-
     1      f5(y(j)-y(i),xmax))
            r2(4,2,i,j)=y(i)*r2(4,1,i,j)+xmax*(f6(y(j+1)-y(i),xmax)-
     1      f6(y(j)-y(i),xmax))
            r4(4,1,i,j)=r2(4,1,i,j)
4.          r4(4,2,i,j)=r2(4,2,i,j)
```

```
c_____________
c  The two following do loops account for the fact the interior
c  angles at the corners are twice as small.
c_____________
      do 5 j=1,mx-1
           r3(1,1,1,j)=2.0d0*r3(1,1,1,j)
           r3(1,2,1,j)=2.0d0*r3(1,2,1,j)
           r3(3,1,1,j)=2.0d0*r3(3,1,1,j)
           r3(3,2,1,j)=2.0d0*r3(3,2,1,j)
           r3(5,1,1,j)=2.0d0*r3(5,1,1,j)
           r3(5,2,1,j)=2.0d0*r3(5,2,1,j)
           r3(1,1,mx,j)=2.0d0*r3(1,1,mx,j)
           r3(1,2,mx,j)=2.0d0*r3(1,2,mx,j)
           r3(3,1,mx,j)=2.0d0*r3(3,1,mx,j)
           r3(3,2,mx,j)=2.0d0*r3(3,2,mx,j)
           r3(5,1,mx,j)=2.0d0*r3(5,1,mx,j)
           r3(5,2,mx,j)=2.0d0*r3(5,2,mx,j)
           r1(1,1,1,j)=2.0d0*r1(1,1,1,j)
           r1(1,2,1,j)=2.0d0*r1(1,2,1,j)
           r1(3,1,1,j)=2.0d0*r1(3,1,1,j)
           r1(3,2,1,j)=2.0d0*r1(3,2,1,j)
           r1(5,1,1,j)=2.0d0*r1(5,1,1,j)
           r1(5,2,1,j)=2.0d0*r1(5,2,1,j)
           r1(1,1,mx,j)=2.0d0*r1(1,1,mx,j)
           r1(1,2,mx,j)=2.0d0*r1(1,2,mx,j)
           r1(5,1,mx,j)=2.0d0*r1(5,1,mx,j)
           r1(5,2,mx,j)=2.0d0*r1(5,2,mx,j)
           r1(3,1,mx,j)=2.0d0*r1(3,1,mx,j)
5          r1(3,2,mx,j)=2.0d0*r1(3,2,mx,j)
      do 6 j=1,my-1
           r3(2,1,mx,j)=2.0d0*r3(2,1,mx,j)
           r3(2,2,mx,j)=2.0d0*r3(2,2,mx,j)
           r3(4,1,1,j)=2.0d0*r3(4,1,1,j)
           r3(4,2,1,j)=2.0d0*r3(4,2,1,j)
           r1(2,1,mx,j)=2.0d0*r1(2,1,mx,j)
           r1(2,2,mx,j)=2.0d0*r1(2,2,mx,j)
           r1(4,1,1,j)=2.0d0*r1(4,1,1,j)
6          r1(4,2,1,j)=2.0d0*r1(4,2,1,j)
      return
      end
c_____________________
c   SUBROUTINE CURRENT IS WHERE THE KINETICS AND THE INFORMATION
c   FROM THE SCHWARZ-CHRISTOFFEL TRANSFORMATION ARE INPUT
c_____________________
      subroutine current(ielec,ikinet,dj)
      implicit double precision(a-h,o-z)
      dimension x(51),y(51),phi(4,51),r1(5,2,51,51),phio(51),
     1 r2(5,2,51,51),r3(5,2,51,51),r4(5,2,51,51),cd1(51),g(100),cd3(51)
      common x,y,phi,r1,r2,r3,r4,my,mx,cd1,xmax,ymax,g,xmaxi
     1,vj(200),vr(200),wins(200),wele(200),xins(200),xele(200),cd3,hl
c:_____________________________
```

```
c       linear kinetics (ikinet=1)
c       Tafel kinetics  (ikinet=2)
c       constant current (ikinet=3)
c_____________________________________
        if (ikinet.eq.1)then
          if (ielec.eq.1)then
             do 1 i=1,mx
1            cd1(i)=-dj*g(i)*(1.0d0-phi(1,i))
          else
             do 2 i=1,mx
2            cd3(i)=-dj*g(i)*phi(3,i)
          end if
        else if (ikinet.eq.2) then
          if (ielec.eq.1)then
             do 3 i=1,mx
3            cd1(i)=-g(i)*dexp(dj-phi(1,i))
          else
             do 4 i=1,mx
4            cd3(i)=-g(i)*dexp(phi(3,i))
          end if
        else
          if (ielec.eq.1)then
             do 5 i=1,mx
5            cd1(i)=-g(i)
          else
             do 6 i=1,mx
6            cd3(i)=-g(i)
          end if
        end if
        return
        end
c_____________________________
c   THE FOLLOWING FUNCTIONS ARE INTEGRALS TO BE USED IN 2-D PROBLEMS.
c   THEY ARE CALLED IN SUBROUTINE FILLMAT.
c_____________________________
        function f1(b,a)
        implicit double precision(a-h,o-z)
        if (a.eq.b) then
           f1=0.0d0
        else
           f1=(b-a)*(dlog(dabs(a-b))-1.0d0)
        end if
        return
        end
c_____________________
        function f2(b,a)
        implicit double precision(a-h,o-z)
        if (a.eq.b) then
            f2=0.0d0
        else
            te=(a-b)**2/2.0d0*(dlog(dabs(b-a))-0.5d0)
```

```
            f2=a*(b-a)*(dlog(dabs(b-a))-1.0d0)+te
        end if
        return
        end
c_______________
        function f3(b,a)
        implicit double precision(a-h,o-z)
        f3=b*dlog(b**2+a**2)-2.0d0*b+2.0d0*a*datan(b/a)
        return
        end
c_______________
        function f4(b,a)
        implicit double precision(a-h,o-z)
        f4=0.5d0*(b**2+a**2)*dlog(b**2+a**2)-0.5d0*b**2
        return
        end
c_______________
        function f5(b,a)
        implicit double precision(a-h,o-z)
        f5=datan(b/a)/a
        return
        end
c_______________
        function f6(b,a)
        implicit double precision(a-h,o-z)
        f6=0.5d0*dlog(a**2+b**2)
        return
        end
c_______________
        function f7(b,a)
        implicit double precision (a-h,o-z)
        f7=(b/(a**2+b**2)-datan(b/a)/a)/2.0d0/a**2
        return
        end
c_______________
        function f8(b,a)
        implicit double precision(a-h,o-z)
        f8=-0.5d0/(b**2+a**2)
        return
        end
c_______________
        function f9(b,a)
        implicit double precision(a-h,o-z)
        f9=-b/(b**2+a**2)/2.0d0+datan(b/a)/a/2.0d0
        return
        end
c_______________
        function fa(p1,p2,z1,z2)
        implicit double precision(a-h,o-z)
        fa=p1-(p2-p1)*z1/(z2-z1)
        return
```

```
      end
c_____________________
      function fb(p1,p2,z1,z2)
      implicit double precision(a-h,o-z)
      fb=(p2-p1)/(z2-z1)
      return
      end
c_____________________
      subroutine readguess
      implicit double precision(a-h,o-z)
      dimension x(51),y(51),phi(4,51),r1(5,2,51,51),phio(51),
     1 r2(5,2,51,51),r3(5,2,51,51),r4(5,2,51,51),cd1(51),g(100),cd3(51)
      common x,y,phi,r1,r2,r3,r4,my,mx,cd1,xmax,ymax,g,xmaxi
     1,vj(200),vr(200),wins(200),wele(200),xins(200),xele(200),cd3,hl
      do 1 i=1,mx/2+1
1     read*,phi(1,2*i-1),phi(3,2*i-1)
      do 2 i=2,mx-1,2
      phi(1,i)=phi(1,i-1)+(-phi(1,i-1)+phi(1,i+1))/2.0d0
2     phi(3,i)=phi(3,i-1)+(-phi(3,i-1)+phi(3,i+1))/2.0d0
      return
      end
c_____________________
      subroutine tread
      implicit double precision(a-h,o-z)
      dimension x(51),y(51),phi(4,51),r1(5,2,51,51),phio(51),
     1 r2(5,2,51,51),r3(5,2,51,51),r4(5,2,51,51),cd1(51),g(100),cd3(51)
      common x,y,phi,r1,r2,r3,r4,my,mx,cd1,xmax,ymax,g,xmaxi
     1,vj(200),vr(200),wins(200),wele(200),xins(200),xele(200),cd3,hl
      read*,mx,my
      read*,hl
      print*,'h/L=',hl
      pi=3.14159265358979d0
      do 1 i=1,200
1     read*,vj(i),wele(i),xele(i)
      do 2 i=1,200
2     read*,vr(i),wins(i),xins(i)
      xmax=vj(200)
      ymax=2.0d0*vr(200)
      x(1)=0.0d0
      ix=200/(mx-1)
      iy=200/(my-1)*2
      do 3 i=2,mx
3     x(i)=vj((i-1)*ix)
      y(1)=0.0d0
      y(my)=2.0d0*vr(200)
      y(my/2+1)=vr(200)
      do 4 i=2,my/2
      y(my-i+1)=vr(200)+vr(200-(i-1)*iy)
4     y(i)=(vr(200)-vr(200-(i-1)*iy))
      g(1)=dsqrt(wele(200)**2-wele(1)**2)/pi
      do 5 i=2,mx-1
```

```
      g(i)=dsqrt(wele(200)**2-wele((i-1)*ix)**2)/pi
5     continue
      g(mx)=0.0d0
      return
      end
c_____________________
      subroutine tprint(iter,ikinet,dj)
      implicit double precision(a-h,o-z)
      character*72 11
      dimension x(51),y(51),phi(4,51),r1(5,2,51,51),phio(51),
     1 r2(5,2,51,51),r3(5,2,51,51),r4(5,2,51,51),cd1(51),g(100),cd3(51)
      common x,y,phi,r1,r2,r3,r4,my,mx,cd1,xmax,ymax,g,xmaxi
     1,vj(200),vr(200),wins(200),wele(200),xins(200),xele(200),cd3,hl
      del=average(ikinet)
      delst=2.0d0*del*hl*x(mx)
c_____________________________________
      if (ikinet.eq.1)then
          bl=(1.0d0-phi(4,my/2+1))/del/y(my/2+1)
          dil=dj*(1.0d0-phi(1,mx))
          print101,dj,dil/delst,bl
      else if (ikinet.eq.2) then
          ec=dj-phi(4,my/2+1)-y(my/2+1)*del-dlog(delst)
          gd=y(my/2+1)*del-phi(4,1)+phi(4,my/2+1)
          dil=dexp(dj-phi(1,mx))
          print102,delst,dil/delst,ec,gd
      else
          ec=dj-phi(4,my/2+1)-y(my/2+1)*del-dlog(delst)
          gd=y(my/2+1)*del-phi(4,1)+phi(4,my/2+1)
          bl=(1.0d0-phi(4,my/2+1))/del/y(my/2+1)
          print103,1.0d0,1.0d0,gd
          print104,1.0d0,bl
      end if
      if (iter.ge.500)then
          print*,'The last run did not converge'
          stop
      end if
101   format(3G13.6)
102   format(4G13.6)
103   format('infinity',4G13.6)
104   format('infinity',3G13.6)
      return
      end
c_________________
c   CALCULATE THE AVERAGE CURRENT DENSITY
      function average(ikinet)
      implicit double precision(a-h,o-z)
      dimension x(51),y(51),phi(4,51),r1(5,2,51,51),phio(51),
     1 r2(5,2,51,51),r3(5,2,51,51),r4(5,2,51,51),cd1(51),g(100),cd3(51)
      common x,y,phi,r1,r2,r3,r4,my,mx,cd1,xmax,ymax,g,xmaxi
     1,vj(200),vr(200),wins(200),wele(200),xins(200),xele(200),cd3,hl
      sum=0.0d0
```

```
      do 1 i=2,mx
      ex=(cdl(i)+cdl(i-1))*(x(i)-x(i-1))/2.0d0
1     sum=sum+ex
      average=dabs(sum/x(mx))
      return
      end
```

```
      program scinf
      implicit double precision(a-h,o-z)
      character*72 ll
      dimension x(51),y(51),phi(4,51),rl(5,2,51,51),phio(51),
     lr2(5,2,51,51),r3(5,2,51,51),r4(5,2,51,51),cdl(51),g(100),phio3(51)
     1,vj(200),vr(200),wins(200),wele(200),xins(200),xele(200),cd3(51)
      common x,y,phi,rl,r2,r3,r4,my,mx,cdl,xmax,ymax,g,xmaxi
     1,vj,vr,wins,wele,xins,xele,cd3,hl
c_____________________
      read*,djint
      dj=djint
      pi=3.14159265358979d0
      damp=0.5d0
      read*,ikinet
      if (ikinet.eq.1)then
           print*,'linear kinetics'
      ll='J          i(L)/iavg          iol          io2          io4'
      print*,ll
      else if (ikinet.eq.2) then
      print*,'Tafel kinetics'
      ll='delta      ln(g0)      ln(gl)      ln(g2)          ln(g4)'
      print*,ll
      else
      print*,'constant current'
      end if
      call tread
      call fillmat
      iter=1
c_____________________
c   initial guess
      do 3 i=1,mx
           philinf=(1.0d0+dj)/(2.0d0+dj)
           phi3inf=1.0d0/(dj+2.0d0)
        phi(1,i)=-philinf-g(i)
3     phi(3,i)=-phi3inf-g(i)
      call current(3,ikinet,dj)
c_____________________
100   call current(1,ikinet,dj)
c_____________________
c   solve for phi2
      do 6 i=2,my-1
      phi(2,i)=0.0d0
      do 7 j=1,mx-1
         a2=fa(phi(1,j),phi(1,j+1),x(j),x(j+1))
         b2=fb(phi(1,j),phi(1,j+1),x(j),x(j+1))
         al=fa(cdl(j),cdl(j+1),x(j),x(j+1))
         bl=fb(cdl(j),cdl(j+1),x(j),x(j+1))
         a3=fa(cd3(j),cd3(j+1),x(j),x(j+1))
         b3=fb(cd3(j),cd3(j+1),x(j),x(j+1))
         a4=fa(phi(3,j),phi(3,j+1),x(j),x(j+1))
         b4=fb(phi(3,j),phi(3,j+1),x(j),x(j+1))
```

```
7       phi(2,i)=phi(2,i)+a1*r2(1,1,i,j)+b1*r2(1,2,i,j)+
     1 a2*r2(2,1,i,j)+b2*r2(2,2,i,j)+a3*r2(3,1,i,j)+b3*r2(3,2,i,j)
     1+a4*r2(5,1,i,j)+b4*r2(5,2,i,j)
        phi(2,i)=phi(2,i)/pi
6       continue
        phi(2,1)=phi(1,1)
        phi(2,my)=phi(3,1)
c_____________________________
c    solve for phi3
        do 12 i=1,mx
        phio3(i)=phi(3,i)
        phi(3,i)=0.0d0
        do 13 j=1,mx-1
           a1=fa(phi(1,j),phi(1,j+1),x(j),x(j+1))
           b1=fb(phi(1,j),phi(1,j+1),x(j),x(j+1))
           a2=fa(cd1(j),cd1(j+1),x(j),x(j+1))
           b2=fb(cd1(j),cd1(j+1),x(j),x(j+1))
           a3=fa(cd3(j),cd3(j+1),x(j),x(j+1))
           b3=fb(cd3(j),cd3(j+1),x(j),x(j+1))
13      phi(3,i)=phi(3,i)+a3*r3(1,1,i,j)+b3*r3(1,2,i,j)+
     1 a2*r3(3,1,i,j)+b2*r3(3,2,i,j)+a1*r3(5,1,i,j)+b1*r3(5,2,i,j)
        do 14 j=1,my-1
           a1=fa(phi(2,j),phi(2,j+1),y(j),y(j+1))
           b1=fb(phi(2,j),phi(2,j+1),y(j),y(j+1))
14      phi(3,i)=phi(3,i)+a1*r3(2,1,i,j)+b1*r3(2,2,i,j)
        phi(3,i)=phi(3,i)/pi
12      phi(3,i)=phio3(i)-damp*(phio3(i)-phi(3,i))
        call current(3,ikinet,dj)
c_____________________________
c    solve for phi1
        do 15 i=1,mx
        phio(i)=0.0d0
        do 16 j=1,mx-1
           a2=fa(cd3(j),cd3(j+1),x(j),x(j+1))
           b2=fb(cd3(j),cd3(j+1),x(j),x(j+1))
           a3=fa(phi(3,j),phi(3,j+1),x(j),x(j+1))
           b3=fb(phi(3,j),phi(3,j+1),x(j),x(j+1))
           a1=fa(cd1(j),cd1(j+1),x(j),x(j+1))
           b1=fb(cd1(j),cd1(j+1),x(j),x(j+1))
16      phio(i)=phio(i)+a1*r1(1,1,i,j)+b1*r1(1,2,i,j)+
     1 a2*r1(3,1,i,j)+b2*r1(3,2,i,j)+a3*r1(5,1,i,j)+b3*r1(5,2,i,j)
        do 17 j=1,my-1
           a1=fa(phi(2,j),phi(2,j+1),y(j),y(j+1))
           b1=fb(phi(2,j),phi(2,j+1),y(j),y(j+1))
17      phio(i)=phio(i)+a1*r1(2,1,i,j)+b1*r1(2,2,i,j)
15      phio(i)=phio(i)/pi
c_____________________________
c   check for errors
        error=0.0d0
        do 30 i=2,mx
        error=dmax1(error,dabs(phi(1,i)-phio(i)))
```

```
30      continue
        if (error.gt.1.d-5) then
            do 35 i=1,mx
35          phi(1,i)=phi(1,i)+damp*(phio(i)-phi(1,i))
            iter=iter+1
            if (iter.ge.500) then
               print*,'greater than 300 iterations','error=',error
               goto 999
            end if
            goto 100
        end if
999     call tprint(iter,ikinet,dj)
        dj=dj+djint
        if (dj.lt.50.0d0*djint) then
           if (dj.ge.6.0d0)damp=0.1d0
           iter=1
           goto 100
        end if
        end
c_______________________
        subroutine fillmat
        implicit double precision(a-h,o-z)
        dimension x(51),y(51),phi(4,51),r1(5,2,51,51),phio(51),
     1  r2(5,2,51,51),r3(5,2,51,51),r4(5,2,51,51),cd1(51),g(100),cd3(51)
        common x,y,phi,r1,r2,r3,r4,my,mx,cd1,xmax,ymax,g,xmaxi
     1,vj(200),vr(200),wins(200),wele(200),xins(200),xele(200),cd3,hl
        do 1 i=1,mx
        do 1 j=1,mx-1
           r1(1,1,i,j)=f1(x(j+1),x(i))-f1(x(j),x(i))
           r1(1,2,i,j)=f2(x(j+1),x(i))-f2(x(j),x(i))
           r1(3,1,i,j)=-0.5d0*(f3(x(j+1)-x(i),ymax)-f3(x(j)-x(i),ymax))
           r1(3,2,i,j)=x(i)*r1(3,1,i,j)-
     1     (f4(x(j+1)-x(i),ymax)-f4(x(j)-x(i),ymax))*0.5d0
           r1(5,1,i,j)=ymax*(f5(x(j+1)-x(i),ymax)-f5(x(j)-x(i),ymax))
           r1(5,2,i,j)=x(i)*r1(5,1,i,j)+ymax*(f6(x(j+1)-x(i),ymax)-
     1     f6(x(j)-x(i),ymax))
           r3(1,1,i,j)=-r1(1,1,i,j)
           r3(1,2,i,j)=-r1(1,2,i,j)
           r3(5,1,i,j)=r1(5,1,i,j)
           r3(5,2,i,j)=r1(5,2,i,j)
           r3(3,1,i,j)=-r1(3,1,i,j)
           r3(3,2,i,j)=-r1(3,2,i,j)
1       continue
        do 2 i=1,mx
        do 2 j=1,my-1
           if (i.eq.1) then
                r1(2,1,i,j)=0.0d0
                r1(2,2,i,j)=0.0d0
                r3(2,1,i,j)=0.0d0
                r3(2,2,i,j)=0.0d0
           else
```

```
                r1(2,1,i,j)=x(i)*(f5(y(j+1),x(i))-f5(y(j),x(i)))
                r1(2,2,i,j)=x(i)*(f6(y(j+1),x(i))-f6(y(j),x(i)))
                r3(2,1,i,j)=-x(i)*(f5(ymax-y(j+1),x(i))-
     1          f5(ymax-y(j),x(i)))
                r3(2,2,i,j)=ymax*r3(2,1,i,j)+
     1          x(i)*(f6(ymax-y(j+1),x(i))-f6(ymax-y(j),x(i)))
             end if
2       continue
        do 3 i=2,my-1
        do 3 j=1,mx-1
           r2(1,1,i,j)=0.5d0*(f3(x(j+1),y(i))-f3(x(j),y(i)))
           r2(1,2,i,j)=0.5d0*(f4(x(j+1),y(i))-f4(x(j),y(i)))
           r2(2,1,i,j)=y(i)*(f5(x(j+1),y(i))-f5(x(j),y(i)))
           r2(2,2,i,j)=y(i)*(f6(x(j+1),y(i))-f6(x(j),y(i)))
           r2(3,1,i,j)=-0.5d0*(f3(x(j+1),ymax-y(i))-
     1     f3(x(j),ymax-y(i)))
           r2(3,2,i,j)=-0.5d0*(f4(x(j+1),ymax-y(i))-
     1     f4(x(j),ymax-y(i)))
           r2(5,1,i,j)=-(y(i)-ymax)*(f5(x(j+1),ymax-y(i))-f5(x(j),ymax-y(i)))
           r2(5,2,i,j)=-(y(i)-ymax)*(f6(x(j+1),ymax-y(i))-f6(x(j),ymax-y(i)))
3       continue
c_______________
c  The next two do loops account for the interior angles at the
c  corners being twice as small.
c_______________
        do 5 j=1,mx-1
             r3(1,1,1,j)=2.0d0*r3(1,1,1,j)
             r3(1,2,1,j)=2.0d0*r3(1,2,1,j)
             r3(3,1,1,j)=2.0d0*r3(3,1,1,j)
             r3(3,2,1,j)=2.0d0*r3(3,2,1,j)
             r3(5,1,1,j)=2.0d0*r3(5,1,1,j)
             r3(5,2,1,j)=2.0d0*r3(5,2,1,j)
             r3(1,1,mx,j)=2.0d0*r3(1,1,mx,j)
             r3(1,2,mx,j)=2.0d0*r3(1,2,mx,j)
             r3(3,1,mx,j)=2.0d0*r3(3,1,mx,j)
             r3(3,2,mx,j)=2.0d0*r3(3,2,mx,j)
             r3(5,1,mx,j)=2.0d0*r3(5,1,mx,j)
             r3(5,2,mx,j)=2.0d0*r3(5,2,mx,j)
             r1(1,1,1,j)=2.0d0*r1(1,1,1,j)
             r1(1,2,1,j)=2.0d0*r1(1,2,1,j)
             r1(3,1,1,j)=2.0d0*r1(3,1,1,j)
             r1(3,2,1,j)=2.0d0*r1(3,2,1,j)
             r1(5,1,1,j)=2.0d0*r1(5,1,1,j)
             r1(5,2,1,j)=2.0d0*r1(5,2,1,j)
             r1(1,1,mx,j)=2.0d0*r1(1,1,mx,j)
             r1(1,2,mx,j)=2.0d0*r1(1,2,mx,j)
             r1(5,1,mx,j)=2.0d0*r1(5,1,mx,j)
             r1(5,2,mx,j)=2.0d0*r1(5,2,mx,j)
             r1(3,1,mx,j)=2.0d0*r1(3,1,mx,j)
5            r1(3,2,mx,j)=2.0d0*r1(3,2,mx,j)
        do 6 j=1,my-1
```

```
            r3(2,1,mx,j)=2.0d0*r3(2,1,mx,j)
            r3(2,2,mx,j)=2.0d0*r3(2,2,mx,j)
            r1(2,1,mx,j)=2.0d0*r1(2,1,mx,j)
            r1(2,2,mx,j)=2.0d0*r1(2,2,mx,j)
6           continue
      return
      end
c_____________________
c   SUBROUTINE CURRENT IS WHERE THE KINETICS AND THE INFORMATION
c   FROM THE SCHWARZ-CHRISTOFFEL TRANSFORMATION ARE INPUT
c_____________________
      subroutine current(ielec,ikinet,dj)
      implicit double precision(a-h,o-z)
      dimension x(51),y(51),phi(4,51),r1(5,2,51,51),phio(51),
     1 r2(5,2,51,51),r3(5,2,51,51),r4(5,2,51,51),cd1(51),g(100),cd3(51)
      common x,y,phi,r1,r2,r3,r4,my,mx,cd1,xmax,ymax,g,xmaxi
     1,vj(200),vr(200),wins(200),wele(200),xins(200),xele(200),cd3,hl
c_____________________________
c     linear kinetics (ikinet=1)
c     Tafel kinetics  (ikinet=2)
c     constant current (ikinet=3)
c_____________________________
      if (ikinet.eq.1)then
           philinf=(1.0d0+dj)/(2.0d0+dj)
           phi3inf=1.0d0/(dj+2.0d0)
        if (ielec.eq.1)then
           do 1 i=1,mx
1          cd1(i)=-dj*g(i)*(1.0d0-phi(1,i)-philinf)-(phi3inf-philinf)
        else
           do 2 i=1,mx
2          cd3(i)=-dj*g(i)*(phi(3,i)+phi3inf)-(phi3inf-philinf)
        end if
      else if (ikinet.eq.2) then
        if (ielec.eq.1)then
           do 3 i=1,mx
3          cd1(i)=-g(i)*dabs(dj)*dexp(-phi(1,i))+dabs(dj)
        else
           do 4 i=1,mx
4          cd3(i)=-g(i)*dabs(dj)*dexp(phi(3,i))+dabs(dj)
        end if
      else
        if (ielec.eq.1)then
           do 5 i=1,mx
5          cd1(i)=-g(i)+1.0d0
        else
           do 6 i=1,mx
6          cd3(i)=-g(i)+1.0d0
        end if
      end if
      return
      end
```

```
c_____________________
c   THE FOLLOWING FUNCTIONS ARE INTEGRALS TO BE USED IN 2-D PROBLEMS.
c   THEY ARE CALLED IN SUBROUTINE FILLMAT.
c_____________________
      function f1(b,a)
      implicit double precision(a-h,o-z)
      if (a.eq.b) then
         f1=0.0d0
      else
         f1=(b-a)*(dlog(dabs(a-b))-1.0d0)
      end if
      return
      end
c_________________
      function f2(b,a)
      implicit double precision(a-h,o-z)
      if (a.eq.b) then
          f2=0.0d0
      else
          te=(a-b)**2/2.0d0*(dlog(dabs(b-a))-0.5d0)
          f2=a*(b-a)*(dlog(dabs(b-a))-1.0d0)+te
      end if
      return
      end
c_______________
      function f3(b,a)
      implicit double precision(a-h,o-z)
      f3=b*dlog(b**2+a**2)-2.0d0*b+2.0d0*a*datan(b/a)
      return
      end
c_____________
      function f4(b,a)
      implicit double precision(a-h,o-z)
      f4=0.5d0*(b**2+a**2)*dlog(b**2+a**2)-0.5d0*b**2
      return
      end
c_______________
      function f5(b,a)
      implicit double precision(a-h,o-z)
      f5=datan(b/a)/a
      return
      end
c_________________
      function f6(b,a)
      implicit double precision(a-h,o-z)
      f6=0.5d0*dlog(a**2+b**2)
      return
      end
c_________________
      function f7(b,a)
      implicit double precision (a-h,o-z)
```

```
      f7=(b/(a**2+b**2)-datan(b/a)/a)/2.0d0/a**2
      return
      end
c_____________________
      function f8(b,a)
      implicit double precision(a-h,o-z)
      f8=-0.5d0/(b**2+a**2)
      return
      end
c_____________________
      function f9(b,a)
      implicit double precision(a-h,o-z)
      f9=-b/(b**2+a**2)/2.0d0+datan(b/a)/a/2.0d0
      return
      end
c_____________________
      function fa(p1,p2,z1,z2)
      implicit double precision(a-h,o-z)
      fa=p1-(p2-p1)*z1/(z2-z1)
      return
      end
c_____________________
      function fb(p1,p2,z1,z2)
      implicit double precision(a-h,o-z)
      fb=(p2-p1)/(z2-z1)
      return
      end
c_____________________
      subroutine tread
      implicit double precision(a-h,o-z)
      dimension x(51),y(51),phi(4,51),r1(5,2,51,51),phio(51),
     1 r2(5,2,51,51),r3(5,2,51,51),r4(5,2,51,51),cd1(51),g(100),cd3(51)
      common x,y,phi,r1,r2,r3,r4,my,mx,cd1,xmax,ymax,g,xmaxi
     1,vj(200),vr(200),wins(200),wele(200),xins(200),xele(200),cd3,hl
      read*,mx,my
      print*,'h/L= 0'
      pi=3.14159265358979d0
      ymax=1.0d0
      xmax=2.0d0
      do 1 i=1,mx
      x(i)=xmax*dfloat(i-1)/dfloat(mx-1)
      pix=2.0d0*dlog(dcosh(pi*x(i)))
      g(i)=dsqrt(1.0d0-dexp(-pix))
1     continue
      do 2 i=1,my
2     y(i)=ymax*dfloat(i-1)/dfloat(my-1)
      return
      end
c_____________________
      subroutine tprint(iter,ikinet,dj)
      implicit double precision(a-h,o-z)
```

```
      character*72 l1
      dimension x(51),y(51),phi(4,51),r1(5,2,51,51),phio(51),
     1 r2(5,2,51,51),r3(5,2,51,51),r4(5,2,51,51),cd1(51),g(100),cd3(51)
      common x,y,phi,r1,r2,r3,r4,my,mx,cd1,xmax,ymax,g,xmaxi
     1,vj(200),vr(200),wins(200),wele(200),xins(200),xele(200),cd3,h1
c_____________________________________________
      if (ikinet.eq.1)then
          philinf=(1.0d0+dj)/(2.0d0+dj)
          phi3inf=1.0d0/(dj+2.0d0)
          v=philinf-phi3inf
          b1=(1.0d0-phi(2,5)-philinf)*dj/v
          b2=(1.0d0-phi(2,9)-philinf)*dj/v
          b4=(1.0d0-phi(2,17)-philinf)*dj/v
          dil=-dj*(1.0d0-phi(1,1)-philinf)/(phi3inf-philinf)
          print101,dj,dil,b1,b2,b4
      else if (ikinet.eq.2) then
          g1=-phi(2,5)
          g2=-phi(2,9)
          g4=-phi(2,17)
          g0=-phi(2,1)
          print101,dj,g0,g1,g2,g4
      else
         print*,'Along insulator:'
         do 10 i=1,my
10         print*,y(i),phi(2,i)+y(i)
         print*,'Along electrode:'
         do 20 i=1,mx
20         print*,x(i),phi(1,i)
      end if
      if (iter.ge.500)then
          print*,'The last run did not converge'
          stop
      end if
101   format(5G13.6)
      return
      end
```

```
      program luggin
      implicit double precision(a-h,o-z)
      dimension zw(0:51),rd(0:51),rp(101),y12(2,0:51,51),
     1y13(2,0:51,101),y21(2,51,51),y22(2,51,51),y31(2,101,51),
     1phi3(101),phi2n(0:51),phi3o(101),phi2(0:51),
     1y23a(51),y13a(0:51),cd(0:51),y23(2,51,101),y32(2,101,51)
     1,phi1(0:51),y31p(2,101,0:51),y21p(2,51,51),philcd(0:51)
      common y21,y22,y23,y31,y32,zw,rp,zstart,zstop,pl,ic,jc
     1,rd,nd,np,nw,pp,damp,pi,y23a,y12,y13,y13a,philcd,y31p,y21p,cd
      pi=3.14159265358979d0
c_____________________
c  pl= dimensionless length of capillary wall
c  nw= # of points on wall where potential is calculated
c  np= # of points on plane where potential is calculated
c_____________________
      call pread
      call fillmat
      call current(0)
      icurr=0
c_____________________________
c  Initial guesses.
      do 3 i=0,nw
3     phi2(i)=pl+1.0d0-(1.0d0-0.75d0/pl)*zw(i)
      do 4 i=0,nd
      phi1(i)=pl+1.0d0
4     continue
      do 5 i=1,np
5     phi3o(i)=0.75d0*(1.0d0-2.0d0/pi*datan(rp(i)**2-1.0d0))
c_____________________
c   calculate the potential on the insulating plane
100   do 10 i=1,np
      phi3(i)=0.0d0
      do 11 j=1,nd
            a=fa(rd(j),rd(j-1),cd(j),cd(j-1))
            b=fb(rd(j),rd(j-1),cd(j),cd(j-1))
            c=fa(rd(j),rd(j-1),phi1(j),phi1(j-1))
            d=fb(rd(j),rd(j-1),phi1(j),phi1(j-1))
11     phi3(i)=phi3(i)+a*y31(1,i,j)+b*y31(2,i,j)+
     1  c*y31p(1,i,j)+d*y31p(2,i,j)
      do 10 j=1,nw
            a=fa(zw(j),zw(j-1),phi2(j),phi2(j-1))
            b=fb(zw(j),zw(j-1),phi2(j),phi2(j-1))
10    phi3(i)=phi3(i)+a*y32(1,i,j)+b*y32(2,i,j)
c_____________________
c   calculate the potential on the disk electrode
      do 70 i=0,nd
      phi1(i)=philcd(i)+(0.6d0*phi3(1)+0.4d0*phi2(nw))*y13a(i)
       do 71 j=1,np-1
        a=fa(rp(j+1)-1.d0,rp(j)-1.d0,phi3(j+1),phi3(j))
        b=fb(rp(j+1),rp(j),phi3(j+1),phi3(j))
71     phi1(i)=phi1(i)+a*y13(1,i,j)+b*y13(2,i,j)
```

```
        do 72 j=1,nw
           a=fa(zw(j),zw(j-1),phi2(j),phi2(j-1))
           b=fb(zw(j),zw(j-1),phi2(j),phi2(j-1))
 72      phi1(i)=phi1(i)+a*y12(1,i,j)+b*y12(2,i,j)
 70     continue
        phi1(nd)=2.0d0*phi1(nd)
        phi1(nd)=phi1(nd-1)
        phi2n(0)=phi1(nd)
c_____________________
c   calculate the potential on the wall
       do 20 i =1,nw
        phi2n(i)=(0.6d0*phi3(1)+0.4d0*phi2(nw))*y23a(i)
          do 21 j=1,np-1
             a=fa(rp(j+1)-1.d0,rp(j)-1.d0,phi3(j+1),phi3(j))
             b=fb(rp(j+1),rp(j),phi3(j+1),phi3(j))
21        phi2n(i)=phi2n(i)+a*y23(1,i,j)+b*y23(2,i,j)
          do 22 j=1,nw
             a=fa(zw(j),zw(j-1),phi2(j),phi2(j-1))
             b=fb(zw(j),zw(j-1),phi2(j),phi2(j-1))
22        phi2n(i)=phi2n(i)+a*y22(1,i,j)+b*y22(2,i,j)
          do 23 j=1,nd
               a=fa(rd(j),rd(j-1),cd(j),cd(j-1))
               b=fb(rd(j),rd(j-1),cd(j),cd(j-1))
               c=fa(rd(j),rd(j-1),phi1(j),phi1(j-1))
               d=fb(rd(j),rd(j-1),phi1(j),phi1(j-1))
23        phi2n(i)=phi2n(i)+a*y21(1,i,j)+b*y21(2,i,j)+
     1    c*y21p(1,i,j)+d*y21p(2,i,j)
20     continue
       phi2n(nw)=2.0d0/3.0d0*phi2n(nw)
c_____________________________
c  Check for convergence
       error=0.0d0
       do 30 i=0,nw
30     error=dmax1(dabs((phi2n(i)-phi2(i))/phi2(i)),error)
       if (error.le.1.d-5) goto 600
       if (error.le.1.d-3)damp=0.1d0
       do 35 i=0,nw
35     phi2(i)=phi2(i)+damp*(phi2n(i)-phi2(i))
       iter=iter+1
       if(iter.le.500)goto 100
600    continue
       if(iter.ge.500)print*,'DID NOT CONVERGE, ERROR = ',error
c_____________________
c   PRINT RESULTS
       print *,'wall'
       print*,zw(0),char(9),phi1(nd)
       do 500 i=1,nw
500    print*,zw(i),char(9),phi2n(i)
       print*,'insulating plane'
       do 501 i=1,np
501    print *,rp(i),char(9),phi3(i)
```

```
      print*,'disk electrode'
      do 502 i=0,nd
502   print*,rd(i),char(9),phil(i)
      do 503 i=0,nd
503   write(7,*),rd(i),phil(i)
      if (icurr.le.18) then
       icurr=icurr+2
       call current(icurr)
       iter=1
       goto 100
      end if
      end
c_____________________________
c   Subroutine to fill the matrix
      subroutine fillmat
      implicit double precision (a-h,o-z)
      dimension zw(0:51),rd(0:51),rp(101),y12(2,0:51,51),
     1y13(2,0:51,101),y21(2,51,51),y22(2,51,51),y31(2,101,51),
     1phi3(101),phi2n(0:51),phi3o(101),phi2(0:51),
     1y23a(51),y13a(0:51),cd(0:51),y23(2,51,101),y32(2,101,51)
     1,phil(0:51),y31p(2,101,0:51),y21p(2,51,51),philcd(0:51)
      common y21,y22,y23,y31,y32,zw,rp,zstart,zstop,pl,ic,jc
     1,rd,nd,np,nw,pp,damp,pi,y23a,y12,y13,y13a,philcd,y31p,y21p,cd
      mw=500
      mp=500
      md=500
      do 1 ic=1,nw
      do 2 jc=1,nw
      if ((ic.eq.jc).or.(ic.eq.(jc-1)))then
          call integ3(zw(jc),zw(jc-1),10*mw,8)
          y22(1,ic,jc)=pp
          call integ3(zw(jc),zw(jc-1),10*mw,9)
          y22(2,ic,jc)=pp
      else
          call integ1(zw(jc),zw(jc-1),mw,1)
          y22(1,ic,jc)=pp
          call integ1(zw(jc),zw(jc-1),mw,2)
          y22(2,ic,jc)=pp
      end if
2     continue
      do 3 jc=1,nd
        call integ1(rd(jc),rd(jc-1),md,7)
        y21p(1,ic,jc)=pp
        call integ1(rd(jc),rd(jc-1),md,21)
        y21p(2,ic,jc)=pp
        call integ1(rd(jc),rd(jc-1),md,3)
        y21(1,ic,jc)=pp
        call integ1(rd(jc),rd(jc-1),md,4)
3     y21(2,ic,jc)=pp
      do 1 jc=1,np-1
      if (ic.eq.nw) then
```

```
            y23(1,ic,jc)=0.0d0
            y23(2,ic,jc)=0.0d0
         else
            call integ2(rp(jc+1),rp(jc),mp,5)
            y23(1,ic,jc)=pp
            call integ2(rp(jc+1),rp(jc),mp,6)
            y23(2,ic,jc)=pp
          end if
1        continue
         do 10 ic=1,np
         do 20 jc=1,nd
            call integl(rd(jc),rd(jc-1),mp,14)
            y31p(1,ic,jc)=pp
            call integl(rd(jc),rd(jc-1),mp,22)
            y31p(2,ic,jc)=pp
            call integl(rd(jc),rd(jc-1),mp,10)
            y31(1,ic,jc)=pp
            call integl(rd(jc),rd(jc-1),mp,11)
20          y31(2,ic,jc)=pp
         do 30 jc=1,nw
            call integl(zw(jc),zw(jc-1),mp,12)
            y32(1,ic,jc)=pp
            call integl(zw(jc),zw(jc-1),mp,13)
30          y32(2,ic,jc)=pp
10       continue
         do 100 ic=0,nd
         do 200 jc=1,nw
         if ((ic.eq.nd).and.(jc.eq.1))then
             call integ3(zw(jc),zw(jc-1),10*mw,26)
             y12(1,ic,jc)=pp
             call integ3(zw(jc),zw(jc-1),10*mw,25)
             y12(2,ic,jc)=pp
         else
           call integl(zw(jc),zw(jc-1),mw,15)
           y12(1,ic,jc)=pp
           call integl(zw(jc),zw(jc-1),mw,16)
           y12(2,ic,jc)=pp
         end if
200      continue
         do 300 jc=1,np-1
            call integ2(rp(jc+1),rp(jc),mp,17)
            y13(1,ic,jc)=pp
            call integ2(rp(jc+1),rp(jc),mp,18)
300         y13(2,ic,jc)=pp
100      continue
         return
         end
c_____________________________
c    Basic Trapezoid integration
         subroutine integl(up,down,m,id)
         implicit double precision(a-h,o-z)
```

```
      dimension zw(0:51),rd(0:51),rp(101),y12(2,0:51,51),
     1y13(2,0:51,101),y21(2,51,51),y22(2,51,51),y31(2,101,51),
     1phi3(101),phi2n(0:51),phi3o(101),phi2(0:51),
     1y23a(51),y13a(0:51),cd(0:51),y23(2,51,101),y32(2,101,51)
     1,phi1(0:51),y31p(2,101,0:51),y21p(2,51,51),phi1cd(0:51)
      common y21,y22,y23,y31,y32,zw,rp,zstart,zstop,pl,ic,jc
     1,rd,nd,np,nw,pp,damp,pi,y23a,y12,y13,y13a,phi1cd,y31p,y21p,cd
      pp=0.0d0
      j=1
      eps=(up-down)/dfloat(m-1)
      do 1 j=2,m
         x=down+eps*dfloat(j-1)
         or2=ord(id,x)
         pp=pp+eps*(or2+or1)/2.0d0
1     or1=or2
      return
      end
c_____________________________
c  Integration "log style"
      subroutine integ2(up,down,m,id)
      implicit double precision(a-h,o-z)
      dimension zw(0:51),rd(0:51),rp(101),y12(2,0:51,51),
     1y13(2,0:51,101),y21(2,51,51),y22(2,51,51),y31(2,101,51),
     1phi3(101),phi2n(0:51),phi3o(101),phi2(0:51),
     1y23a(51),y13a(0:51),cd(0:51),y23(2,51,101),y32(2,101,51)
     1,phi1(0:51),y31p(2,101,0:51),y21p(2,51,51),phi1cd(0:51)
      common y21,y22,y23,y31,y32,zw,rp,zstart,zstop,pl,ic,jc
     1,rd,nd,np,nw,pp,damp,pi,y23a,y12,y13,y13a,phi1cd,y31p,y21p,cd
      up1=up-1.0d0
      down1=down-1.0d0
      x1=down1
      h=dlog(up1/down1)/dfloat(m-1)
      or1=ord(id,down1)
      if ((id.eq.17).and.(jc.eq.1))then
          y13a(ic)=or1*down1
      else if ((jc.eq.1).and.(id.eq.5)) then
          y23a(ic)=or1*down1
      end if
      pp=0.0d0
      do 1 j=2,m
         x2=down1*dexp(h*dfloat(j-1))
         or2=ord(id,x2)
         b=dlog(or2/or1)/h
         pp=pp+(x2*or2-x1*or1)/(1.0d0+b)
         x1=x2
1     or1=or2
      return
      end
c_____________________________
c  This is for the addition and subtraction of singular values.
      subroutine integ3(up,down,m,id)
```

```
      implicit double precision(a-h,o-z)
      dimension zw(0:51),rd(0:51),rp(101),y12(2,0:51,51),
     1y13(2,0:51,101),y21(2,51,51),y22(2,51,51),y31(2,101,51),
     1phi3(101),phi2n(0:51),phi3o(101),phi2(0:51),
     1y23a(51),y13a(0:51),cd(0:51),y23(2,51,101),y32(2,101,51)
     1,phi1(0:51),y31p(2,101,0:51),y21p(2,51,51),phicd(0:51)
      common y21,y22,y23,y31,y32,zw,rp,zstart,zstop,pl,ic,jc
     1,rd,nd,np,nw,pp,damp,pi,y23a,y12,y13,y13a,phicd,y31p,y21p,cd
      call integ1(up,down,m,id)
      dif=up-down
      if (mod(id,2).ne.0)then
            te=0.5d0*dif**2*(dlog(dif/4.0d0)-0.5d0)
            if(id.eq.25)then
                 corr=te
                 goto 111
            end if
            if (dabs(zw(ic)-up).le.0.0001d0)te=-te
            corr=zw(ic)*dif*(dlog(dif/4.0d0)-1.0d0)+te
      else
        corr=dif*(dlog(dif/4.0d0)-1.0d0)
      end if
111   pp=pp-corr/2.0d0/pi
      return
      end
c_____________________________________
      subroutine integ4(up,down,m,id,icurr)
      implicit double precision(a-h,o-z)
      dimension zw(0:51),rd(0:51),rp(101),y12(2,0:51,51),
     1y13(2,0:51,101),y21(2,51,51),y22(2,51,51),y31(2,101,51),
     1phi3(101),phi2n(0:51),phi3o(101),phi2(0:51),
     1y23a(51),y13a(0:51),cd(0:51),y23(2,51,101),y32(2,101,51)
     1,phi1(0:51),y31p(2,101,0:51),y21p(2,51,51),phicd(0:51)
      common y21,y22,y23,y31,y32,zw,rp,zstart,zstop,pl,ic,jc
     1,rd,nd,np,nw,pp,damp,pi,y23a,y12,y13,y13a,phicd,y31p,y21p,cd
      jc=icurr
      call integ1(up,down,m,id)
      corr=0.0d0
      if (id.eq.19) then
         dif=up-down
         corr=dif*(dlog(dif)-1.0d0)
         y=dcos(pi/2.0d0*(1.d0-rd(ic)))
         pp=pp+corr/pi*P(icurr,y)
      end if
      return
      end
c_____________________________________
      function fa(x2,x1,p2,p1)
      implicit double precision(a-h,o-z)
      fa=p1-(p2-p1)*x1/(x2-x1)
      return
      end
```

```
c_____________________________
      function fb(x2,x1,p2,p1)
      implicit double precision(a-h,o-z)
      fb=(p2-p1)/(x2-x1)
      return
      end
c_____________________________
c  This simulates a Pascal case statement for use in integration.
       function ord(id,x)
       implicit double precision(a-h,o-z)
       dimension zw(0:51),rd(0:51),rp(101),y12(2,0:51,51),
     1y13(2,0:51,101),y21(2,51,51),y22(2,51,51),y31(2,101,51),
     1phi3(101),phi2n(0:51),phi3o(101),phi2(0:51),
     1y23a(51),y13a(0:51),cd(0:51),y23(2,51,101),y32(2,101,51)
     1,phi1(0:51),y31p(2,101,0:51),y21p(2,51,51),phi1cd(0:51)
       common y21,y22,y23,y31,y32,zw,rp,zstart,zstop,pl,ic,jc
     1,rd,nd,np,nw,pp,damp,pi,y23a,y12,y13,y13a,phi1cd,y31p,y21p,cd
       if (id.eq.1) then
          ord=-f2(x,zw(ic),1.0d0,1.0d0)
       else if (id.eq.2) then
          ord=-f2(x,zw(ic),1.0d0,1.0d0)*x
       else if (id.eq.3) then
          ord=-f1(0.0d0,zw(ic),x,1.0d0)*x
       else if (id.eq.4) then
          ord=-f1(0.0d0,zw(ic),x,1.0d0)*x**2
       else if (id.eq.5) then
          ord=f3(pl,zw(ic),x+1.0d0,1.d0)*(x+1.0d0)
       else if (id.eq.6) then
          ord=f3(pl,zw(ic),x+1.d0,1.d0)*x*(x+1.0d0)
       else if (id.eq.7) then
          ord=f3(0.0d0,zw(ic),x,1.0d0)*x
       else if (id.eq.8) then
       if (dabs(x-zw(ic)).le.1d-8) then
        ord=-0.5d0/pi*(1.0d0-dlog(2.0d0))
       else
        ord=-f2(x,zw(ic),1.0d0,1.0d0)+
     1 dlog((x-zw(ic))**2/16.0d0)/4.0d0/pi
       end if
       else if (id.eq.9) then
       if (dabs(x-zw(ic)).le.1d-8)then
        ord=-x/2.d0/pi*(1.0d0-dlog(2.0d0))
       else
        ord=(-f2(x,zw(ic),1.0d0,1.0d0)+dlog((x-zw(ic))**2/16.0d0)
     1   /4.0d0/pi)*x
       end if
       else if (id.eq.10) then
          ord=-f1(0.0d0,pl,x,rp(ic))*x
       else if (id.eq.11) then
          ord=-f1(0.0d0,pl,x,rp(ic))*x**2
       else if (id.eq.12) then
          ord=-f2(x,pl,1.0d0,rp(ic))
```

```
      else if (id.eq.13) then
         ord=-f2(x,pl,1.0d0,rp(ic))*x
      else if (id.eq.14) then
         ord=f3(0.0d0,pl,x,rp(ic))*x
      else if (id.eq.15) then
         ord=-f2(x,0.0d0,1.0d0,rd(ic))
      else if (id.eq.16) then
         ord=-f2(x,0.0d0,1.0d0,rd(ic))*x
      else if (id.eq.17) then
         ord=f3(pl,0.0d0,x+1.0d0,rd(ic))*(x+1.0d0)
      else if (id.eq.18) then
         ord=f3(pl,0.0d0,x+1.0d0,rd(ic))*x*(x+1.d0)
      else if (id.eq.19) then
        yq=dcos(pi/2.d0*(1.d0-rd(ic)))
        y=dcos(pi/2.d0*(1.d0-x))
        if (dabs(x-rd(ic)).le.1d-7)then
         ord=-dlog(8.0d0*rd(ic))/pi*P(jc,yq)
        else
         ord=-f1(0.0d0,0.0d0,x,rd(ic))*x*P(jc,y)-
     1    P(jc,yq)*dlog((x-rd(ic))**2)/pi/2.0d0
        end if
      else if (id.eq.20) then
         y=dcos(pi/2.d0*(1.d0-x))
         ord=-x/(rd(ic)+x)*P(jc,y)
      else if (id.eq.21) then
         ord=f3(0.0d0,zw(ic),x,1.0d0)*x**2
      else if (id.eq.22) then
         ord=f3(0.0d0,pl,x,rp(ic))*x**2
      else if (id.eq.26) then
      if (x.le.1d-8) then
       ord=-0.5d0/pi*(1.0d0-dlog(2.d0))
      else
       ord=-f2(x,0.0d0,1.0d0,1.0d0)+dlog(x**2/16.0d0)/4.0d0/pi
      end if
      else if (id.eq.25) then
      if (x.le.1d-8)then
       ord=-x/2.d0/pi*(1.0d0-dlog(2.0d0))
      else
       ord=(-f2(x,0.d0,1.0d0,1.0d0)+dlog(x**2/16.0d0)/4.0d0/pi)*x
      end if
      else
          print*,'Invalid ID number'
          stop
      end if
      return
      end
c_____________________________
c   This is the Green's function for axisymmetric problems.
      function f1(z,zq,r,rq)
      implicit double precision(a-h,o-z)
      pi=3.14159265358979d0
```

```
      w=((r-rq)**2+(z-zq)**2)/((r+rq)**2+(z-zq)**2)
      f1=2.0d0/pi*el(w)/dsqrt((z-zq)**2+(r+rq)**2)
      return
      end
c_____________________________
c   This is the r-component of the gradient of the Green's function
      function f2(z,zq,r,rq)
      implicit double precision(a-h,o-z)
      pi=3.14159265358979d0
      w=((r-rq)**2+(z-zq)**2)/((r+rq)**2+(z-zq)**2)
      zd=z-zq
      f2=-(e2(w)*(r**2-rq**2-zd**2)/((r-rq)**2+zd**2)+el(w))/2.0d0/r/
     1 dsqrt((r+rq)**2+zd**2)*2.0d0/pi
      return
      end
c_____________________________
c  This is the z-component of the gradient of the Green's function.
      function f3(z,zq,r,rq)
      implicit double precision(a-h,o-z)
      pi=3.14159265358979d0
      w=((r-rq)**2+(z-zq)**2)/((r+rq)**2+(z-zq)**2)
      zd=z-zq
      f3=-2.0d0/pi*zd*e2(w)/((r-rq)**2+zd**2)/dsqrt(zd**2+(r+rq)**2)
      return
      end
c_____________________________
c   Complete Elliptic Integral of the First Kind
      function el(w)
      implicit double precision (a-h,o-z)
      dimension a(5),b(5)
      data a / 1.38629436112d0,.09666344259d0,.03590092383d0
     1,.03742563713d0,.01451196212d0/
      data b/ .5d0,.12498593597d0,.06880248576d0,
     1 .03328355346d0,.00441787012d0/
      d=a(1)+a(2)*w+a(3)*w**2+a(4)*w**3+a(5)*w**4
      el=d+(b(1)+b(2)*w+b(3)*w**2+b(4)*w**3+b(5)*w**4)*dlog(1.0d0/w)
      return
      end
c_____________________________
c   Complete Elliptic Integral of the Second Kind
      function e2(w)
      implicit double precision (a-h,o-z)
      dimension c(4),d(4)
      data c / .44325141463d0,.06260601220d0,.04757383546d0,
     1 .01736506451d0/
      data d/ .2499836831d0,.09200180037d0,.04069697526d0,
     1 .00526449639d0/
      a=1.0d0+c(1)*w+c(2)*w**2+c(3)*w**3+c(4)*w**4
      e2=a+(d(1)*w+d(2)*w**2+d(3)*w**3+d(4)*w**4)*dlog(1.0d0/w)
      end
c_____________________________
```

```
      subroutine pread
      implicit double precision(a-h,o-z)
      dimension zw(0:51),rd(0:51),rp(101),y12(2,0:51,51),
     1y13(2,0:51,101),y21(2,51,51),y22(2,51,51),y31(2,101,51),
     1phi3(101),phi2n(0:51),phi3o(101),phi2(0:51),
     1y23a(51),y13a(0:51),cd(0:51),y23(2,51,101),y32(2,101,51)
     1,phi1(0:51),y31p(2,101,0:51),y21p(2,51,51),philcd(0:51)
      common y21,y22,y23,y31,y32,zw,rp,zstart,zstop,pl,ic,jc
     1,rd,nd,np,nw,pp,damp,pi,y23a,y12,y13,y13a,philcd,y31p,y21p,cd
      read*,np,nw,nd
      read*,pl
      zstop=100.00d0
      zstart=0.01d0
      damp=0.5d0
      hp=dlog(zstop/zstart)/(dfloat(np-1))
      do 1 i=0,nw-5
1     zw(i)=(pl-0.1d0)*dfloat(i)/dfloat(nw-5)
      do 100 i=1,5
100   zw(nw-5+i)=pl-0.1d0+0.1d0*dfloat(i)/dfloat(5)
      do 2 i=1,np
2     rp(i)=1.0d0+zstart*exp(hp*dfloat(i-1))
      do 3 i=0,nd
3     rd(i)=dfloat(i)/dfloat(nd)
      return
      end
c_____________________
      subroutine current(icurr)
      implicit double precision(a-h,o-z)
      dimension zw(0:51),rd(0:51),rp(101),y12(2,0:51,51),
     1y13(2,0:51,101),y21(2,51,51),y22(2,51,51),y31(2,101,51),
     1phi3(101),phi2n(0:51),phi3o(101),phi2(0:51),
     1y23a(51),y13a(0:51),cd(0:51),y23(2,51,101),y32(2,101,51)
     1,phi1(0:51),y31p(2,101,0:51),y21p(2,51,51),philcd(0:51)
      common y21,y22,y23,y31,y32,zw,rp,zstart,zstop,pl,ic,jc
     1,rd,nd,np,nw,pp,damp,pi,y23a,y12,y13,y13a,philcd,y31p,y21p,cd
      do 1 i=0,nd
      x=dcos(pi/2.0d0*(1.0d0-rd(i)))
1     cd(i)=-P(icurr,x)
      md=1000
      do 2 ic=1,nd-1
         call integ4(rd(ic),0.0d0,md,19,icurr)
         philcd(ic)=-pp
         call integ4(1.0d0,rd(ic),md,19,icurr)
         philcd(ic)=philcd(ic)-pp
2     continue
      ic=nd
      call integ4(1.0d0,0.0d0,md,19,icurr)
      philcd(nd)=-pp
      ic=0
      call integ4(1.0d0,0.0d0,md,20,icurr)
      philcd(0)=-pp
```

```
      return
      end
c_____________________________
c  Calculation of Legendre Polynomials
      function P(n,x)
      implicit double precision(a-h,o-z)
      p1=1.d0
      p2=x
      if(n-1)1,2,3
1     P=p1
      return
2     P=p2
      return
3     nm1=n-1
      do 4 nu=1,nm1
      P=(x*dfloat(2*nu+1)*p2-dfloat(nu)*p1)/dfloat(nu+1)
      p1=p2
4     p2=P
      return
      end
```

LAWRENCE BERKELEY LABORATORY
TECHNICAL INFORMATION DEPARTMENT
1 CYCLOTRON ROAD
BERKELEY, CALIFORNIA 94720